

**Nanostructured transition metal oxynitrides for energy
storage devices**

by

Olga Kartachova
M.Sc.

Submitted in fulfilment of the requirements for the degree of
Doctor of Philosophy

Deakin University

November, 2013



**DEAKIN UNIVERSITY
ACCESS TO THESIS - A**

I am the author of the thesis entitled

*Nanostructured transition metal oxynitrides
for energy storage devices*
submitted for the degree of *Doctor of Philosophy*

This thesis may be made available for consultation, loan and limited copying in accordance with the Copyright Act 1968.

'I certify that I am the student named below and that the information provided in the form is correct'

Full Name: *Olga Kardachova*
(Please Print)

Signed: Signature Redacted by Library

Date: *7/4/2014*



**DEAKIN UNIVERSITY
CANDIDATE DECLARATION**

I certify the following about the thesis entitled (10 word maximum)

Nanostructured transition metal oxynitrides
for energy storage devices

submitted for the degree of Doctor of Philosophy

- a. I am the creator of all or part of the whole work(s) (including content and layout) and that where reference is made to the work of others, due acknowledgment is given.
- b. The work(s) are not in any way a violation or infringement of any copyright, trademark, patent, or other rights whatsoever of any person.
- c. That if the work(s) have been commissioned, sponsored or supported by any organisation, I have fulfilled all of the obligations required by such contract or agreement.

I also certify that any material in the thesis which has been accepted for a degree or diploma by any university or institution is identified in the text.

'I certify that I am the student named below and that the information provided in the form is correct'

Full Name: Olga Kardachova
(Please Print)

Signed: Signature Redacted by Library

Date: 29.11.2013

Acknowledgements

I express my gratitude to:

- My principal supervisor Prof. Ying (Ian) Chen for providing me with the opportunity to work in his research group, for providing the guidance throughout my research and for his openness to new ideas
- My associate supervisor Dr. A. M. Glushenkov for his important advices, his patience and his day-to-day support
- Deakin University for the postgraduate research scholarship
- Dr. H. Zhang and Dr. Y. Chen for performing transmission electron microscopy characterisations
- Dr. X. J. Dai and Dr. R. Jones for performing X-ray photoelectron spectroscopy measurements
- Dr. C. Pozo-Gonzalo for performing electrocatalytic measurements
- Dr. C. Pozo-Gonzalo, Dr. A. A. J. Torriero, Dr. P. C. Howlett and Prof. M. Forsyth for providing me with the opportunity to learn the rotating disk electrode technique and to use the equipment
- Dr. D. M. Fabijanic for synthesising materials with a fluid bed furnace
- Dr. S. Poissonnet for performing wavelength dispersive spectroscopy measurements
- Dr. P. Lamb for important advices throughout my thesis
- Prof. R. Horn for organising very useful seminars
- Mr. R. Lovett, Mr. R. Pow and Ms. M. Wright for technical support
- Dr. Jane Allardyce
- All members of the IFM Nanotechnology group
- My family for their support
- Dr. M. Fielding and his family

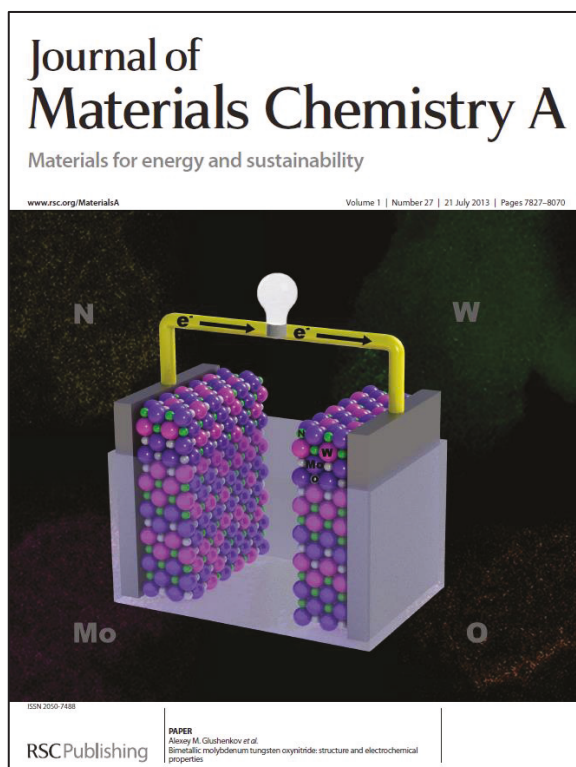
Journal publications from this thesis:

- Results presented in Chapter 3 have been published in the article:

O. Kartachova, A. M. Glushenkov, Y. Chen, H. Zhang, X. J. Dai and Y. Chen, “Electrochemical capacitance of mesoporous tungsten oxynitride in aqueous electrolytes”, *Journal of Power Sources* 220 (2012), 298-305. Permissions have been obtained from the publisher (Elsevier Limited, UK) to reuse the article in a thesis (licence number 3261740798635).

- Results presented in Chapter 4 have been published in the article (as a cover paper):

O. Kartachova, A. M. Glushenkov, Y. Chen, H. Zhang and Y. Chen, “Bimetallic molybdenum tungsten oxynitride: structure and electrochemical properties”, *Journal of Materials Chemistry A* 1 (2013), 7889-7895. Reproduced by permission of The Royal Society of Chemistry.



Full article: pubs.rsc.org/en/content/articlelanding/2013/ta/c3ta10836h

- Results presented in Chapter 6 have been published in the article:

C. Pozo-Gonzalo, O. Kartachova, A. A. J. Torriero, P. C. Howlett, A. M. Glushenkov, D. M. Fabijanic, Y. Chen, S. Poissonnet and M. Forsyth “Nanoporous transition metal oxynitrides as catalysts for the oxygen reduction reaction”, *Electrochimica Acta* 103 (2013), 151-160. Permissions have been obtained from the publisher (Elsevier Limited, UK) to reuse the article in a thesis (licence number 3261741398473).

Abstract

In this thesis, transition metal oxynitrides, possessing unique physico-chemical properties, are explored as candidates for applications in energy storage devices. More specifically, their electrochemical performance in supercapacitors is evaluated and their electrocatalytic activity towards oxygen reduction reaction is tested. In order to better understand their performance, a number of gaps in the knowledge are addressed.

For electrode materials in supercapacitors, understanding the charge storage mechanism is of great importance, as it enables improvement of their performance. For some nitrides and oxynitrides, however, the mechanism remains unclear. In this work, tungsten oxynitride $W_{0.75}(N,O)$ is synthesised, extensively characterised and electrochemically tested in a range of electrolytes. The influence of the electrolyte on the electrochemical properties is discussed and the possible charge storage mechanism is explored.

In addition to monometallic nitrides and oxynitrides, synthesis of the bimetallic compounds, with superior physico-chemical properties, has been reported in the field of catalysis. In supercapacitors, however, bimetallic oxynitrides remain almost unexplored as active electrode materials. In this thesis, bimetallic molybdenum tungsten oxynitride $MoW(N,O)$ is produced and its electrochemical properties are evaluated. Additionally, electrochemical impedance spectroscopy measurements are performed in order to compare the performance of the bimetallic compounds and the monometallic oxynitrides.

Furthermore, it has previously been reported that a number of transition metal nitrides and oxynitrides have the ability to form an oxide layer on their surface, and properties of this layer are changing with time, the process also known as ageing. The influence of the ageing on the electrochemical performance of these compounds in supercapacitors has, however, never been studied. In this work, the synthesised $W(N,O)$ and $Mo(N,O)$ undergo a controlled ageing process by exposing the samples to the ambient air for different periods, and their electrochemical properties are compared. Additionally, the role of the passivation in the ageing process is studied.

Finally, many transition metal nitrides and oxynitrides demonstrate good electrocatalytic activities towards oxygen reduction reaction. In this work, electrocatalytic activities of Mo(N,O), V(N,O) and W(N,O) are compared and the oxygen reduction mechanism of Mo(N,O) is studied in detail.

Contents

Chapter 1. Introduction and literature review	5
1.1 BACKGROUND.....	5
1.2 THESIS OBJECTIVES	8
1.3 REVIEW OF RELATED LITERATURE	10
1.3.1 <i>Physico-chemical properties and applications of transition metal nitrides and oxynitrides.....</i>	<i>10</i>
1.3.2 <i>Transition metal nitrides and oxynitrides as candidates for applications in supercapacitors.....</i>	<i>12</i>
1.3.3 <i>Applications of transition metal nitrides and oxynitrides as electrocatalysts for oxygen reduction reaction.....</i>	<i>18</i>
1.4 THESIS STRUCTURE	23
Chapter 2. Experimental techniques	24
2.1 SYNTHESIS TECHNIQUES	24
2.1.1 <i>Temperature-programmed reduction.....</i>	<i>24</i>
2.1.2 <i>Monitoring of the ageing process</i>	<i>26</i>
2.2 CHARACTERISATION TECHNIQUES	26
2.2.1 <i>X-ray diffraction</i>	<i>26</i>
2.2.2 <i>Electron microscopy</i>	<i>27</i>
2.2.3 <i>Low temperature nitrogen adsorption</i>	<i>31</i>
2.2.4 <i>X-ray photoelectron spectroscopy</i>	<i>31</i>
2.3 ELECTROCHEMICAL TESTING TECHNIQUES.....	32
2.3.1 <i>Electrode preparation.....</i>	<i>32</i>
2.3.2 <i>Cyclic voltammetry</i>	<i>33</i>

2.3.3 Galvanostatic charge and discharge measurements.....	36
2.3.4 Electrochemical impedance spectroscopy	37
2.3.5 Rotating disk and ring/disk electrode measurements.....	39

Chapter 3. Electrochemical properties of mesoporous tungsten oxynitride in supercapacitors 42

3.1 INTRODUCTION	42
3.2 EXPERIMENTAL	43
3.3 CHARACTERISATION AND ELECTROCHEMICAL PROPERTIES OF TUNGSTEN OXYNITRIDE.....	45
3.4 CONCLUSIONS.....	58

Chapter 4. Structure and electrochemical capacitance of bimetallic molybdenum tungsten oxynitride 60

4.1 INTRODUCTION	60
4.2 EXPERIMENTAL	61
4.3 STRUCTURE AND ELECTROCHEMICAL PROPERTIES OF MoW(N,O).....	63
4.4 CONCLUSIONS.....	73

Chapter 5. Ageing of molybdenum and tungsten oxynitrides and its influence on the electrochemical capacitance 74

5.1 INTRODUCTION	74
5.2 EXPERIMENTAL	75

5.3 COMPARISON OF THE STRUCTURE AND ELECTROCHEMICAL PERFORMANCE OF NON-PASSIVATED SAMPLES EXPOSED TO AMBIENT AIR FOR DIFFERENT PERIODS.	77
5.3.1 <i>Characterisation of tungsten oxynitride</i>	77
5.3.2 <i>Characterisation of molybdenum oxynitride</i>	81
5.3.3 <i>Influence of ageing on the electrochemical properties of tungsten oxynitride</i>	85
5.3.4 <i>Influence of ageing on the electrochemical properties of molybdenum oxynitride</i>	88
5.4 INFLUENCE OF THE PASSIVATION OF TUNGSTEN OXYNITRIDE ON THE AGEING PROCESS.....	91
5.5 DISCUSSION: IMPLICATIONS OF THE AGEING ON THE PREPARATION AND STORAGE OF TRANSITION METAL OXYNITRIDES	97
5.6 CONCLUSIONS	98

Chapter 6. Transition metal oxynitrides: structure and electrocatalytic performance for the oxygen reduction reaction	100
6.1 INTRODUCTION	100
6.2 EXPERIMENTAL	101
6.3 CHARACTERISATION OF MOLYBDENUM, TUNGSTEN AND VANADIUM OXYNITRIDES	104
6.4 ELECTROCATALYTIC PERFORMANCE OF MOLYBDENUM, TUNGSTEN AND VANADIUM OXYNITRIDES AND OXYGEN REDUCTION MECHANISM OF MOLYBDENUM OXYNITRIDE	107
6.4.1 <i>Comparison of the electrocatalytic performance of Mo(N,O), W(N,O) and V(N,O)</i> ...	107
6.4.2 <i>Investigation of the oxygen reduction mechanism for molybdenum oxynitride</i>	110
6.5 CONCLUSIONS	112

Chapter 7. Summary and recommendations114

References117

Chapter 1. Introduction and literature review

1.1 Background

Today, technological progress is driven by the availability, performance and cost of power sources. The development of cheap and reliable energy storage systems therefore becomes of critical importance for new application areas. In the consumer electronics sector, for instance, the miniaturisation of portable electronic devices such as mobile phones, computers or music players, needs safe and efficient power sources with low weight and volume [1]. In residential applications, the growing use of variable and intermittent output of renewable power sources such as solar cells requires energy storage technologies for satisfying the peak demand for both stand-alone and grid-connected systems [1-4]. Additionally, safe and reliable energy storage systems, with long operating lives are necessary for hybrid and electric vehicles [3, 5].

A number of energy storage technologies exist today: they include mechanical energy storage technologies such as flywheels, compressed air or pumped hydro storage technologies, thermal energy storage, and electrochemical energy storage systems such as batteries, supercapacitors or fuel cells [1, 6]. Among these technologies, electrochemical energy storage systems offer the greatest flexibility in size and design, combined with high efficiency and low maintenance [1, 4]. Therefore, they are promising candidates for use in a wide range of areas, from portable electronics such as mobile phones and computers, to large scale applications including the storage of energy generated by solar cells or wind turbines for residential and industrial applications [1, 4].

Among electrochemical energy storage devices, lithium-ion (Li-ion) batteries have attracted attention in recent years due to their advantages over other types of rechargeable batteries such as higher energy density and lower self-discharge rate [3, 4]. One of the key parameters determining the energy density of electrochemical cells is the voltage, *i.e.* the difference in the electric potential between its terminals [1, 7]. Due to the fact that lithium has a low redox potential versus a standard hydrogen electrode, Li-based electrochemical systems have demonstrated promising energy storage performances [4, 8]. Additionally, lithium is the lightest metal and the small ionic radius of Li^+ facilitates its diffusion in solids [8]. However, one of the disadvantages of lithium-ion batteries lies in the fact that they do not possess high rate capabilities and therefore are not able to operate in conditions where power is required in the pulse form such as load levelling or power backup systems [4, 9]. Another disadvantage of lithium-ion batteries resides in the fact that they will not satisfy future needs for applications in the transportation sector in terms of energy density. It is expected that electric cars with future lithium-ion batteries will be able to be driven for 500 miles (805 km) on a single charge. The weight of their battery pack, however, will exceed 500 kg [10].

In order to satisfy these requirements of high power or energy densities, alternative energy storage systems are being developed. For high-power applications, supercapacitors, possessing higher power densities than lithium-ion batteries, are currently investigated and are often used complementarily with batteries [11]. Another type of power sources being actively studied is lithium-air batteries, with energy densities 5-10 times higher than that of current Li-ion batteries [10, 12].

The price, weight and performance of these new electrochemical energy storage devices are mainly dependant on their active electrode materials. In supercapacitors, for instance, the choice of materials affects several operational characteristics including the power and energy densities, cyclic stability and the price [13]. Similarly, in lithium-air batteries, the performance of the air electrode containing the electrocatalyst for the oxygen reduction reaction affects the cost, the overall efficiency of the device, the charge/discharge rate, the capacity

retention as well as the cycling life [14-16]. Additionally, many active electrode materials used in energy storage systems today are toxic or hazardous. Efforts are therefore directed towards developing safer and better performing compounds.

Nitrides and oxynitrides of transition metals from groups 4-6 are a class of materials possessing a unique set of physico-chemical characteristics including a high conductivity, hardness, mechanical stability, resistance to corrosion and a catalytic activity [17]. Due to their versatile properties, these compounds have been extensively used in past years for a number of applications including integrated circuits, coatings and catalysis [18-20]. Recently, however, nitrides and oxynitrides of transition metals have been studied as active electrode materials in the energy conversion and storage devices including dye-sensitised solar cells, lithium-ion batteries, metal-air batteries and supercapacitors [21].

Among these applications, transition metal nitrides have demonstrated particularly promising electrochemical properties in supercapacitors and have achieved, on one side, attractive specific capacitance values due to the pseudocapacitive charge storage mechanism, and, on another side, high rate capabilities due to their good intrinsic conductivities [22, 23]. Additionally, these materials have shown a Pt-like electrocatalytic activity as electrocatalysts for oxygen reduction reaction (ORR) in lithium-air batteries [21]. These new uses of transition metal nitrides and oxynitrides still require better understanding of their electrochemical and electrocatalytic properties. The work presented in this thesis will therefore be focused on the applications of these compounds in supercapacitors and as electrocatalysts for oxygen reduction reaction, and several gaps in the knowledge will be addressed.

1.2 Thesis objectives

Due to their unique physico-chemical properties, nitrides and oxynitrides of transition metals are actively investigated today as candidates for use in the electrodes of supercapacitors and as electrocatalysts for the oxygen reduction reaction. These new areas of application require a more detailed investigation of these compounds in order to achieve a better understanding of their electrochemical and electrocatalytic mechanisms, as several aspects of their performance have not been covered in the literature. The work presented in this thesis is focused on some of these issues.

In supercapacitors, the understanding of the charge storage mechanism enables optimisation of the material in order to improve its performance. For example, the identification of active species participating in the charge storage processes on the surface could help to maximise the performance of electrode materials by adapting their surface composition, for instance, by oxidation. For some transition metal nitrides and oxynitrides, however, the charge storage mechanism is not clear. Additionally, in supercapacitors, only monometallic nitrides and oxynitrides have been studied, almost exclusively, as active electrode materials, while bimetallic nitrides and oxynitrides have not been characterised. Furthermore, it has previously been observed that properties of transition metal nitrides and oxynitrides are evolving with time; in fact, these compounds have the ability to form an oxide layer on the surface, and properties of this oxide layer are changing upon storage of the compounds in the ambient air (ageing). The influence of ageing on the electrochemical properties of transition metal nitrides and oxynitrides in supercapacitors has, however, never been explored. Finally, although a number of transition metal nitrides and oxynitrides have demonstrated a Pt-like electrocatalytic behaviour, many compounds have not been extensively studied. The detailed literature review highlighting these gaps in the knowledge is presented in the following section. This thesis is mainly focused on molybdenum, tungsten and vanadium oxynitrides, which exhibit unique physico-chemical characteristics, typical for a number of nitrides and oxynitrides of transition metals from groups 4-6.

In summary, this research work aims to:

- Explore the possible charge storage mechanism for tungsten nitrides and oxynitrides in supercapacitors
- Evaluate the influence of the addition of the second metal in the crystal lattice of oxynitrides on their electrochemical properties
- Establish the influence of the ageing of nitrides and oxynitrides in the ambient air on their electrochemical performance and discuss the implications of ageing on the synthesis and storage procedures of these compounds
- Characterise the electrocatalytic activity of molybdenum oxynitride towards oxygen reduction reaction

1.3 Review of related literature

1.3.1 Physico-chemical properties and applications of transition metal nitrides and oxynitrides

Transition metal nitrides of groups 4-6 are also called interstitial nitrides or interstitial alloys, as non-metal atoms are located in the interstices between the metal atoms due to the small atomic radius of nitrogen, which can fit into the lattices of these transition metals [24, 25]. High electrical and thermal conductivities of transition metal nitrides of groups 4-6 are attributed to the predominantly metallic bonding, with contributions of ionic and covalent components [17, 24]. The good catalytic activities of these compounds, which are comparable to platinum, could be explained by the electron transfer from the non-metals to transition metals, as well as by the expansion of the metal lattice, resulting in the contraction of the d-band [25]. Another important characteristic of this group of materials is their ability to form a range of non-stoichiometric phases [17]. Additionally, oxygen is often present in the crystal lattice, leading to the formation of oxynitrides [25]. The difference between the nitrides and oxynitrides, as well as between several non-stoichiometric phases is not visible on the X-ray diffraction patterns, making it difficult to distinguish between these compounds [17].

Due to their versatile properties, transition metal nitrides and oxynitrides attracted attention in recent years as candidates for application in energy conversion and storage devices. In lithium-ion batteries, thin films of vanadium nitride [26] and chromium nitride [27] have demonstrated reversible capacities of approximately 800 [26] and 1200 mAh g⁻¹[27], respectively, as anode materials. Furthermore, thin films of Co₃N [28], Fe₃N [28], Mn₃N₂ [29], RuN [30] and V₂ON [31] have reached reversible capacities between approximately 300 and 900 mAh g⁻¹. In addition to thin films, nanostructured transition metal nitrides such as CrN [32], CoN [33] and (Ni_{0.33}Co_{0.67})N [34] nanoparticles, as well as CoN nanoflakes [35] have demonstrated capacity values between 400 and 990 mAh g⁻¹. It has been reported that the main mechanism responsible for the electrochemical

performance of these compounds as anode materials is a partial or complete conversion reaction with lithium [21]. In addition to applications in lithium-ion batteries, compounds including vanadium nitride [22, 36-39], tungsten nitride [40, 41], molybdenum nitride [36, 42-44] and titanium nitride [45, 46], as well as titanium and vanadium oxynitrides [47] have also been investigated as active electrode materials for supercapacitors and have shown typical capacitance values between 30 and 350 F g⁻¹. These compounds have predominantly demonstrated good rate capabilities due to their high intrinsic conductivities. Furthermore, nearly ideal rectangular shapes of cyclic voltammetry curves have typically been observed for a number of these materials.

Additionally, the electrocatalytic properties of transition metal nitrides and oxynitrides enable their application as counter-electrodes in dye-sensitised solar cells (DSSCs) and as electrocatalysts for oxygen reduction reaction (ORR) [21]. More specifically, DSSCs using nitrides of iron [48], vanadium [48, 49], molybdenum [48, 50] and tungsten [48, 50] as counter-electrodes for the reduction of triiodide ions, have reached up to 92 % of the photovoltaic performance of DSSCs using Pt as counter-electrodes [48-50]. Furthermore, nitrides and oxynitrides including TiN [51, 52], molybdenum nitrides MoN [53, 54] and Mo₂N [54, 55], as well as zirconium [56] and tantalum [57] oxynitrides have demonstrated good electrocatalytic activity for oxygen reduction reaction. For many of these compounds, a four-electron ORR pathway has been reported.

The work in this thesis is focused on the electrochemical performance of transition metal nitrides and oxynitrides in supercapacitors and on their electrocatalytic performance as catalysts for oxygen reduction reaction. Sections 1.3.2 and 1.3.3 below present a detailed review of the related literature on the applications of these compounds as active materials in supercapacitors, and as electrocatalysts for ORR, respectively.

1.3.2 Transition metal nitrides and oxynitrides as candidates for applications in supercapacitors

Supercapacitors are energy storage devices possessing higher power densities than batteries, and therefore can be discharged at higher currents [58]. This characteristic enables their application, often complementarily to batteries, in industrial, residential or automotive areas, where energy is required in a pulse form, typically for a time range between 10^{-2} and 10^2 seconds [11, 59]. In hybrid electric vehicles, for instance, supercapacitors are used to recover braking energy and for engine starting [11], while in cellular phones, supercapacitors could deliver pulse power and therefore help to increase the lifetime of batteries [59]. Another example of high-power applications of these charge storage devices is smart grids, which require power quality control and load smoothing [11]. In addition to higher power densities, supercapacitors often possess longer cycling life than batteries. This is due to the fact that their charge storage mechanism only involves the surface or sub-surface layers of the active materials and not the bulk, as it is the case with batteries, and therefore no significant phase or composition changes of the electrode materials occur [11, 58, 60].

Most of the supercapacitors available on the market today are electrochemical double-layer capacitors (EDLCs). Their electrodes are composed of carbon-based active materials, which store the charge at the electrode/electrolyte interface as an electrical double layer (EDL), which forms due to the separation of ion and electron charges [59, 60]. However, despite high power densities and good cyclic stability, the amount of energy stored in a double-layer is limited, and the specific capacitance values of EDLCs are typically between 20 and 50 $\mu\text{F cm}^{-2}$ [61, 62]. This limitation introduces challenges in the new application areas of supercapacitors, particularly in the automotive sector where the weight and size of the power source is of significant importance [59]. Efforts are therefore directed towards developing active electrode materials with higher capacitance values.

One type of materials actively investigated today and possessing higher specific capacitance values when compared to carbon-based materials are transition metal oxides, which are able to store the charge through Faradaic reactions, in addition

to the electric double-layer [58, 61, 63-65]. This type of charge storage mechanism, also known as pseudocapacitance, involves a charge transfer across the electrode/electrolyte interface [58, 61] and the specific capacitance values per unit of electrode area, associated with pseudocapacitive processes, are typically orders of magnitude higher when compare to EDL, due to the superior energy densities associated with Faradaic processes [58, 66-68]. Among transition metal oxides, amorphous hydrous ruthenium oxide ($\text{RuO}_2 \cdot x\text{H}_2\text{O}$) is a benchmark material possessing a pseudocapacitive charge storage mechanism with specific capacitance values exceeding 700 F g^{-1} ($>1000 \mu\text{F cm}^{-2}$) [67, 69]. However, the high cost of ruthenium prevents the wide use of this material. Manganese oxide (MnO_2) is considered as a cheaper and less toxic alternative to ruthenium oxide with reported specific capacitance values of above 350 F g^{-1} [70-79]. MnO_2 has been extensively studied and its charge storage mechanism has been investigated. Manganese oxide exists in a wide range of crystalline structures or degrees of crystallinity, and two principal pseudocapacitive charge storage mechanisms have been identified, depending on the crystalline form and the type of ions present in the electrolyte [72-74, 76, 78-83]. One of these mechanisms is reversible adsorption of ions or protons on the surface [71, 79], and it has been reported that this process is predominantly characteristic of poorly crystalline forms of MnO_2 [80]. Another charge storage mechanism is ion or proton intercalation into the lattice, mainly reported for crystalline phases of manganese oxides, and the specific capacitance, in this case, is dependent on the crystal structure [75-77, 80-82].

However, despite promising capacitive properties, many transition metal oxides suffer from poor intrinsic conductivity, which results in the low rate capability. Efforts have been made to resolve this issue, as the rate capability, and therefore the ability to work with high currents, is a very important characteristic of supercapacitors. One of the methods to improve the rate capability of transition metal oxides involves the production of composites with carbon-based materials [84]. However, despite improved rate capabilities, these composites suffer from lower energy densities. Another strategy consists of the use of transition metal oxides in the form of thin films [85]. The drawback of this method is the low content of the active materials. Efforts are therefore directed towards developing a

material for supercapacitors which possesses both a pseudocapacitive charge storage mechanism with high specific capacitance values, and a high intrinsic conductivity.

In recent years, several transition metal nitrides and oxynitrides have become promising candidates for applications in supercapacitors due to their high surface areas, good intrinsic conductivities and resistance to corrosion [21]. One of the most important performance parameters of supercapacitors is the rate capability, which can be defined as the ability to maintain the charge storage characteristics at high charge or discharge currents. Transition metal nitrides and oxynitrides, due to their good conductivities, have shown promising performance at high currents. For instance, vanadium nitride (VN), with typical maximum specific capacitance values between 161 and 273 F g⁻¹ [22, 36-38], has demonstrated 79 % of the initial capacitance retention upon 20-fold increase of the current load from 0.05 to 1 A g⁻¹ in 1M H₂SO₄ and 84 % in 3M NaCl electrolytes, respectively [22]. Additionally, TiN-VN core-shell fibres, showing the specific capacitance of 262 F g⁻¹ in 1M KOH electrolyte at 2 A g⁻¹, have retained approximately 64 % of this value at 10 A g⁻¹ [23].

Furthermore, in addition to high rate capabilities, transition metal nitrides and oxynitrides often possess a symmetric, nearly rectangular shape of cyclic voltammograms, as well as triangular galvanostatic charge and discharge curves, demonstrating an almost ideal capacitive behaviour [22, 36, 40, 42, 44]. Examples of compounds possessing rectangular CV curves include W₂N [40] or TiN [46] in KOH solution, as well as γ -Mo₂N in H₂SO₄ electrolyte [36, 42]. The shape of the cyclic voltammograms of transition metal nitrides and oxynitrides is, however, affected by the electrolyte used. Vanadium nitrides, for instance, shows several redox peaks on the surface of cyclic voltammograms in KOH solution [22, 37, 39], while a more rectangular shape of the CV curves is observed in the neutral NaCl aqueous electrolyte [22].

Additionally, good cyclic stabilities have been reported for some transition metal nitrided and oxynitrides. For instance, VN has demonstrated less than 10 % of the initial capacitance loss after 1000 CV cycles in 1M KOH electrolyte at the scan

rate of 50 mV s^{-1} [39], while $\gamma\text{-Mo}_2\text{N}$ retained 94.9 % of the initial capacitance after 6000 cycles in 1M H_2SO_4 and 94.7% in 1M KCl electrolytes, respectively, at the scan rate of 100 mV s^{-1} [44]. Additionally, tungsten nitrides WN and W_2N lost approximately 20 % and 27 %, respectively, of the initial capacitance values after 500 cycles in 1M KOH electrolyte at the scan rate of 50 mV s^{-1} [40, 41]. It is, however, difficult to compare the cycling life of several compounds, as different scan rates have been used for measuring their cyclic stabilities. It would be useful, in my view, to investigate the stability of the electrode materials upon the galvanostatic charging and discharging, in addition to cyclic voltammetry, as an emulation of the real application. Additionally, the cycling life of transition metal nitrides and oxynitrides has usually been tested in one electrolyte only, and the influence of the electrolyte on the stability has not been studied in detail.

Transition metal nitrides and oxynitrides have predominantly demonstrated pseudocapacitive charge storage mechanisms, in addition to the electrical double-layer in aqueous electrolytes, characterised by orders of magnitude higher specific capacitance values per electrode area compared to the EDL [58]. It has been proposed that the pseudocapacitive charge storage mechanism of VN in 1M KOH electrolyte, for instance, could be attributed to the presence of vanadium oxides or oxynitrides on the surface, which interact with OH^- ions [39]. Later, Thompson *et al.* have reported, using the ion isolation method, that OH^- ions are, in fact, the active species participating in the charge storage process, while K^+ ions are not involved [36]. Despite the fact that several transition metal nitrides and oxynitrides have been studied as electrode materials in supercapacitors, the charge storage mechanism of some compounds such as, for example, tungsten nitrides and oxynitrides, is not clear. Similarly to other nitrides, tungsten nitrides have demonstrated nearly ideal shapes of cyclic voltammetry curves and specific capacitance values of 100 F g^{-1} and 30 F g^{-1} have been reported for W_2N and WN, respectively, in 1M KOH electrolyte [40, 41]. The charge storage mechanism of these compounds has, however, not been explored in detail. In fact, both authors proposed that the charge is mainly stored in the electrical double-layer due to the rectangular shape of the cyclic voltammogram, however, the double layer mechanism does not correlate with the specific capacitance values per area of $\sim 200 \mu\text{F cm}^{-2}$ and $\sim 64 \mu\text{F cm}^{-2}$ for W_2N and WN, respectively, which are higher

than the values associated with a EDL charge storage [40, 41]. Later, Thompson *et al.* proposed the existence of a pseudocapacitive charge storage mechanism in addition to the EDL for tungsten nitride in 1M KOH electrolyte [36]. A more detailed investigation of the charge storage mechanism of tungsten nitrides and oxynitrides is therefore needed. Furthermore, these compounds have only been tested in 1M KOH solution, and no detailed data exist on their performance in acid and neutral electrolytes.

In addition to monometallic transition metal nitrides and oxynitrides, synthesis of bimetallic compounds has previously been reported. For instance, in the field of catalysis, a partial substitution of one transition metal by another in the lattice has led, as a result, to changes in the physico-chemical properties and therefore catalytic performances of the materials [86-88]. More specifically, vanadium molybdenum oxynitride [88] and cobalt molybdenum nitride [86] have shown higher catalytic performances when compared to the monometallic compounds. In supercapacitors, however, bimetallic nitrides and oxynitrides have not been studied in detail, and electrochemical performance of the mixed γ -Mo₂N and Co₃Mo₃N phase has only been reported [89]. When compared to the pure γ -Mo₂N, a higher capacitance of 109.9 F g⁻¹, an improved cyclic stability, as well as a better rate capability have been reported for the γ -Mo₂N and Co₃Mo₃N “composite material” in 3.5 M H₂SO₄ electrolyte [89]. No data, however, exist on the electrochemical performance of pure bimetallic compounds in supercapacitors, and the effect of the second metal addition in the crystal lattice of transition metal nitrides and oxynitrides on their capacitive properties has not been explored.

Additionally, transition metal nitrides and oxynitrides have another important intrinsic property affecting their electrochemical activity. It is known from previous studies that several nitrides and oxynitrides of transition metals tend to form oxide layers on the surface at room temperature, and could therefore be regarded as “core-shell” structures, with a nitride “core” and a thin oxide “shell” [90-92]. The presence of the oxidised species on the surface of transition metal nitrides and oxynitrides could be an important factor determining their pseudocapacitive charge storage properties. In vanadium nitride, for instance, the

charge storage mechanism has been attributed to the existence of various oxidised compounds on the surface of VN, which interact with OH⁻ ions in 1M KOH electrolyte [36, 39]. It has also been reported that the properties of the oxide layer on the surface of nitrides and oxynitrides are changing with time. This process, also known as ageing, has been reported for molybdenum and tungsten oxynitrides. In fact, X-ray photoelectron spectroscopy data have demonstrated an increase in the amount of WO₃ on the surface of WN_{0.59}O_{0.24} after a storage in the air at room temperature for 80 days [90]. Additionally, elemental analysis has also revealed a higher amount of oxygen in molybdenum oxynitride samples stored in the ambient air [91, 92]. This room temperature oxidation process involves the surface or sub-surface layers of oxynitrides, as no changes in the X-ray diffraction patterns could be detected [90-92]. The variation of oxide layer composition with time on the surface of nitrides or oxynitrides could therefore have an effect on their capacitive properties, and this influence should be investigated in more detail. For instance, the effect of the passivation as well as the ageing should be studied in relation to the electrochemical performance, in order to determine the optimal preparation and storage conditions for these electrode materials.

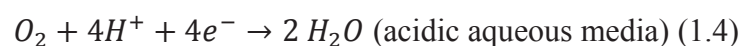
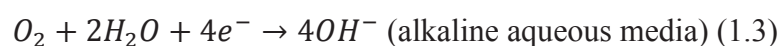
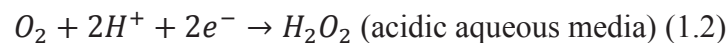
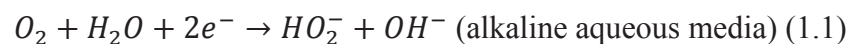
Finally, it is important to highlight again that although several compounds are described in the literature as “nitrides”, they could, in reality, contain a certain percentage of oxygen [17]. For example, Brousse *et al.* [47] have produced a range of compounds by a temperature-programmed reduction of vanadium oxides by varying the nitridation time, temperature as well as heating rate, and obtained products with a varying oxygen content, with oxygen still present at synthesis temperatures as high as 1000°C [47]. The fact that several compounds are often denoted as “nitrides” without presenting an elemental analysis, makes it difficult to perform the comparison between the materials reported in the literature. The synthesised materials should therefore be investigated in detail in order to assign the correct phases. For simplicity, the compounds are denoted in this thesis according to their respective descriptions in publications and referred to as “nitrides and oxynitrides”.

In summary, although transition metal nitrides and oxynitrides possess promising electrochemical properties in supercapacitors, a number of gaps in the knowledge

should be addressed in order to gain a better understanding the advantages and limitations of this class of compounds. First, the charge storage mechanism of some compounds such as, for instance, tungsten nitrides and oxynitrides, has not been studied in detail and should therefore be clarified. Additionally, pure bimetallic nitride and oxynitride compounds have never been investigated as electrode materials for supercapacitors. Finally, the influence of the ageing, or the evolution of the oxide layer on the surface of nitrides and oxynitrides with time, has never been addressed in relation to the capacitive properties of these compounds.

1.3.3 Applications of transition metal nitrides and oxynitrides as electrocatalysts for oxygen reduction reaction

The oxygen reduction reaction (ORR) is an important process, which enables several biological mechanisms such as, for instance, the respiration, to happen [93]. In energy storage devices, the ORR occurs at the cathode of the metal-air batteries and regenerative fuel cells, and its mechanism in the aqueous media is similar between these two systems [10, 14-16, 94]. The ORR in these electrochemical devices involves the reduction of O_2 into H_2O or H_2O_2 , depending on the reaction pathway, and processes via several steps: adsorption of oxygen on the surface of the electrocatalyst, electron transfer to oxygen from the anode, breaking of the oxygen bond and finally, desorption of products [14, 93]. This reaction can proceed via two-electron or four-electron mechanisms, and its pathways are affected by the type of catalyst, its active sites, crystalline structure, as well as the electrolyte [12, 15, 16, 93]:



In reality, ORR pathways are more complex and could involve a series “2x2” electron pathways, where the two-electron reduction is followed by further two-electron reduction or disproportionation of the peroxide [15, 93]. Additionally, the combination of both two- and four-electron pathways is also possible [15]. In order to obtain the maximum efficiency of the charge storage device, as well as to avoid the corrosion of the electrode material by the peroxide formed, a four-electron pathway is preferred in fuel cells and metal-air batteries [15, 93]. Since the ORR mechanism is, to a large extent, dependant on the activity of the electrocatalyst [14, 15, 95], research is focused on studying ORR pathways for different materials in order to develop a cheap and efficient catalyst.

The most studied electrocatalysts for ORR are noble metals-based compounds, such as platinum and its alloys. These generally demonstrate overall four-electron oxygen reduction mechanisms, and they are considered as benchmark electrocatalysts [15, 93, 96, 97]. However, despite the good electrocatalytic performance, the high cost of noble metals prevents their wide application [14, 15]. Efforts have therefore been devoted to develop less costly alternatives to noble metal-based catalysts.

In this regard, carbon-based materials, characterised by high surface areas and high conductivities, have been considered as less expensive alternatives to Pt, and have predominantly demonstrated electrocatalytic activity towards ORR via the two-electron mechanism [15, 93, 98-100]. The introduction of impurities has, however, enabled a significant improvement in their electrocatalytic performance [14, 15, 99, 101-103]. For instance, carbon nanotube-graphene complexes containing iron and nitrogen impurities have shown a higher ORR activity when compared to the purified nanostructures, demonstrated by the shift in the onset potential of ~100 mV and a lower percentage of H₂O₂ generated, thus approaching the activity of platinum on carbon black (Pt/C) [99]. Furthermore, for nitrogen-doped carbon nanotubes, the number of transferred electrons of n=3.9 has been calculated, while only n=1.8 was reported for nitrogen-free carbon nanotubes [103]. Additionally, the electrocatalytic activity of carbon-based materials varies depending on their morphology, allotropes, and concentration of the edge planes [15]. For instance, graphene nanosheets, possessing a large amount of edge sites

for oxygen adsorption, have shown an improved electrocatalytic performance, demonstrated by higher discharge capacity as electrode material in Li-air batteries when compared to other types of carbons in non-aqueous electrolytes [104]. Furthermore, a four-electron ORR mechanism has often been reported for heteroatom-doped graphene-based materials [105].

Another class of materials actively investigated as catalysts for oxygen reduction reaction are transition metal compounds, including transition metal oxides carbides, nitrides, carbonitrides, oxynitrides and chalcogenides [15, 94]. Among these materials, transition metal oxides have attracted considerable attention. Manganese oxides, for instance, exist in a variety of phases, including MnO, MnO₂, Mn₂O₃, Mn₃O₄ or Mn₅O₈, and a range of chemical compositions and crystalline arrangements [106-110]. The electrocatalytic performance of manganese oxides towards ORR has been extensively studied and it has been demonstrated that the number of transferred electrons is influenced by numerous parameters including the phase, crystal structure or morphology, with a number of compounds demonstrating high activity towards ORR via an overall four-electron process [15, 106, 107, 109-111]. Other transition metal oxides including Co₃O₄ [112-114] or TiO₂ [115, 116] have shown attractive electrocatalytic activities towards ORR, and oxygen reduction reaction pathways for these materials have been dependent on the type of the support, oxidation state or crystalline structure of the compounds, as well as on the electrolyte [93, 112, 113, 115, 116]. Additionally, La-based perovskites with a general formula LaMO₃ (M=Ni, Co, Fe, Mn and Cr) demonstrated promising electrocatalytic performance [95] and promoted the oxygen reduction reaction predominantly via the four-electron pathway [95, 117]. However, despite lower costs when compared to noble metals, transition metal oxides are generally semiconductors and therefore possess limited intrinsic conductivities [95]. Furthermore, many of these compounds demonstrate a poor resistance to corrosion [95]. There is, therefore, a need for an electrocatalyst that does not only satisfy the price and efficiency criteria but also possesses a high intrinsic conductivity and good corrosion resistance.

The unique intrinsic properties of transition metal nitrides and oxynitrides including the electrochemical activity, high conductivity and resistance to

corrosion in a range of electrolytes make them promising candidates for applications as electrocatalysts for ORR in air electrodes [21, 93]. One of the most studied compounds in this field is titanium nitride [51, 52, 118-120]. In fact, TiN has been studied as a catalyst for ORR several decades ago in the alkaline electrolyte, and has shown a significantly higher electrocatalytic performance than that of pure titanium as well as better resistance to corrosion [51]. More specifically, TiN has demonstrated a higher onset potential for ORR (0.8 V when compared to 0.3 V for pure Ti), as well as a twice higher limiting current [51]. The mechanisms of the oxygen reduction reaction and electrocatalytic activities of transition metal nitrides and oxynitrides are, however, complex, and depend on several parameters including the morphology or phase. For instance, ORR has been studied for the nano-sized and micro-sized TiN, and it has been reported that the nano-sized TiN not only demonstrates a higher catalytic activity but also a different pathway for the oxygen reduction reaction [52]. It has been proposed that the ORR proceeds via a dual-path in nano-sized TiN, combining both direct four-electron and series two-electron pathways, while a series two-electron ORR mechanism occurs in micro-sized TiN [52].

Other nitrides including CrN, Mn₄N, Fe₂N, Co₃N and Ni₃N have also demonstrated electrocatalytic activities for ORR [121]. The number of electrons transferred (n) increases in the following order: Ni₃N ($n=2.6$) < Fe₂N ($n=2.9$) < Co₃N ($n=3.2$) < CrN ($n=3.3$) < Mn₄N ($n=3.9$) [121]. In addition, the electrocatalytic performances of bimetallic compounds such as cobalt molybdenum nitride [122] and cobalt tungsten nitride [123], as well as oxynitrides of zirconium and tantalum [56, 57] have been evaluated.

Among transition metal nitrides and oxynitrides, a promising catalytic activity has been reported for two phases of molybdenum nitrides: MoN and Mo₂N, and the number of transferred electrons $n=3.8$ has been calculated for both materials [53, 124], indicating overall four-electron ORR pathways. The oxygen reduction mechanism for these compounds is, however, not clear. The electrocatalytic activities of these materials have been reported for the carbon-supported compounds, and Lee *et al.* have recently proposed that carbon supports could have a synergetic influence on the electrocatalytic activity of transition metal nitrides

[125]. More specifically, TiN electrocatalysts supported on carbon nanostructures have shown higher onset potentials and larger ORR limiting currents when compared to pure TiN, not only due to high surface area supports provided by nanocarbons, but by the decreased charge transfer resistances as well [125]. The electrocatalytic activity of the pure, unsupported molybdenum nitrides and oxynitrides towards ORR should therefore be further explored.

Although the larger portion of this thesis is attributed to the performance of transition metal nitrides and oxynitrides in supercapacitors, Chapter 6 is dedicated to the electrocatalytic performance of molybdenum oxynitride as a catalyst for the oxygen reduction reaction.

1.4 Thesis structure

This thesis is divided into seven chapters presenting different aspects of the work within the wider research question. **Chapter 1** defines the research context and contains a review of the existing literature on the application of transition metal nitrides and oxynitrides in the energy storage devices. More specifically, the application of these compounds as active electrode materials in supercapacitors and as electrocatalysts for oxygen reduction reaction (ORR) is explored. This chapter also highlights the gaps in the knowledge to be addressed and defines the objectives of the thesis. **Chapter 2** briefly summarises experimental methods used to synthesise, characterise and test materials in supercapacitors and as electrocatalysts for ORR. **Chapters 3-6** contain experimental results and their discussions. **Chapter 3** is focused on tungsten oxynitride and its electrochemical properties in supercapacitors. This chapter particularly addresses the investigation of the charge storage mechanism and the performance of tungsten oxynitride in different electrolytes. In **Chapter 4**, electrochemical properties of the bimetallic oxynitride (molybdenum tungsten oxynitride) in supercapacitors are reported for the first time. **Chapter 5** is focused on investigating the influence of the ageing on the electrochemical performance of oxynitride powders exposed to the ambient air for different periods. In **Chapter 6**, the activity of molybdenum oxynitride as an electrocatalyst for ORR is studied and compared to tungsten and vanadium oxynitrides. This chapter includes an extensive characterisation of these compounds. **Chapter 7** contains conclusions and possible directions for future research.

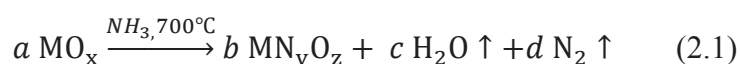
Chapter 2. Experimental techniques

In this chapter, synthesis and characterisation techniques used in this thesis are briefly presented. More detailed descriptions are given in Chapters 3-6 or in textbooks presented in the section “References”.

2.1 Synthesis techniques

2.1.1 Temperature-programmed reduction

Transition metal compounds described in this thesis are synthesised by a temperature-programmed reduction (TPR) technique, extensively described in the literature [18, 19, 126-128]. This procedure consists of placing a precursor in a stream of the reactive gas and progressively increasing the temperature with a fixed heating rate [18]. In this work, precursors are transition metal oxides in a powder form, while the reactive gas is ammonia (NH₃). For a number of transition metal oxides, TPR in ammonia gas occurs in two stages: reduction of the oxide and the progressive replacement of oxygen in the crystal lattice with nitrogen; while oxygen reacts with hydrogen to form water, nitrogen is incorporated in the lattice [126, 127]. This process produces the porous morphology of the samples, and as a result, the oxide precursors transform into the nitride or oxynitride products with high surface areas [19, 91, 127]:



In order to produce monometallic compounds, commercially available transition metal oxide precursors are used. To produce bimetallic products, however, a

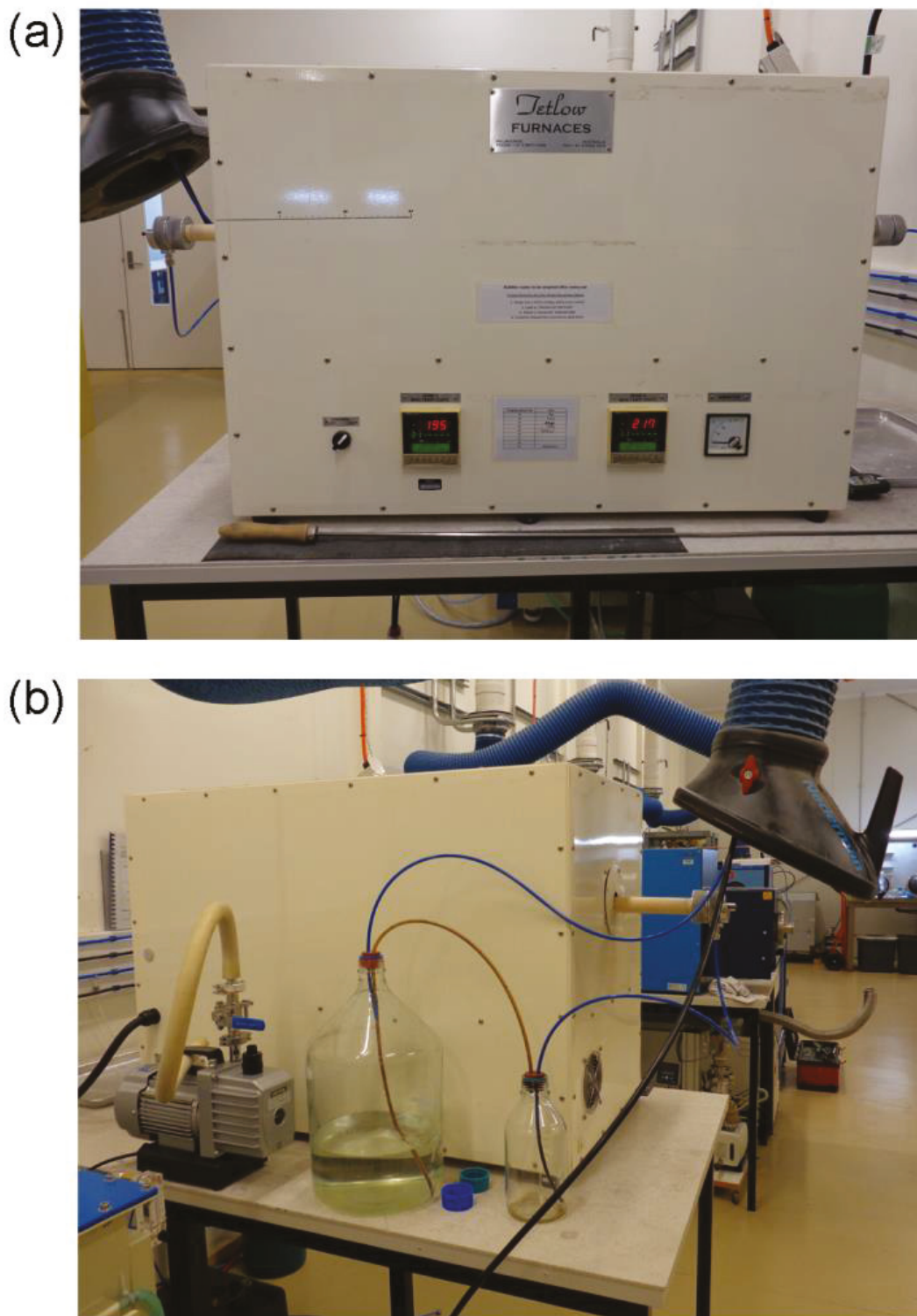


Figure E1. Front (a) and rear views (b) of the tube furnace setup for the temperature-programmed reduction in the ammonia gas.

special bimetallic oxide precursor is prepared using a ball milling and annealing process. The detailed synthesis procedure of the bimetallic precursor is described in Chapter 4.

In a typical temperature-programmed experiment, approximately one gram of the oxide precursor, placed in an alumina crucible, is loaded in the tube furnace (Tetlow Kilns & Furnaces Pty Ltd, Australia) (Figure E1). The temperature is subsequently raised to the final nitridation temperature with a fixed heating rate, kept at this temperature for the required period, and then cooled down to the room temperature naturally. Throughout the experiment, the flow of the reactive gas (NH_3) is fixed.

Due to their pyrophoric character, transition metal compounds presented in this thesis require passivation, *i.e.* the formation of a protective oxide layer on the surface prior the exposure to air as a standard synthesis procedure [90, 91, 128]. In order to evaluate the effect of the passivation on the ageing of the samples (Chapter 5), passivated and non-passivated compounds are produced. If the passivation of the products is required, a special gas mixture, consisting of Ar with 0.1 vol.% O_2 , is passed over the sample at a fixed flow rate during one hour. Pure argon gas is used in case of the non-passivated products.

2.1.2 Monitoring of the ageing process

In order to study the evolution of the synthesised products in the ambient air (the ageing), the passivated and non-passivated samples produced by the temperature-programmed reduction technique are stored in open containers for different time periods in a drawer of a cabinet at room temperature.

2.2 Characterisation techniques

2.2.1 X-ray diffraction

X-ray diffraction (XRD) is used in this work to identify crystalline phases present in the synthesised samples. The working principle of the XRD analysis is based on the interaction of the X-ray beam with a crystalline structure of the material. When the incident beam interacts with a long-range, periodic arrangement of atoms, X-rays are diffracted from the atomic planes of a crystal by the electrons according to the Bragg's law [129]:

$$2 d \sin(\theta) = n \lambda \quad (2.2),$$

where, λ is the wavelength of the incident X-ray beam, n is the order of reflection, d is the interplanar spacing and θ is the angle of incidence of the X-ray beam [129]. Diffraction angles as well as the intensities of the diffraction are related to the atomic arrangements in unit cells, and could therefore be used to identify crystalline structures [129]. Peak positions, peak intensities and full widths at half maximums are determined by data fitting with X'Pert HighScore software.

The synthesised powders are characterised by PANalytical X'Pert PRO diffractometer with an incident Cu K-alpha radiation ($\lambda=0.15418$ nm). The sample holder and the detector are rotated relative to the X-ray source (Bragg-Brentano arrangement), and the intensity of the diffraction is measured as a function of the diffraction angle [130]. In a typical experiment, the step size, spot size, holding time per step, accelerating voltage and current are set to 0.05 degrees, 5 mm x 5 mm, 3 s, 40 kV and 30 mA, respectively. Depending on the measurement requirements and the nature of the sample, these parameters are adjusted. Samples are characterised in the ambient air, within few days after the synthesis.

2.2.2 Electron microscopy

2.2.2.1 Scanning electron microscopy

In this thesis, scanning electron microscopy (SEM) is used to study the morphology of the synthesised samples. More specifically, SEM is used to investigate particle sizes, as well as to visualise shapes and sizes of pores in the porous products (Figure E2). When a sample is irradiated with an electron beam, it results in a release of a range of signals from the irradiated zone [131]. These include characteristic X-rays, luminescence, secondary and backscattered electrons [131]. In this work, secondary electrons (SE) are used to study the morphology of the materials, as the escape depth of SE is in the range of tens-hundreds of angstroms, which enables achievement of a good visualisation of the mesopores on the surface of the samples [131]. In a typical experiment, the electron beam is scanned over an area of the specimen, and secondary electrons are detected in order to form the image [131].

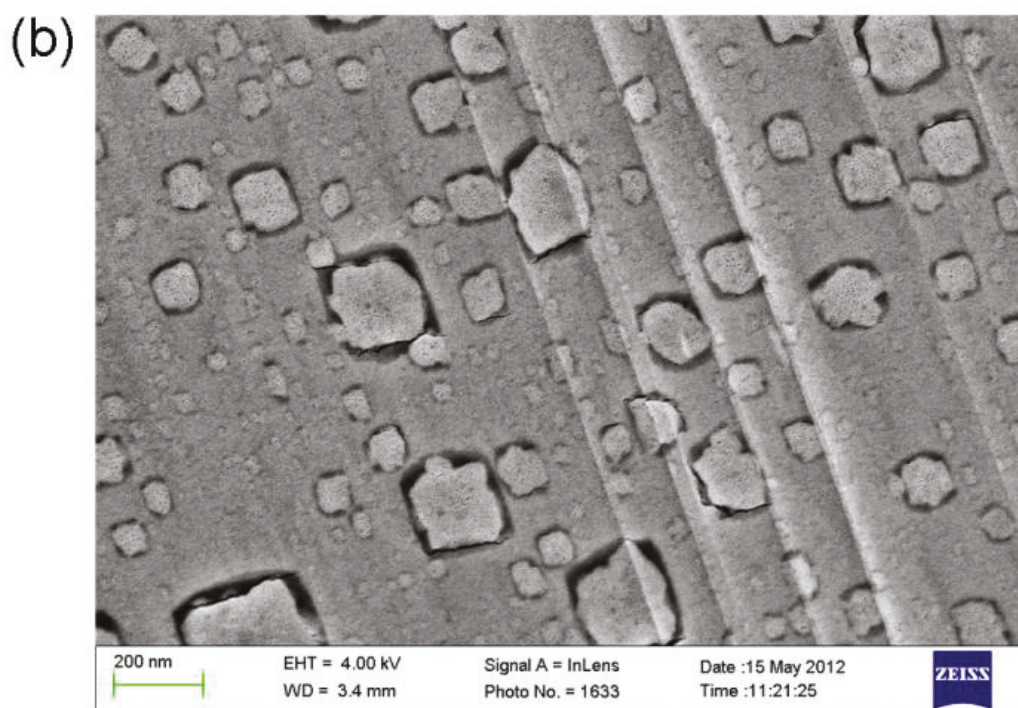
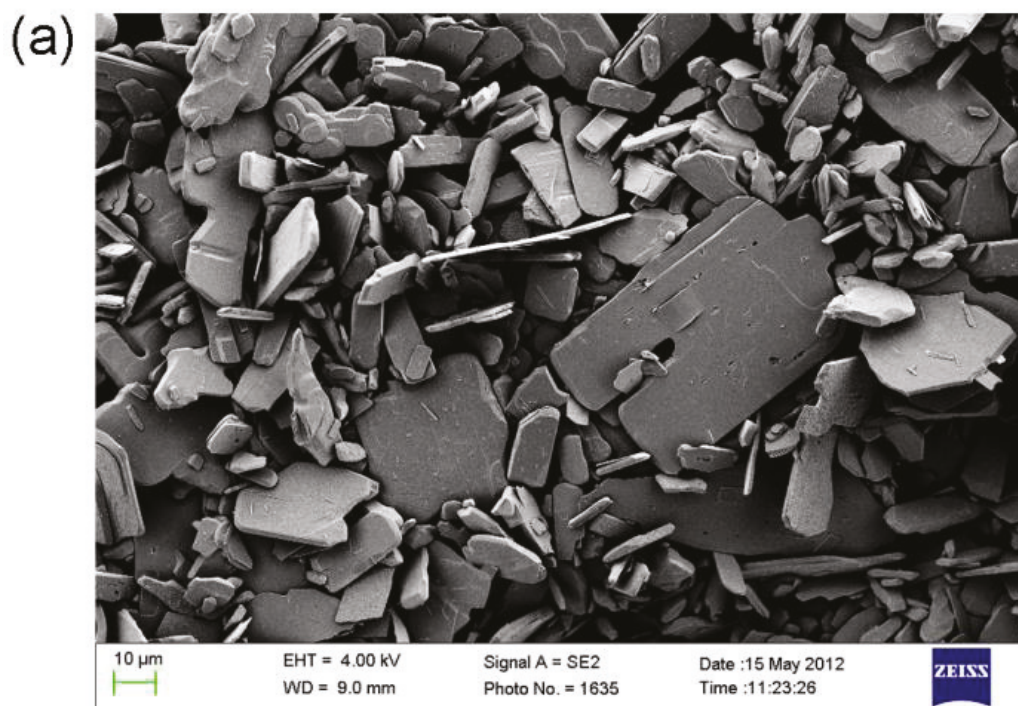


Figure E2. Low-resolution (a) and high-resolution (b) SEM images of molybdenum oxynitride powder.

The synthesised materials are investigated with Carl Zeiss SUPRA 55VP scanning electron microscope. Powder samples are deposited onto the conductive carbon tape and irradiated with an incident beam. For high-resolution images (Figure E2 b), the accelerating voltages of the beam and working distances are kept low, in

the range of 3-5 kV and 3-5 mm, respectively, in order to achieve a better contrast and resolution of the surface features. In this case, an in-lens detector is used.

2.2.2.2 Electron microprobe and wavelength dispersive spectroscopy

Similar to SEM, wavelength dispersive spectroscopy (WDS) X-ray analysis is based on the interaction of the incident electron beam with electrons of the specimen. In this case, however, characteristic X-rays and not the secondary electrons are detected, which enables quantitative characterisation of the elemental composition, as the wavelength of the emitted photon is related to the atomic number of the element from which the emission occurs, and the intensity of the emitted line is proportional to its concentration [132]. Characteristic X-rays are detected with an electron micro probe analyser (EMPA), equipped with a crystal spectrometer [131]. In order to separate the characteristic wavelength in the polychromatic beam of radiation, an analysing crystal with a known interplanar spacing is used [132]. Since each wavelength diffracts from that crystal at a particular discrete (Bragg) angle (equation 2.2), measuring diffraction angles therefore enables determination of the characteristic wavelength [132].

Elemental analysis of the synthesised materials is performed using the electron micro probe analysis (EMPA) with CAMECA SX50 instrument, at the voltage of 15 kV and the current of 40 nA. Prior the analysis, a calibration is performed with standards for each element. Powder samples are pressed into pellets and polished, and the analysis is performed at thirty points for each sample.

2.2.2.3 Transmission electron microscopy

Transmission electron microscopy (TEM) is used in this work to obtain more detailed information on the morphology and structure of the sample, such as, for instance, crystalline structure or grain sizes in crystalline samples, which could not be analysed with the SEM, or to confirm the presence of crystalline phases measured with the X-ray diffraction. Additionally, TEM enables chemical characterisation of the samples with nanometre-level resolution, as well as visualisation of the distribution of a particular element. Similar to SEM, TEM is based on the interaction of the incident beam of electrons with the specimen. In

TEM, however, the voltage of the incident beam is typically a hundred times higher than that used in SEM, and since the sample is thin, TEM enables the incident electrons to penetrate through the specimen. Therefore, in TEM, inelastic and elastic scattering of the incident beam by electrons or nuclei of the atoms in the sample are used as a source of information, and not the secondary signals as it is the case with the SEM [133-135].

In case of the elastic scattering, the kinetic energy of the electrons does not change after interaction with the specimen, and scattering of the incident beam at different angles contributes to the image contrast [133-136]. Both electrons scattered in the direction parallel to the incident beam and electrons scattered at wide angles can be used to form TEM images (bright-field and dark-field, respectively) [133-136]. Additionally, in crystalline samples, incident electrons are diffracted according to the Bragg's law (equation 2.2) and produce electron diffraction patterns, which give information about the crystalline nature of the specimen [133-135].

In the case of the inelastic scattering, incident electrons can induce ionisations of the atoms in the specimen or plasmon excitations, which result in the decrease of the kinetic energy of the electrons exiting the sample [133, 136]. Core excitations are used in the Electron Energy-Loss Spectrometry (EELS), which records the energy losses and gives the information about the elements present in the sample, while plasmon excitations enable identification of the number of phases [136]. In the imaging mode, it is possible to obtain energy-filtered TEM (EFTEM) images, showing the distribution of a particular element in the sample, by using a three-window method, which consists of using two images recorded below and one image recorded above the ionisation edge of the specific element [133, 136].

TEM characterisation of the samples is performed with an FEI Titan instrument, equipped with a scanning unit (STEM) and a Gatan Imaging Filter (GIF), using an operating voltage of 300 kV. Samples are stored in an inert gas atmosphere prior the TEM analysis and characterised within two weeks after the synthesis.

2.2.3 Low temperature nitrogen adsorption

Low temperature nitrogen (N_2) adsorption is used in this thesis to measure surface areas of the materials, as well as to analyse their pore size distributions. This information could be obtained from the adsorption isotherm, measured when the sample is brought in contact with a gas (N_2) at various definite pressures and at a constant temperature of liquid nitrogen [137]. Adsorption isotherm represents the amount of the adsorbed gas as a function of p/p_0 , where p is the equilibrium pressure and p_0 is the saturation vapour pressure [137]. In porous materials, the isotherm has a hysteresis loop between the adsorption and desorption branches due to the capillary condensation of the gas in the pores [137]. The surface area of the materials is calculated from the amount of the adsorbate using the Brunauer-Emmett-Teller (BET) method, while the pore size distribution is evaluated with the Barrett-Joiner-Helenda (BJH) method [137, 138]. BJH model is combining two mechanisms to describe the equilibrium between the adsorbed and non-adsorbed gas during the desorption: the adsorption on pore walls and the capillary condensation [139].

In this thesis, low temperature nitrogen adsorption measurements are performed by using Micrometrics Tristar 3000 instrument. Prior to analysis, samples are degassed at a temperature of 300°C using Micrometrics SmartPrep programmable degas system during two hours under the flow of nitrogen gas.

2.2.4 X-ray photoelectron spectroscopy

In this thesis, X-ray photoelectron spectroscopy (XPS) is used to determine the oxidation states of metals present on the surface of the samples. This technique is based on measurement of kinetic energies of photoelectrons, emitted from the atoms/ions after ionisations induced by the incident X-ray beam, which enables identification of the elemental composition (except hydrogen, helium and elements heavier than uranium), as well as investigation of the chemical environment of these elements [140, 141]. The characterisation is based on the fact that kinetic energies of the emitted photoelectrons are proportional to their



Figure E3. The author connects cables of a potentiostat to a three-electrode supercapacitor cell (the image is reproduced with permission from Deakin University).

binding energies, which are dependent on several parameters, such as the number of protons, distance between the nuclei and core electrons, density of electrons around the atom/ion/molecule and interactions of electrons [140].

XPS measurements are performed using X-ray photoelectron spectrometer (Thermo Fisher Scientific) and Kratos AXIS Nova instrument (Kratos Analytical Ltd, Manchester, UK) with monochromatic Al $K\alpha$ X-rays.

2.3 Electrochemical testing techniques

2.3.1 Electrode preparation

In order to perform the electrochemical analysis, electrodes are prepared by mixing the active oxynitride materials with carbon-based compounds and the binder in specific ratios depending on the type of experiments. For applications in supercapacitor electrodes, materials are mixed with carbon nanopowder (Sigma-

Aldrich, #699632) and poly(vinylidene)fluoride (PVDF, Sigma-Aldrich) in an agate mortar, using N-methyl-2-pyrrolidone (NMP, anhydrous, 99.5 %, Sigma-Aldrich) as a solvent. The slurry is subsequently coated onto Ti foils and dried in vacuum in a conventional oven at 90° C. The weight of the electrode materials is typically between 2 and 3 mg. For testing, three electrode cells (Figure E3) or symmetric sandwich cells are assembled in a Teflon holder, which is also used to separate the components of the cell, and filled with electrolytes under vacuum. In symmetric cells, microporous polyethylene film (MTI Corp., USA) is used as a separator. Either a Solartron Analytical 1470E potentiostat/galvanostat or an Ivium-*n*-stat electrochemical analyser is used for electrochemical measurements.

In order to investigate the electrocatalytic performance towards oxygen reduction reaction, the active materials are mixed with Super PTM Li carbon (TIMCAL) and PVDF (Solvay) in NMP (Solvay) by sonication. Slurries are deposited onto a glassy carbon disk with a pipette and dried in vacuum at 55°C in a conventional oven. Electrocatalytic performance is measured by rotating disk electrode (RDE) or rotating ring-disk electrode (RRDE) methods with the Biologic VMP3/Z multi-channel potentiostat and RRDE-3A rotating ring/disk electrode apparatus (ALS Co. Ltd, Japan).

2.3.2 Cyclic voltammetry

In this thesis, cyclic voltammetry (CV) is used to evaluate the capacitive properties of materials as potential candidates for applications in supercapacitors. In a typical experiment, electrochemical cells (in a three electrode or symmetric cell setup), are connected to a potentiostat and the potential is cycled at a constant sweep rate between two voltage values, while the current response is measured [58]. This technique enables analysis of the capacitive properties of a material from the shape of the cyclic voltammogram. Additionally, it is possible to determine the potential window, in which the electrode material is stable in a particular electrolyte.

When performing the cyclic voltammetry and applying a constant scan rate $\nu = dV/dt$, the current response I could be represented as [58]:

$$I = C \frac{dV}{dt} \quad (2.3)$$

Here, C represents the capacitance. If no Faradaic charge transfer processes take place across the electrode/electrolyte interface, C represents the double-layer capacitance only and could be defined as C_{dl} [58]:

$$I = C_{dl} \frac{dV}{dt} \quad (2.4)$$

while if Faradaic processes occur, C represents pseudocapacitance [58]:

$$I = C_{\varphi} \frac{dV}{dt} \quad (2.5)$$

In this case, the double-layer charging process also contributes to the total response current, but normally represents only a small percentage of the pseudocapacitive current [58].

If the electrode material has an ideal capacitive behaviour, the shape of current response as a function of the potential (cyclic voltammogram) is close to a rectangle (Figure E4 a):

$$\pm I = C (\pm v) \quad (2.6)$$

In reality, C could vary with potential and cyclic voltammetry curve, in that case, exhibits peaks (Figure E4 b) [58].

The criteria for the selection of materials as candidates for application in supercapacitors, based on the CV evaluation, are the mirror-symmetrical and nearly rectangular cyclic voltammograms.

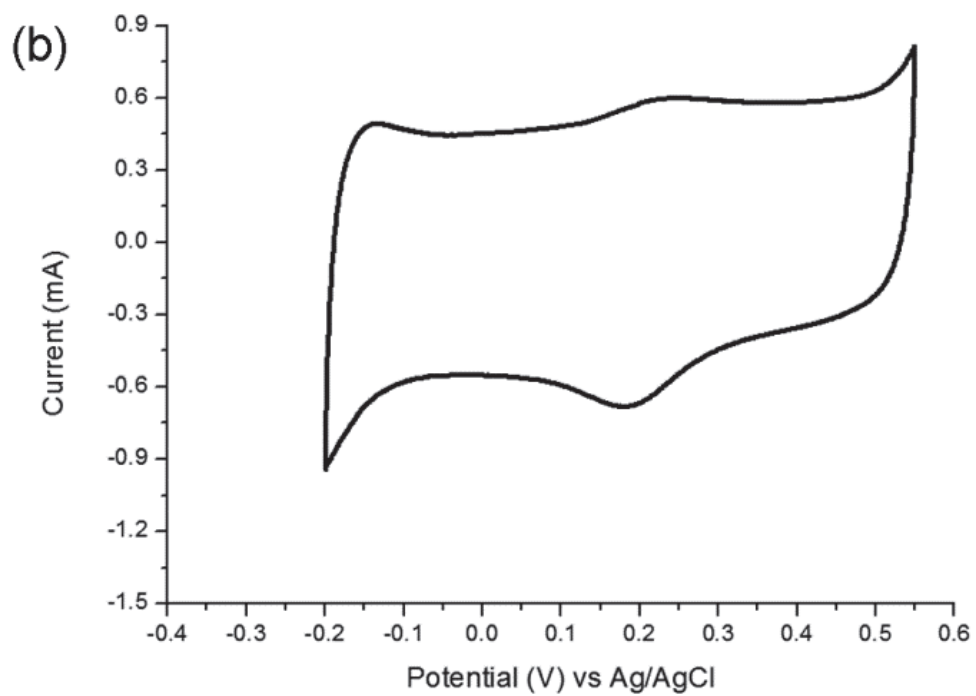
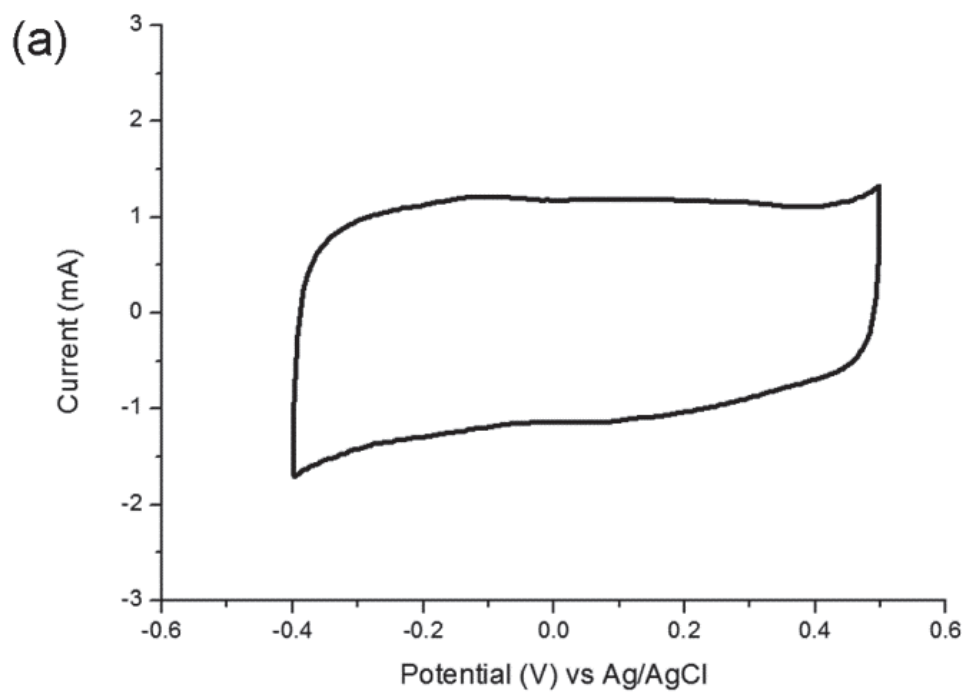


Figure E4. Cyclic voltammograms (3rd cycle) of tungsten oxynitride (a) and molybdenum tungsten oxynitride (b) in 1M H₂SO₄ electrolyte at the scan rate of 5 mV s⁻¹.

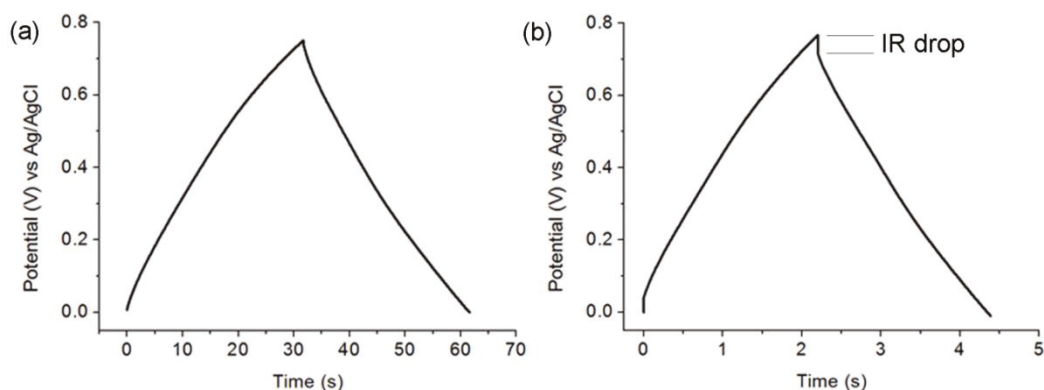


Figure E5. Galvanostatic charge and discharge curves of molybdenum tungsten oxynitride at the current density of 0.5 (a) and 5 A g⁻¹ (b) assembled in a symmetric cell in 1M H₂SO₄ electrolyte (3rd cycle).

2.3.3 Galvanostatic charge and discharge measurements

Galvanostatic charge and discharge measurements are used to determine the specific capacitance of the synthesised materials in supercapacitors. In a typical experiment, a constant current density (I) is supplied within a potential window (ΔV), and the charging/discharging time (Δt) is measured. For a nearly ideal capacitive behaviour of the electrode material, the specific capacitance (C) (defined in the section 2.3.2) is calculated with the formula [58, 142]:

$$C = \frac{I\Delta t}{\Delta V} \quad (2.7)$$

In case of a nearly ideal supercapacitor material, the shape of the galvanostatic charge and discharge curve is close to a triangle (Figure E5 a). It is also possible to compare resistances of the cells from the voltage drop (IR drop) occurring upon the inversion of the current (Figure E5 b) [142].

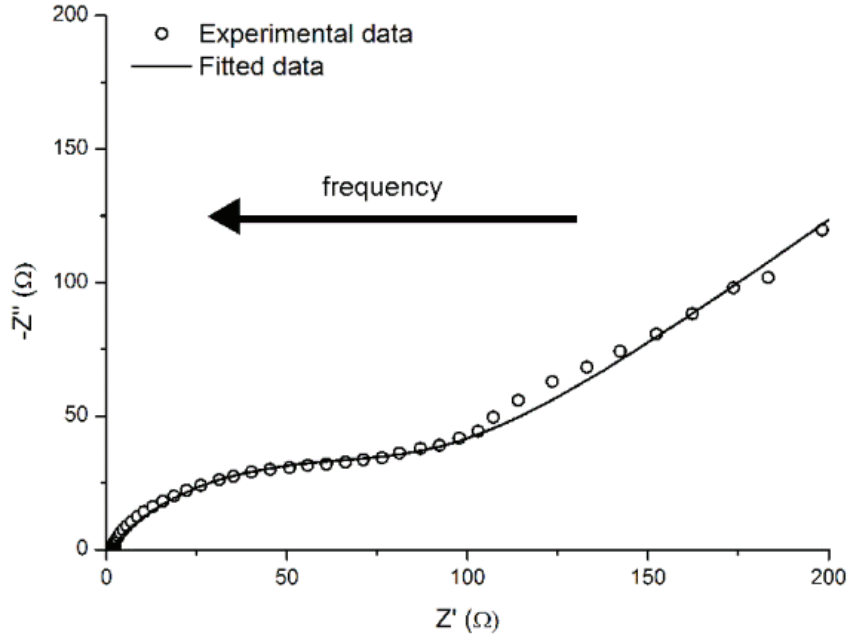


Figure E6. Impedance spectrum of molybdenum oxynitride electrodes assembled in a symmetric supercapacitor in 1M H₂SO₄ electrolyte, represented with a Nyquist plot, where Z' is Z_{real} and Z'' is Z_{im}.

2.3.4 Electrochemical impedance spectroscopy

In an electrochemical system, several phenomena occur as a response to an AC voltage input. They include electron transport towards the electrode/electrolyte interface through a conductor, double-layer charging or charge transfer reactions [143]. These processes occur with different time constants and impedance spectroscopy enables extraction and analysis of useful data separately [143]. When the electrochemical system, which could be modelled with an equivalent circuit containing elements such as resistors, capacitors or inductors, is stimulated with an AC voltage input, the current response, as a result, will present a phase shift, dependent on the ratio of these elements [144]. If $V(t) = V_A \sin(\omega t)$ is the applied voltage with a frequency f , where $\omega = 2\pi f$, and the response current signal is $I(t) = I_A \sin(\omega t + \varphi)$, where φ is the phase shift, then the impedance Z could be expressed in the following form [144]:

$$Z = \frac{V(t)}{I(t)} = \frac{V_A \sin(\omega t)}{I_A \sin(\omega t + \varphi)} = Z_A \frac{\sin(\omega t)}{\sin(\omega t + \varphi)} \quad (2.8)$$

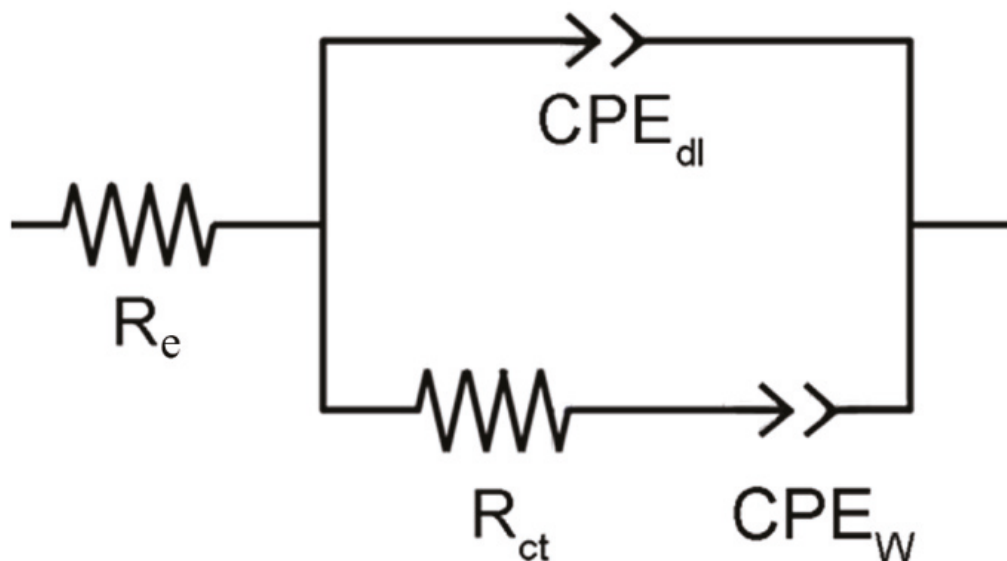


Figure E7. Example of an equivalent circuit used for fitting of the experimental data. R_e and R_{ct} are the electrolyte and charge transfer resistances, respectively, while CPE_{dl} and CPE_w are constant phase elements, used to represent the double layer capacitance and diffusion impedance for a porous material.

This expression could also be written using Euler’s formula $exp(j\varphi) = \cos(\varphi) + jsin(\varphi)$ as a complex function with a combination of “real” and “imaginary” parts [144]:

$$Z = Z_A(\cos(\varphi) + jsin(\varphi)) = Z_{real} + jZ_{im} \quad (2.9)$$

In a typical experiment, a voltage input is applied to the electrochemical system with a varying frequency and the output impedance response is measured [144]. When plotting Z_{real} on the x-axis and Z_{im} on the y-axis, impedance spectrum could be represented with a Nyquist plot (Figure E6) [144]. An example of the equivalent circuit used to model the impedance data for molybdenum oxynitride electrodes, assembled in a symmetric supercapacitor in 1M H_2SO_4 electrolyte, is given in Figure E7.

In this thesis, electrochemical impedance spectroscopy is used to compare the intrinsic properties of monometallic and bimetallic oxynitrides applied as supercapacitor electrode materials, as frequency-response behaviour is affected by the characteristics of the analysed materials [58]. Impedance measurements are

performed with an Ivium-*n*-stat electrochemical analyser operating in a frequency range between 50 kHz and 0.05 Hz in a symmetric cell configuration at the open circuit potential. Fitting of the data is performed with the ZView software.

2.3.5 Rotating disk and ring/disk electrode measurements

Rotating disk and ring/disk electrode techniques (RDE and RRDE, respectively), are used to investigate the electrocatalytic activity of the synthesised materials towards oxygen reduction reaction (ORR) and to determine the ORR pathway from the number of transferred electrons and the amount of hydrogen peroxide generated. In a rotating disk electrode measurement, a three-electrode setup is used, whereby the working electrode spins at a fixed rotation rate, thus increasing the mass transport of the reactants and products towards and away from the electrode, respectively [93, 145]. In this thesis, RDE is used for cyclic voltammetry measurements. At the onset potential of the ORR, the current is controlled by the reaction kinetics and could be defined as [93, 145]:

$$i_k = nFAkC \quad (2.10)$$

Where *n* is the number of transferred electrons, *F* is the Faraday constant, *A* is the area of the electrode, *k* is the rate constant and *C* is the concentration of species (O₂) in the bulk [93, 145]. When the steady-state (where the reaction rate is determined by the mass transport rate at a particular rotation speed) is achieved, the diffusion-controlled (limiting) current is defined as [93, 145]:

$$i_d = 0.62nFAD^{2/3}\omega^{1/2}\nu^{-1/6}C \quad (2.11)$$

Where *D* is the diffusion coefficient of the species, ω is the rotation rate and ν is the viscosity of the electrolyte [93, 145].

The total number of transferred electrons could be calculated by plotting the current in the diffusion-controlled potential range as a function of the rotation rate, and by using the Koutecky-Levich expression for the total current [93, 145]:

$$i^{-1} = i_k^{-1} + i_d^{-1} \quad (2.12)$$

In order to calculate the number of transferred electrons, the following values are used in the equations 2.10-2.12:

F	96485 C mol ⁻¹
A	0.1256 cm ²
D	1.74 x 10 ⁻⁵ cm ² s ⁻¹
v	0.01 cm ² s ⁻¹
C	1.19 x 10 ⁻⁶ mol cm ⁻³

The rotating ring-disk electrode measurement is used to determine the amount of hydrogen peroxide (H₂O₂) produced and thus confirm the ORR mechanism. In this setup, the rotating electrode is equipped with a platinum ring and the measurement is performed in a four-electrode arrangement. The ring detects reaction products swept away from the rotating disk and by using the ring (I_R) and disk (I_D) current densities, the ratio of H₂O₂ formed from one O₂ molecule could be calculated [93, 145]:

$$X_{H_2O_2} = \frac{2I_R/N}{I_D + I_R/N} \quad (2.13)$$

Where N is the collection efficiency of the electrode, calculated as a ratio of the ring and disk current densities measured in 5 mM K₃[Fe(CN)₆] in 0.1 M KCl aqueous solution. The behaviour of [Fe(CN)₆]³⁻/[Fe(CN)₆]⁴⁻ ions during RRDE measurements is well studied, and helps to determine the ratio of the species reduced on the disk reaching the ring: the ring current is produced upon oxidation of [Fe(CN)₆]⁴⁻, generated on the disk by reduction of [Fe(CN)₆]³⁻ [93, 145]. A schematic view of the RRDE setup is presented on Figure E8.

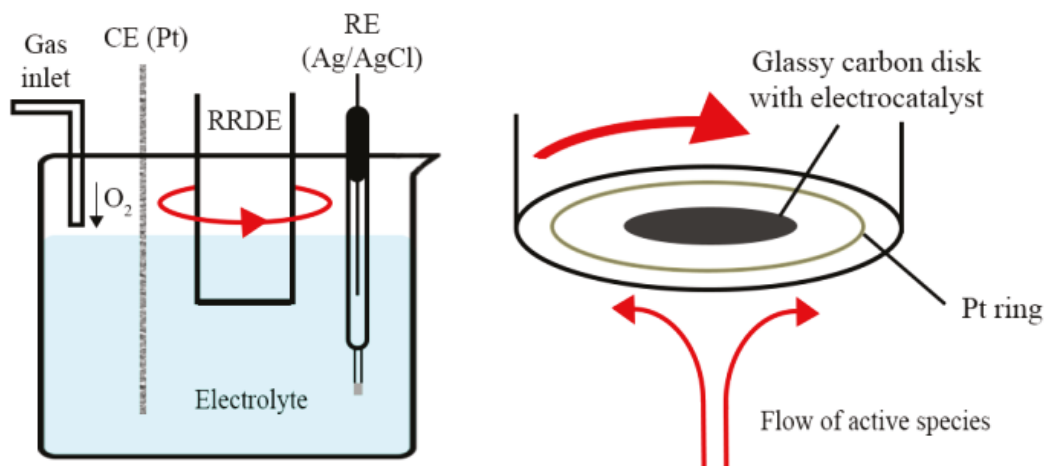


Figure E8. Schematic view of the RRDE setup (left) and a more detailed representation of the rotating electrode (right). CE and RE represent counter and reference electrodes, respectively.

Chapter 3. Electrochemical properties of mesoporous tungsten oxynitride in supercapacitors

3.1 Introduction

Among several transition metal nitrides and oxynitrides investigated as supercapacitor electrode materials, the nature of the charge storage mechanism of tungsten nitrides and oxynitrides remains unclear. Choi and Kumta [41] synthesised tungsten nitride by a temperature-programmed reduction and assigned the phase to WN. This material has demonstrated nearly rectangular CV curves, with the highest capacitance of 30 F g^{-1} measured at the scan rate of 2 mV s^{-1} in 1M KOH electrolyte [41]. Later, Park *et al.* [40] produced tungsten nitride nanoplates and denoted the phase as W_2N . Similar to WN, this product has shown rectangular CV curves, with the highest specific capacitance value of approximately 100 F g^{-1} in 1M KOH electrolyte at the scan rate of 50 mV s^{-1} [40]. Both authors claimed that the main charge storage process of tungsten nitrides is the double-layer mechanism based on the shape of cyclic voltammograms. Thompson *et al.*, however, analysed W_2N in 1M KOH electrolyte and reported the specific capacitance value per area of $60 \mu\text{F cm}^{-2}$, which is higher than the values expected for the double-layer and therefore proposed a presence of a pseudocapacitive charge storage process [36]. The exact nature of the charge storage mechanism for this compound should, therefore, be investigated in more detail.

For manganese oxide MnO_2 , which is an extensively investigated material possessing pseudocapacitive properties, two types of charge storage mechanisms have been reported: pseudocapacitive ion/proton adsorption [71, 79] and ion/proton intercalation into the crystal lattice [74-77], the latter accompanied by the expansion and shrinkage of the lattice visible on XRD patterns, which show

the variation of peak positions and intensities between the charged and discharged materials [74, 75]. These two processes are used as a basis for investigation of a charge storage mechanism of the synthesised tungsten oxynitride.

Furthermore, capacitive properties of transition metal nitrides and oxynitrides have predominantly been tested in one electrolyte only. It would be, in my view, important to investigate electrochemical properties of these compounds in different electrolytes, as they could vary significantly. For example, vanadium nitride has shown variations of the shape of cyclic voltammograms depending on the electrolyte, with a nearly rectangular shape observed in NaCl solution, while redox peaks have been recorded in KOH electrolyte [22]. Additionally, although a number of transition metal nitrides and oxynitrides have shown good cyclic stabilities, measurements have mainly been performed by cyclic voltammetry. In my view, galvanostatic charging and discharging is a more appropriate technique to measure the cycling life as it is an emulation of the application of a real device. Finally, similar to capacitive properties, cyclic stability should be evaluated in a range of different electrolytes.

In this chapter, tungsten oxynitride is synthesised by a temperature-programmed reduction of the tungsten oxide precursor in NH_3 . The compound is extensively characterised by X-ray diffraction and transmission electron microscopy with electron energy loss spectroscopy in order to assign the correct phase to the compound. Furthermore, the morphology of the synthesised material is investigated with scanning electron microscopy and low temperature nitrogen adsorption. The electrochemical properties of tungsten oxynitride are characterised in acid, alkaline and neutral electrolytes: 1M H_2SO_4 , 1M KOH, 3M KCl, 3M NaCl, 1M LiCl and 1M CaCl_2 . Finally, the possible charge storage mechanism is explored and cyclic stability is tested in 1M H_2SO_4 , 1M KOH, 3M NaCl solutions.

3.2 Experimental

Tungsten oxynitride was synthesised by a temperature-programmed reduction of the WO_3 precursor (Fluka, 95410). One gram of tungsten oxide was placed in an

alumina crucible inside a tube furnace (Tetlow Kilns & Furnaces Pty Ltd, Australia) and the furnace was subsequently filled argon (in order to remove air), which was later replaced with NH_3 . Temperature-programmed reduction was performed by progressively raising the temperature to 700 °C with the heating rate of 180 °C h^{-1} , keeping the furnace at that temperature for two hours and letting the furnace to cool down to the room temperature with the ammonia flow fixed to 0.2 l min^{-1} throughout the experiment. Before bringing the samples in contact with air, the synthesised material was passivated with a special gas mixture (Ar + 0.1 vol.% O_2) during one hour with the flow rate of 0.5 l min^{-1} .

The morphology of the product was characterised with scanning electron microscopy (Carl Zeiss Supra SUPRA 55VP) and low temperature N_2 adsorption, performed with Micrometrics Tristar 3000 system. The measured isotherm was used to calculate the surface area of the material with the Brunauer-Emmett-Teller (BET) and the pore size distribution with Barrett-Joiner-Helenda (BJH) methods, respectively. X-ray diffraction (PANalytical X'Pert PRO diffractometer with Cu K-alpha radiation ($\lambda=0.15418$ nm)) was used to evaluate the crystal structure of the synthesised powder. A more detailed characterisation of the product was performed by transmission electron microscopy (FEI Titan instrument operating at 300 kV). Electron energy loss spectroscopy (EELS) was recorded in the TEM nanoprobe diffraction mode with a 2 mm aperture, spectrometer channel resolution of 0.1 eV, convergence angle of 9 mrad, collection angle of 2.9 mrad and a 10-20 s acquisition time. Energy-filtered TEM (EFTEM) maps of W, N and O were obtained via the three-window method. The surface composition of the samples was investigated with X-ray photoelectron spectroscopy (XPS, Thermo Fischer Scientific X-ray photoelectron spectrometer), with a K-alpha X-ray beam focused on a 400 μm spot, with survey spectra collected at the pass energy of 100 eV and high-resolution peaks obtained at 20 eV. The measured binding energies were corrected with the position of the C 1s peak.

Tungsten oxynitride electrodes were prepared by mixing 85 wt.% of the synthesised powder, 10 wt.% of carbon nanopowder, and 5 wt.% of PVDF in NMP as a solvent. The resulting slurry was coated onto Ti foils and dried in vacuum overnight at 90° C. Electrochemical characterisation of tungsten

oxynitride electrodes was performed in 1M H₂SO₄, 1M KOH, 3M KCl, 3M NaCl, 1M LiCl and 1M CaCl₂ electrolytes in a three-electrode cell setup. In the acid and neutral electrolytes, Ag/AgCl reference electrode and a Pt wire as a counter electrode were used, while for tests in the alkaline solution, the Ag/AgCl reference electrode was replaced by Hg/HgO.

In order to investigate the possible pseudocapacitive charge storage mechanism of tungsten oxynitride, charged and discharged electrodes were characterised by the XRD. These electrodes were prepared by the galvanostatic charge and discharge cycling between -0.4 and 0.5 V in 1M H₂SO₄ and between -0.8 to 0.2 V in 3M KCl electrolytes for ten cycles. The cycling was interrupted at -0.4 or 0.5 V in 1M H₂SO₄ and at -0.8 or 0.2 V in 3M KCl, respectively. Charged and discharged electrodes were subsequently cleaned with deionised water and dried at the room temperature.

Cyclic stability measurements were performed by galvanostatic charge and discharge cycling in 1M H₂SO₄, 1M KOH and 3M NaCl solutions, and cyclic voltammetry curves were recorded after every hundred cycles.

3.3 Characterisation and electrochemical properties of tungsten oxynitride

The synthesised sample is first characterised with the scanning electron microscopy (Figure 3.1) in order to evaluate its morphology. SEM images show that the produced dark grey powder is composed of particles with sizes of approximately 20-30 μm (Figure 3.1 a) and pores of diameters less than 20 nm could be observed with a higher magnification (Figure 3.1 b).

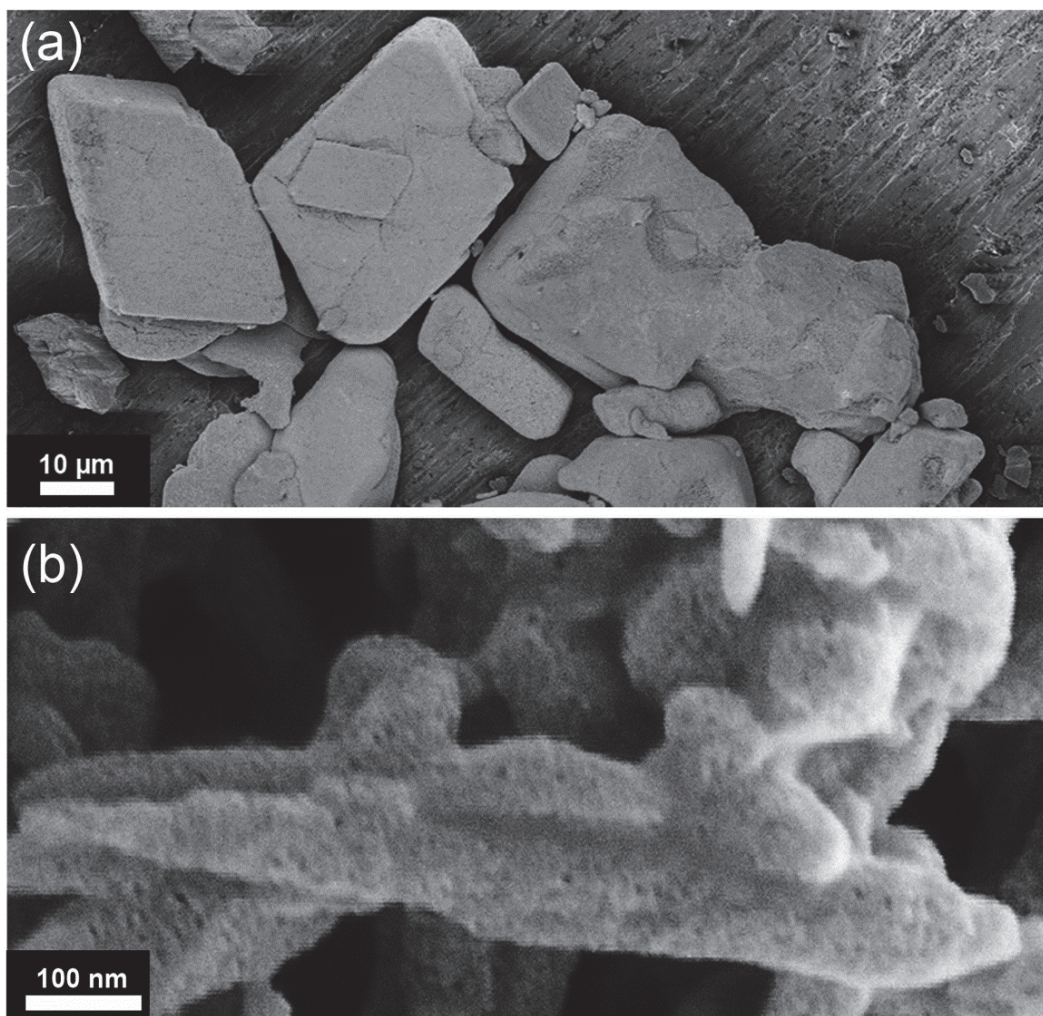


Figure 3.1. SEM images of the synthesised material, depicting its morphology at low (a) and high (b) magnifications.

In order to investigate the porosity of the synthesised material in more detail, low temperature nitrogen (N_2) adsorption experiments are performed. The pore size distribution, calculated with the BJH method, reveals that the produced compound is mesoporous, with the maximum of the distribution centred at approximately 5 nm, with no pores larger than 14 nm detected (Figure 3.2), in agreement with the information revealed by the SEM images (Figure 3.1). The specific surface area of the product is $42 \text{ m}^2 \text{ g}^{-1}$ ($\pm 0.342 \text{ m}^2 \text{ g}^{-1}$), which is identical to the previously reported value for tungsten nitride produced by the temperature-programmed reduction of the tungsten oxide precursor [36].

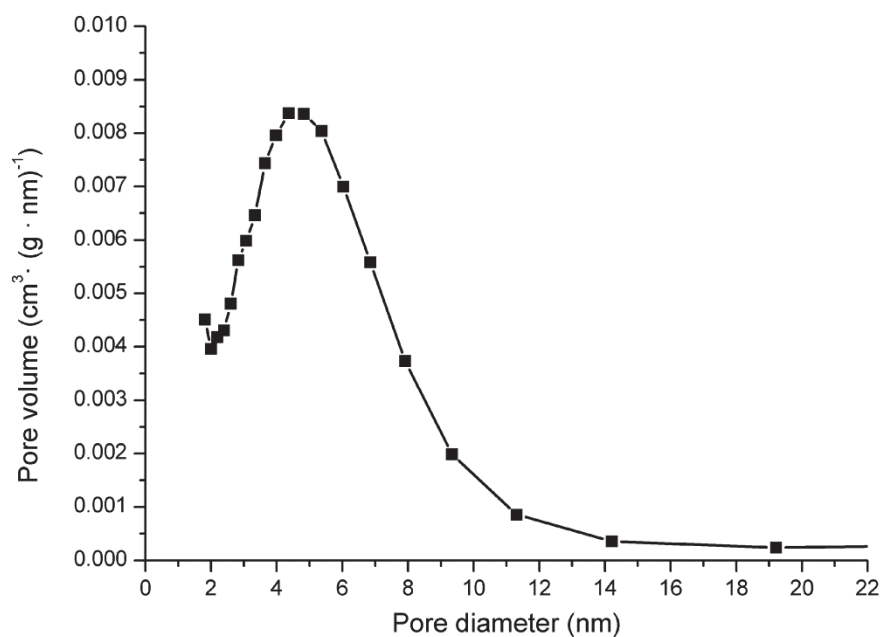


Figure 3.2. Pore size distribution of the material produced by the temperature-programmed reduction.

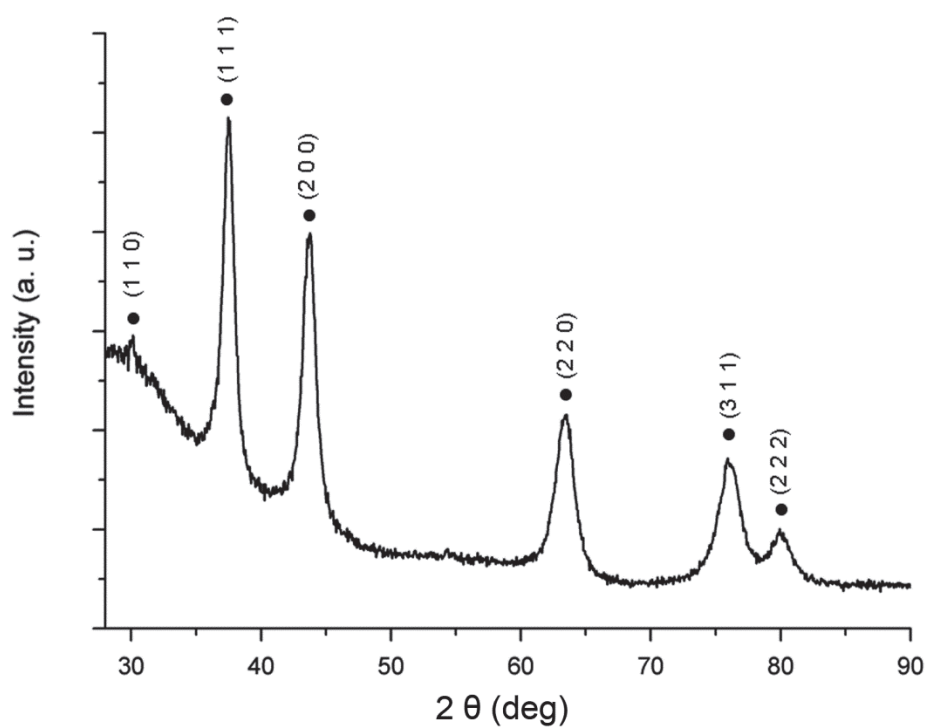


Figure 3.3. X-ray diffraction pattern of the synthesised material, revealing diffraction peaks at 30.1°, 37.5°, 43.7°, 63.4°, 76.1° and 80.1° (marked with “•” symbol). The slope of the background is due to the signal from the sample holder (Scotch tape).

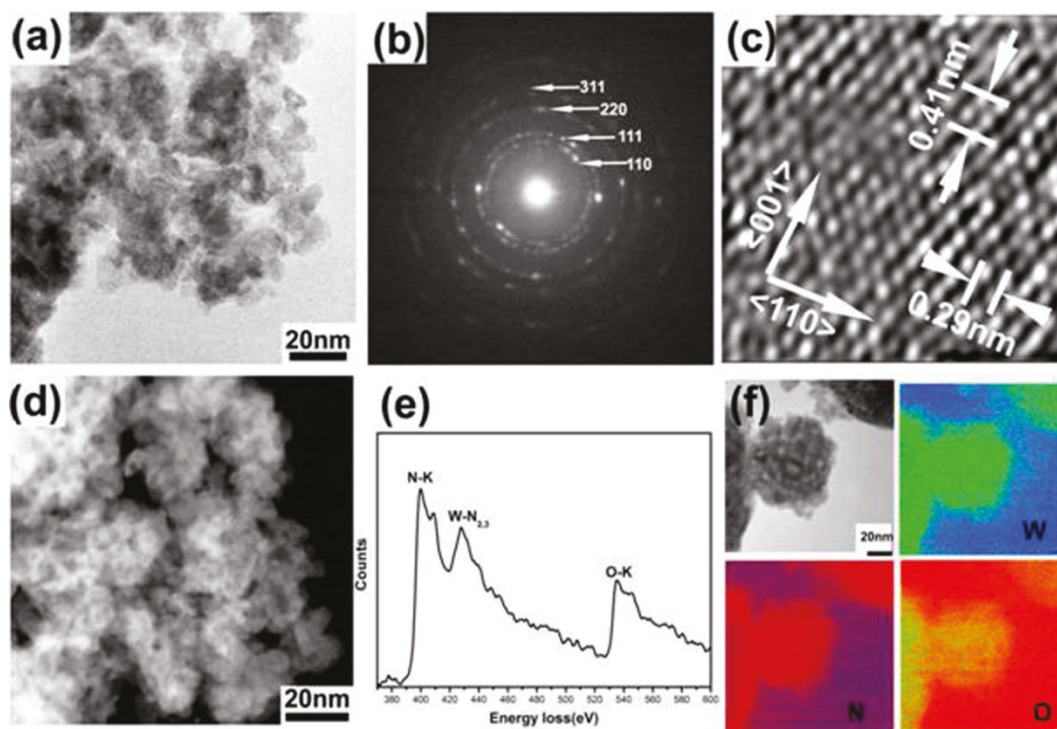


Figure 3.4. Transmission electron microscopy images of the produced material: the bright-field (a), electron diffraction pattern (b), high-resolution TEM (HRTEM) (c), high angle annular dark-field (HAADF) (d), electron energy loss spectrum (e) and EFTEM maps acquired with a three-window method with the corresponding bright-field image (f).

Phase identification of transition metal nitrides and oxynitrides could be complex, as several non-stoichiometric compounds, as well as various oxynitrides with different oxygen content have nearly identical XRD patterns [47]. In fact, the X-ray diffraction pattern (Figure 3.3) of the synthesised compound presents six peaks, which could be attributed to two known phases: W_3N_4 (Powder Diffraction File #: 75-1002) or $W_{0.75}(N,O)$ (Powder Diffraction File #: 25-1255). A more detailed characterisation is therefore required in order to identify the correct phase.

TEM characterisation (Figure 3.4) is performed for studying the synthesised material in more detail. Electron diffraction pattern reveals the polycrystalline, diamond cubic structure of the sample with $a = 0.413$ nm (Figure 3.4 b). Bright-field TEM shows that the crystallite sizes have diameters of approximately 3-8 nm (Figure 3.4 a). HAADF image (Figure 3.4 d) depicts the porosity of the sample, while HRTEM (Figure 3.4 c) demonstrates the resolved lattice fringes corresponding to the (011) and (100) planes of a cubic crystal, and the [011]

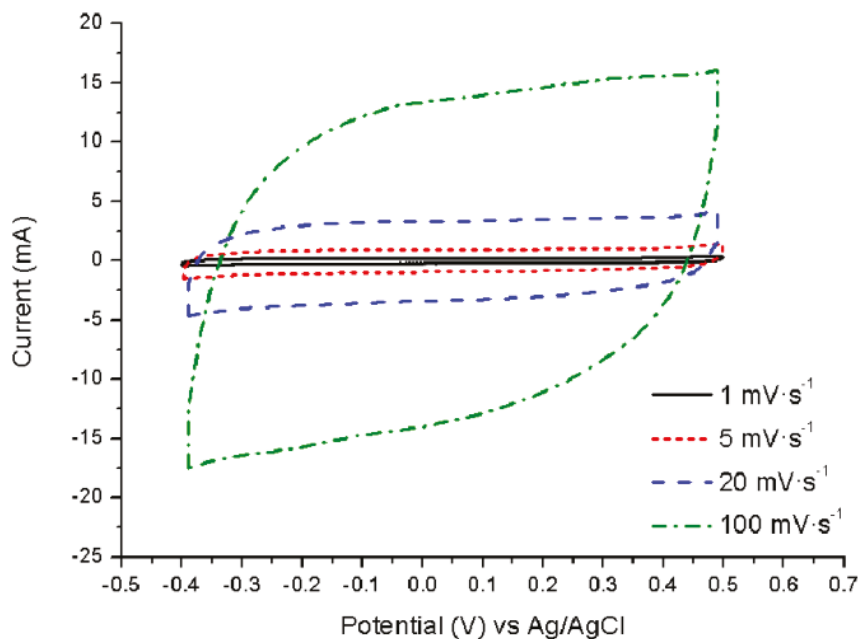


Figure 3.5. Cyclic voltammograms of tungsten oxynitride in 1M H₂SO₄ electrolyte.

direction in the zone axis of this image. Electron diffraction pattern (Figure 3.4 b) confirms the data obtained from the XRD pattern (Figure 3.3), indicating that the synthesised material corresponds to W₃N₄ (Powder Diffraction File #: 75-1002) or W_{0.75}(N,O) (Powder Diffraction File #: 25-1255). The EELS spectrum (Figure 3.4 e), however, shows the presence of oxygen in the compound, in addition to tungsten and nitrogen, and EFTEM maps of W, N and O (Figure 3.4 f) reveal that these elements are distributed throughout the sample. The oxygen and nitrogen are not distributed homogeneously and the O/N atomic ratio, calculated from the electron energy loss data along a line scan, varies between 0.3 and 1. Based on the XRD and TEM analysis, it could be concluded that the main phase in the synthesised material is tungsten oxynitride, with a composition most likely similar to W_{0.75}(N,O).

Cyclic voltammetry measurements in 1M H₂SO₄ electrolyte (Figure 3.5) reveal nearly ideal, rectangular shapes of cyclic voltammograms (CVs) in the potential range between -0.4 V and 0.5 V at the scan rates of 1 mV s⁻¹, 5 mV s⁻¹, 20 mV s⁻¹ and 100 mV s⁻¹, indicating nearly ideal capacitive properties of tungsten oxynitride, as well as a high reversibility of the charge storage mechanism. The nearly rectangular shape of the CV is retained at high scan rates.

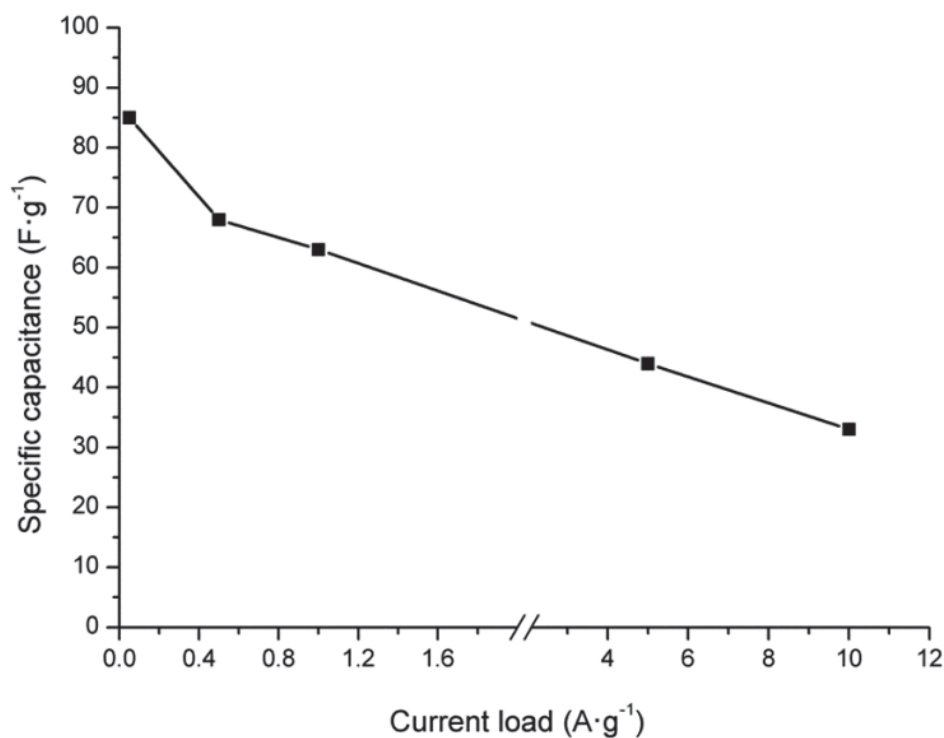


Figure 3.6. Rate capability of tungsten oxynitride electrode in 1M H₂SO₄ electrolyte.

The maximum specific capacitance, measured with the galvanostatic charge and discharge method at the current load of 0.05 A g⁻¹ in 1M H₂SO₄ electrolyte, is 85 F g⁻¹. Despite this modest maximum value, approximately 40% of the initial capacitance is retained upon a 200-fold increase of the current load, reaching 33 F g⁻¹ at the high current density of 10 A g⁻¹, indicating a good rate capability of tungsten oxynitride (Figure 3.6).

Galvanostatic charge and discharge curves at the current load of 0.5 A g⁻¹, depicted on figure 3.7 a, have a triangular shape, with a Coulombic efficiency close to 100 %. At 5 A g⁻¹, however, a small IR drop is observed upon the inversion of the current (Figure 3.7 b) due to limitations of the conductivity, as electrodes were prepared by mixing the material with a conductive carbon and an insulating binder via the conventional procedure.

In addition to the 1M H₂SO₄ solution, tungsten oxynitride works in a range of neutral aqueous electrolytes containing alkaline (Figure 3.8) and alkaline-earth (Figure 3.9) metal cations. In fact, W_{0.75}(N₃O) demonstrated specific capacitance

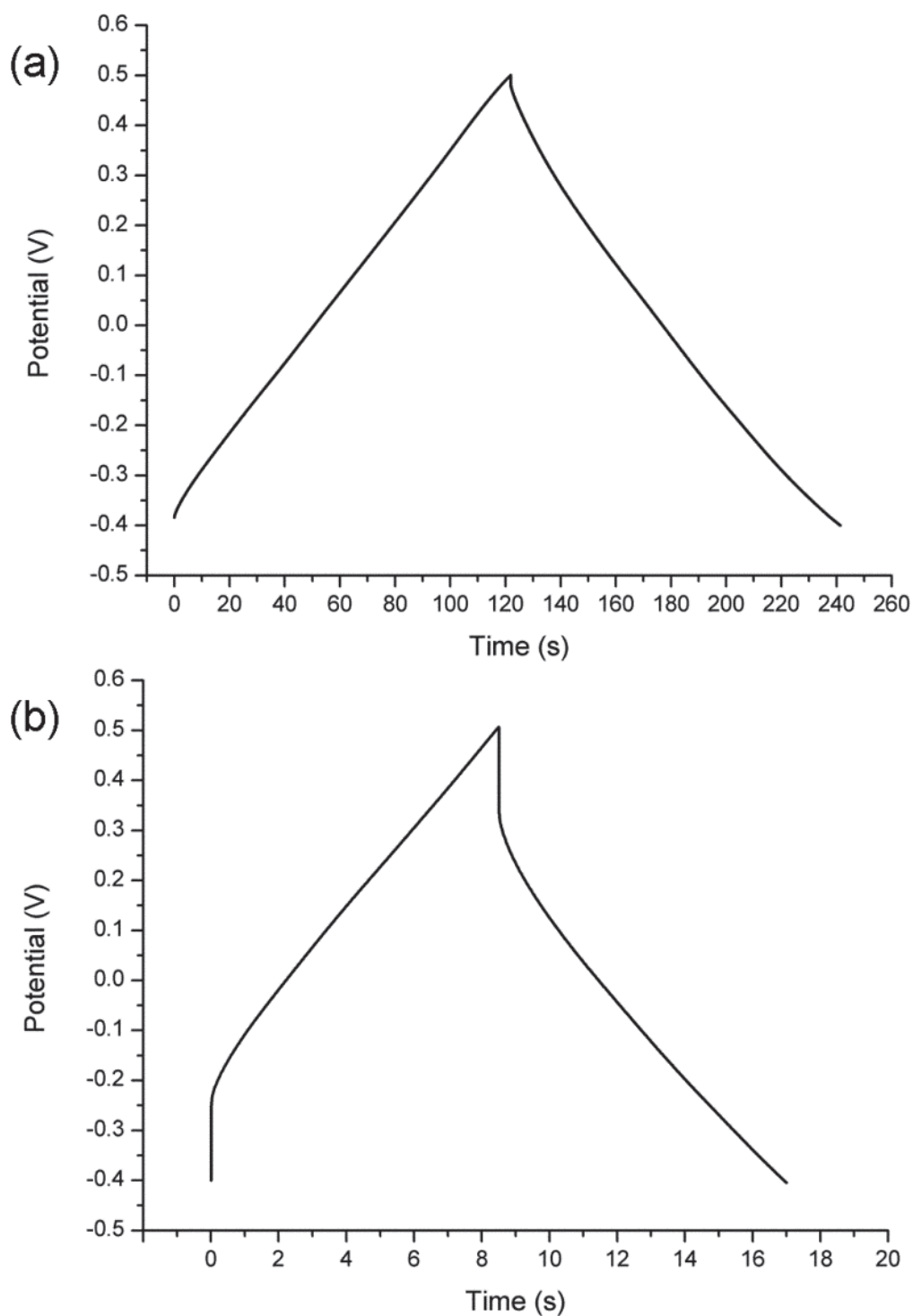


Figure 3.7. Galvanostatic charge and discharge curves of tungsten oxynitride in 1M H₂SO₄ electrolyte at the current loads of 0.5 A g⁻¹ (a) and 5 A g⁻¹ (b).

values of 16 F g⁻¹, 18 F g⁻¹, 28 F g⁻¹ and 39 F g⁻¹ in 3M NaCl, 3M KCl, 1M LiCl and 1M CaCl₂, respectively, at the current load of 0.5 A g⁻¹. The CV shapes are less rectangular when compared to 1M H₂SO₄ electrolyte and are varying depending on the presence of the particular cations.

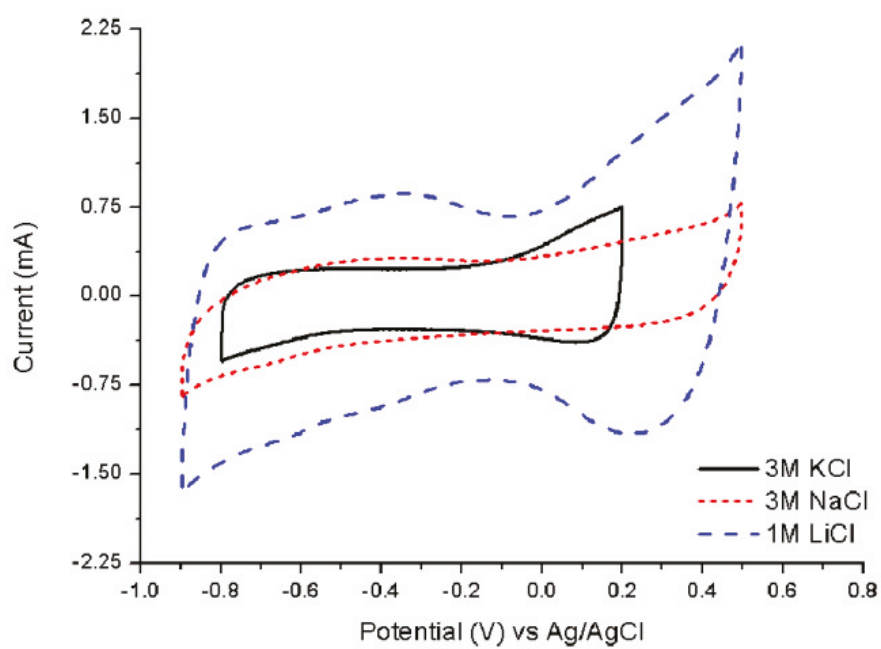


Figure 3.8. Cyclic voltammograms (3rd cycle) of $W_{0.75}(N,O)$ in 3M KCl, 3M NaCl and 1M LiCl solutions at the scan rate of 5 mV s^{-1} .

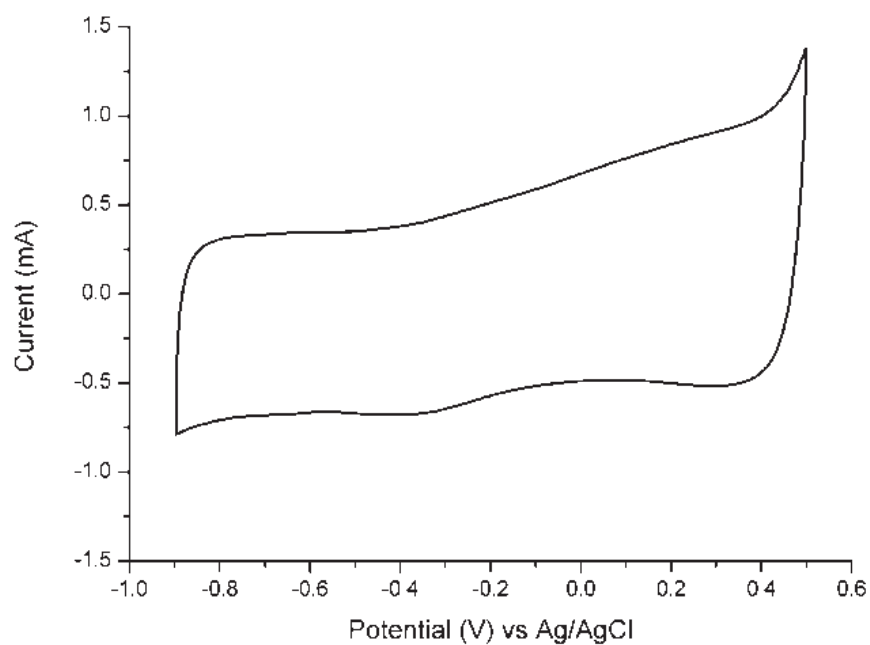


Figure 3.9. Cyclic voltammogram (3rd cycle) of $W_{0.75}(N,O)$ in 1M $CaCl_2$ electrolyte at the scan rate of 5 mV s^{-1} .

In order to investigate the charge storage mechanism of tungsten oxynitride, the material is tested in 1M KOH electrolyte, as reported in the literature [40, 41], in the potential range between -1.1 V and -0.3 V. As a result, a nearly ideal, rectangular shape of the CV curves is observed, similar to the behaviour previously observed in 1M KOH electrolyte in the same potential window [40, 41], and a capacitance value of 57 F g^{-1} is reached at the current load of 0.5 A g^{-1} . The difference between the measured specific capacitance and the 30 F g^{-1} , as well as the 100 F g^{-1} reported for WN [41] and W_2N [40] phases, respectively, could result from the difference in the stoichiometry and the nature of crystalline phases, since the surface areas of the synthesised tungsten oxynitride and the compounds reported in the literature are similar. The main charge storage mechanism of tungsten nitrides has previously been attributed to EDLC [40, 41], however, when evaluating the specific capacitance values per electrode area, $\sim 200 \mu\text{F cm}^{-2}$ and $\sim 136 \mu\text{F cm}^{-2}$ are estimated in 1M H_2SO_4 and 1M KOH electrolytes, respectively. The calculated specific capacitance values are an order of magnitude higher when compared to the values expected for the EDLC mechanism, typically between $20\text{-}50 \mu\text{F cm}^{-2}$ [61, 62]. It could therefore be concluded that for tungsten oxynitride, a pseudocapacitive charge storage process is present in addition to the formation of the electric double-layer. Similar observations have been made by Thompson *et al.* [36].

In order to investigate the nature of the charge storage mechanism of $\text{W}_{0.75}(\text{N},\text{O})$ in more detail, two pseudocapacitive processes are evaluated as possibly applicable to tungsten oxynitride: pseudocapacitive ion/proton adsorption [71, 79] and ion/proton intercalation [75-77], previously reported for MnO_2 . For this extensively investigated material, the pseudocapacitive ion/proton intercalation is accompanied by the expansion and shrinkage of the crystal lattice, visible from the reversible shifts of the diffraction peaks when comparing the XRD patterns of the charged and discharged electrodes. In fact, ion intercalation into crystalline MnO_2 results in the reversible shift of XRD peaks [75, 146]. In order to evaluate ion/proton intercalations as a possible charge storage mechanism, XRD patterns of the charged and discharged tungsten oxynitride electrodes in 1M H_2SO_4 and

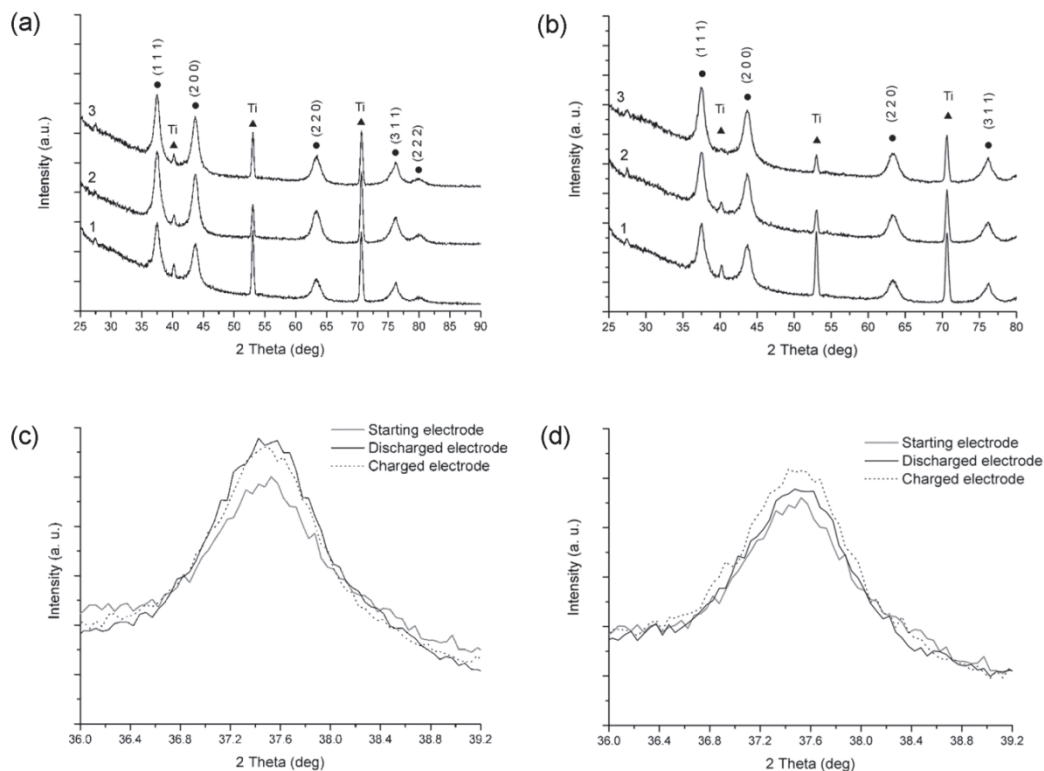


Figure 3.10. (a, b) XRD patterns of the starting tungsten oxynitride electrode (pattern 1), as well as discharged (pattern 2) and charged (pattern 3) electrodes in 1M H₂SO₄ (a) and 3M KCl electrolytes (b). The difference in the relative intensities between the spectra 1, 2 and 3 could result from variations of the sample thickness. The magnified (1 1 1) diffraction peaks for 1M H₂SO₄ and 3M KCl electrolytes are presented in figures c and d, respectively. The symbol “●” represents characteristic peaks of tungsten oxynitride, while peaks of the Ti current collector are denoted with “▲”.

3M KCl electrolytes are compared (Figure 3.10). The measured XRD patterns (Figure 3.9), however, did not show any changes in peak positions or in the full widths at half maximums (FWHM) for the most intense (1 1 1) diffraction peak (Figure 3.10 c, d), as well as for (200), (220) and (311) peaks (Figure 3.11). Furthermore, no loss in the crystallinity could be detected. It is therefore concluded, from the absence of changes in the XRD patterns, that no bulk intercalation takes place. The pseudocapacitive cation adsorption on the surface is therefore a possible charge storage mechanism for tungsten oxynitride, as it does not involve the bulk of the material, in agreement with the observed XRD data.

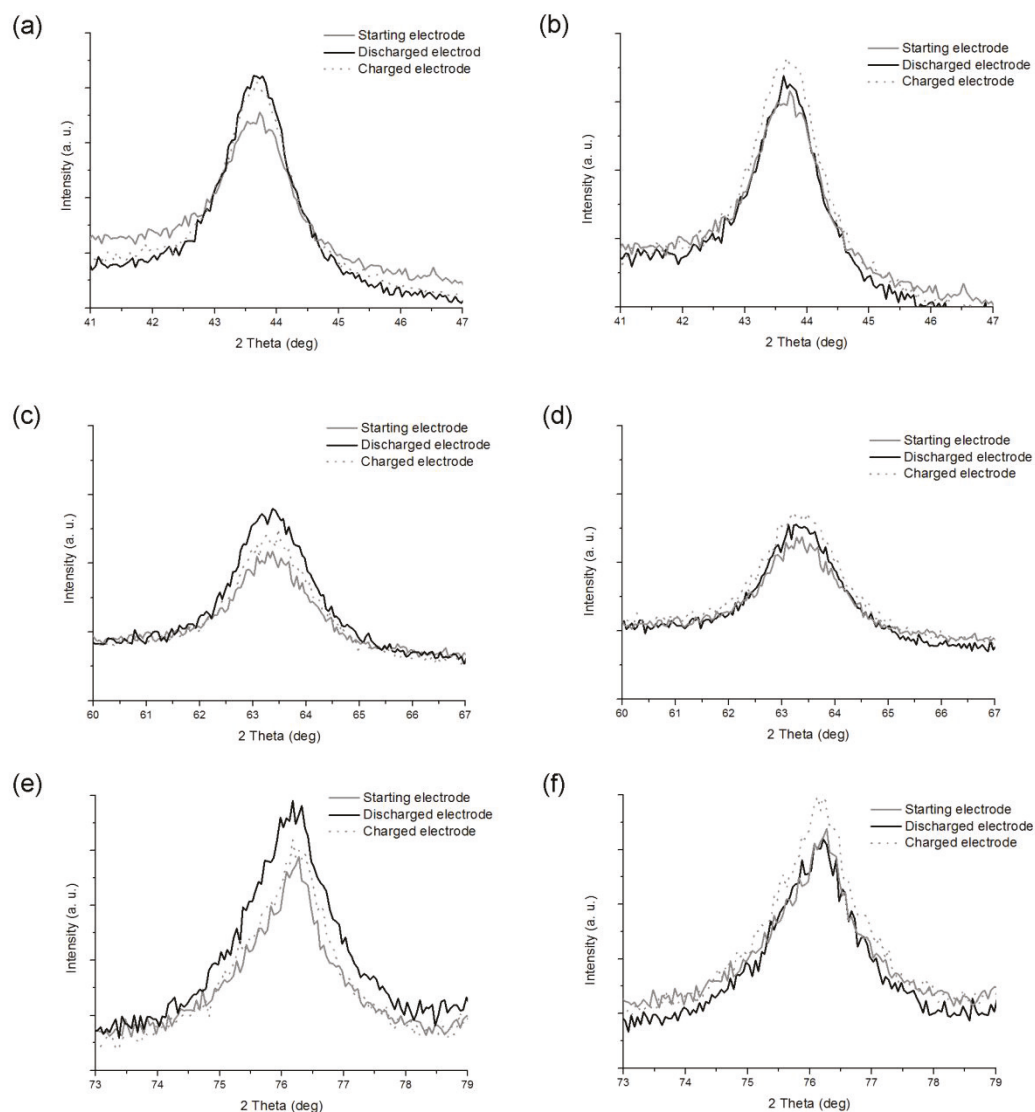


Figure 3.11. The magnified (200) (a, b), (220) (c, d) and (311) (e, f) diffraction peaks for 1M H₂SO₄ (a, c, e) and 3M KCl (b, d, e) electrolytes.

Finally, the cyclic stability of tungsten oxynitride is tested in three different electrolytes: 1M H₂SO₄, 3M NaCl and 1M KOH by performing multiple galvanostatic charge and discharge cycles at the current load of 0.5 A g⁻¹ (Figure 3.12) and recording cyclic voltammograms at the scan rate of 5 mV s⁻¹ after a specific number of cycles (Figure 3.12, inserts). In 1M H₂SO₄ electrolyte, the distortion of the CV curves is observed after 200 galvanostatic charge and discharge cycles (Figure 3.12 a, insert), accompanied by a loss of the electrochemical reversibility (Figure 3.12 a).

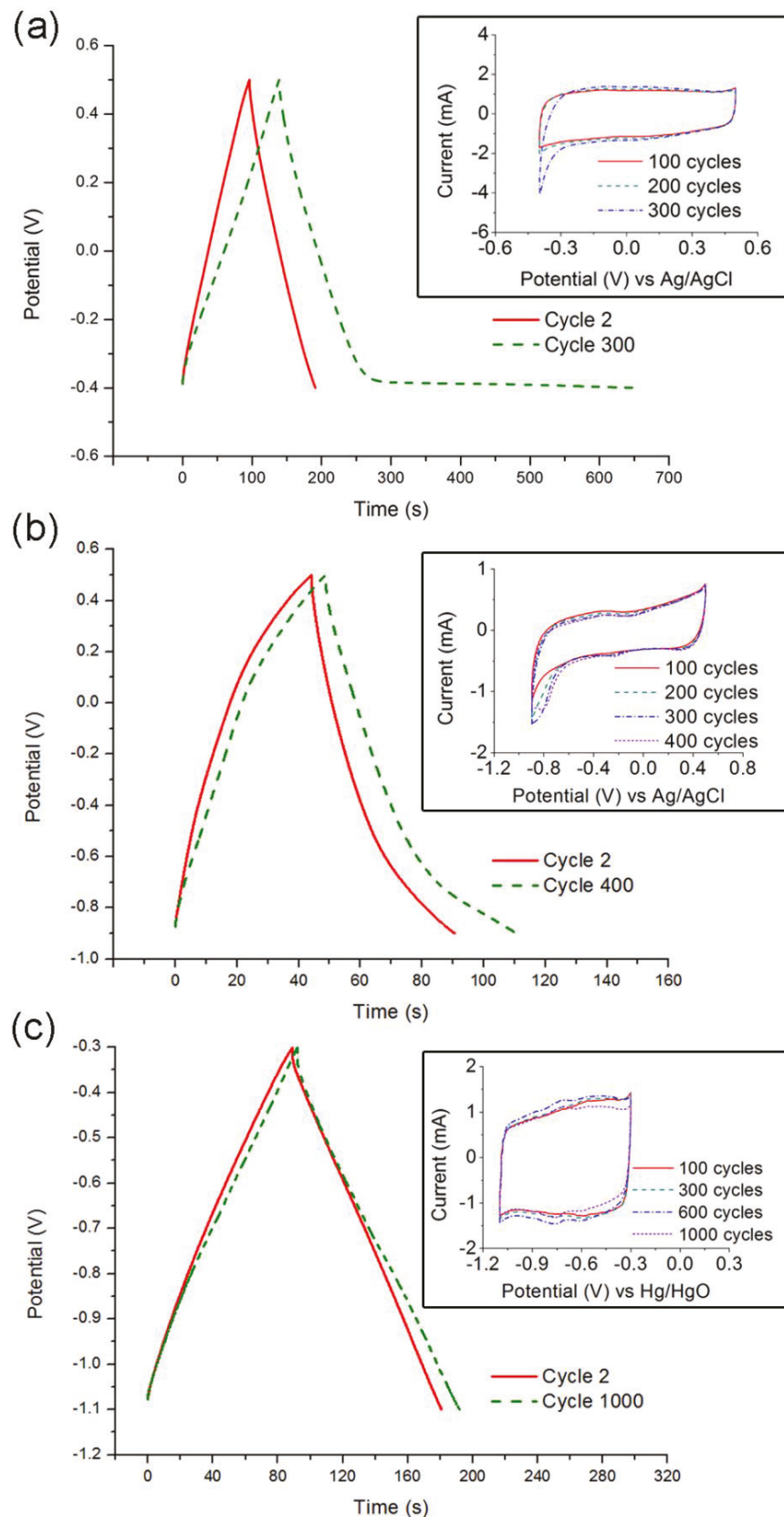


Figure 3.12. Cyclic stability of tungsten oxynitride: galvanostatic charge/discharge curves measured for the 2nd and 300th cycles in 1M H₂SO₄ (a), the 2nd and 400th cycles in 3M NaCl (b) and the 2nd and 1000th cycles in 1M KOH electrolytes (c). CV curves measured after selected cycles are presented in inserts.

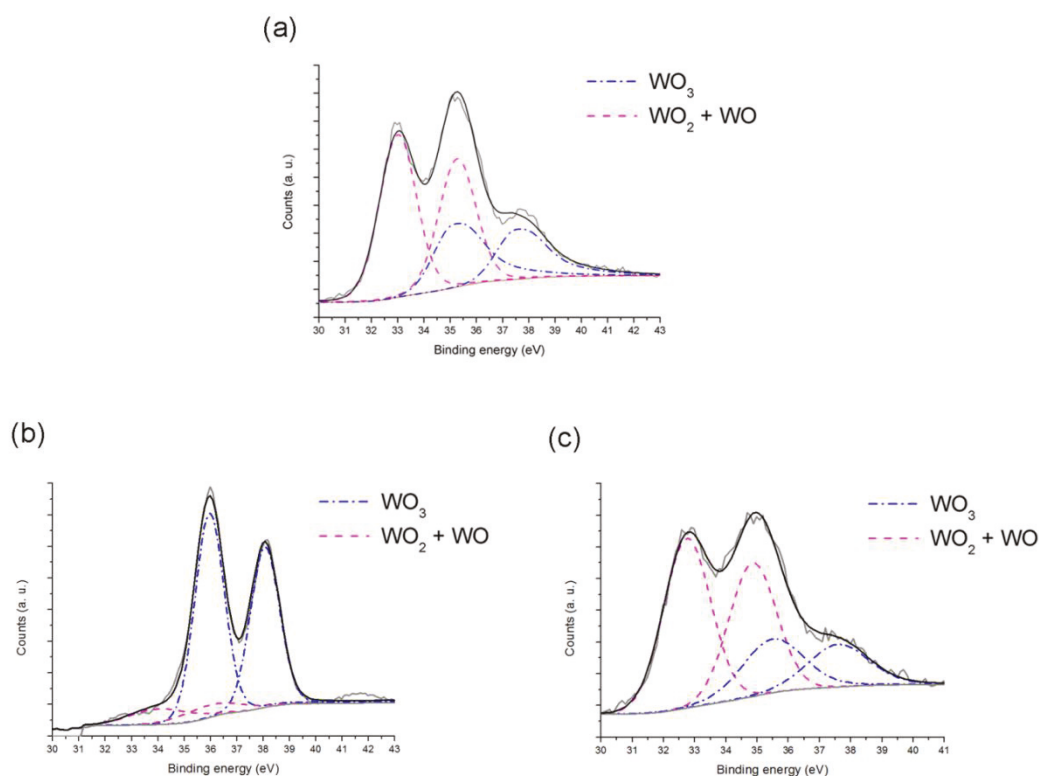


Figure 3.13. XPS spectra deconvoluted peaks of W 4f core levels for tungsten oxynitride as-prepared electrode (a) and after multiple (> 160) galvanostatic charge and discharge cycles in 1M H_2SO_4 (b) and 1M KOH (c) electrolytes.

A faster degradation of the reversibility is observed in 3M NaCl electrolyte (Figure 3.12 b). In 1M KOH, however, tungsten oxynitride demonstrates a reasonable stability and only minor increases in specific capacitance values (1 % and 9 %, respectively) could be measured between the first and the 1000th cycle from the galvanostatic charge and discharge curves (Figure 3.12 c).

In order to investigate the cyclic stability of tungsten oxynitride in more detail, XPS spectra of tungsten oxynitride electrodes are compared before and after testing for multiple (>160) galvanostatic charge and discharge cycles in 1M H_2SO_4 and 1M KOH electrolytes in order to evaluate changes in the surface characteristics of the samples (Figure 3.13). The cycling was stopped when the discharge curves in 1M H_2SO_4 electrolyte became asymmetric. The W 4f spectrum of the as-prepared electrode (Figure 3.13 a) could be deconvoluted into four components, with two sets of core levels, based on the previously reported

data [90]. The first doublet, with binding energies of 36.98 and 35.08 eV, is characteristic of WO_3 species, while the second doublet, with binding energies of 35.04 and 32.96 eV, could be attributed to the mixed WO_2 and WO phase [90, 147, 148]. XPS analysis reveals that the synthesised oxynitride is possibly covered with a passivating layer composed of a mixture of tungsten oxides. This layer is not visible on the TEM images (Figure 3.4) and could therefore be very thin. No peaks corresponding to the mixed nitride species $\text{W}_2\text{N} + \text{WN}$, with binding energies of 34.2 and 32.0 eV, could be detected, in agreement with literature, where Ar^+ sputtering has been used to remove the surface oxide layer in order to reveal these mixed nitride phases [90, 147].

When compared to the as-prepared sample, XPS of tungsten oxynitride electrodes cycled in 1M KOH electrolyte present no visible changes (Figure 3.13 c), as opposed to electrodes cycled in 1M H_2SO_4 electrolyte, where an increase in the intensity of peaks corresponding to WO_3 species is observed (Figure 3.13 b). It could therefore be concluded that the poor stability of tungsten oxynitride electrodes in 1M H_2SO_4 electrolyte could result from the progressive oxidation of the material. In 1M KOH electrolyte, however, the surface composition of tungsten oxynitride remains nearly unchanged. This is in agreement with the observation by Thompson *et al.*, where the highest stability of VN and W_2N in alkaline electrolytes has been reported [36].

3.4 Conclusions

In this chapter, tungsten oxynitride is synthesised by a temperature-programmed reduction and extensively characterised by SEM, low temperature N_2 adsorption, XRD, TEM, EELS and XPS. The analysis reveals that the synthesised material is mesoporous, and its phase is assigned to $\text{W}_{0.75}(\text{N},\text{O})$, as a closest match, according to the XRD and EELS data. The specific surface area of tungsten oxynitride is $42 \text{ m}^2 \text{ g}^{-1}$ and the maximum of the pore size distribution is centred around 5 nm. The surface of tungsten oxynitride is possibly covered with a very thin, nitrogen-poor passivating layer, composed of WO_3 and $\text{WO}_2 + \text{WO}$ tungsten oxide species.

Electrochemical characterisation of tungsten oxynitride is performed in the acid, alkaline and a range of neutral aqueous electrolytes containing alkaline and alkaline-earth metal cations: 1M H₂SO₄, 1M KOH, 3M KCl, 3M NaCl, 1M LiCl and 1M CaCl₂. The specific capacitances of 85 F g⁻¹ and 57 F g⁻¹ are measured in 1M H₂SO₄ and 1M KOH electrolytes, respectively, and nearly ideal, rectangular shapes of the CV curves are observed. In neutral electrolytes containing alkaline and alkaline-earth metal cations, the specific capacitance values, as well as the shapes of cyclic voltammetry curves are dependent on the presence of particular cations. Based on the measured specific capacitance values per electrode area, it is concluded that a pseudocapacitive charge storage mechanism exists in addition to the formation of the electric double-layer.

In order to investigate the charge storage mechanism of tungsten oxynitride in more detail, two pseudocapacitive processes, previously proposed for MnO₂, are evaluated: ion/proton adsorption and ion/proton intercalation into the crystal lattice. Based on the XRD characterisation of the charged and discharged samples, no bulk intercalation could be detected. It is therefore concluded that the possible charge storage mechanism is the pseudocapacitive ion/proton adsorption.

Cyclic stability of tungsten oxynitride is evaluated in 1M H₂SO₄, 3M NaCl and 1M KOH electrolytes and the highest stability is observed in 1M KOH, while a loss of reversibility is observed in 1M H₂SO₄ and 3M NaCl. Additionally, XPS spectra of the as-prepared electrodes are compared to the electrode cycled in 1M H₂SO₄ and 1M KOH solutions after multiple cycles. Cycling in 1M H₂SO₄ results in the progressive oxidation of tungsten oxynitride, revealed by an increase of the WO₃/WO₂ + WO ratio on the surface, while in 1M KOH, the surface composition remains nearly unchanged.

Chapter 4. Structure and electrochemical capacitance of bimetallic molybdenum tungsten oxynitride

4.1 Introduction

Rate capability is an important performance criterion of supercapacitors, as it determines its ability to work at high charge and discharge currents. This property is particularly useful for high power applications in the transport, residential, telecommunication and consumer electronics sectors [11, 59, 68]. Transition metal nitrides and oxynitrides, possessing pseudocapacitive charge storage properties, have demonstrated good rate capabilities due to their high intrinsic conductivities [23, 149], as opposed to many transition metal oxides.

It has previously been reported that the transition metal in the nitrides and oxynitride compounds could be partially substituted by another metal. As a result, bimetallic compounds with altered physico-chemical properties are produced [86-88]. It has been observed, for instance, that catalytic properties of the bimetallic catalysts, obtained by the addition of second metals such as Ti, Ce, Zr or Co in the crystal lattice of molybdenum nitride, are improved when compared to the performance of the pure γ -Mo₂N [86]. Additionally, vanadium molybdenum oxynitride V_{2.0}Mo_{1.0}O_{1.7}N_{2.4} has demonstrated a higher specific surface area when compared to the monometallic VN and Mo₂N, as well as a higher catalytic performance (normalised to the surface area) [88]. In supercapacitors, however, research has been almost exclusively focused on monometallic nitride and oxynitride compounds. Data exist on the γ -Mo₂N and Co₃Mo₃N “composite material”, which has shown higher specific capacitance values, as well as an improved cyclic stability in 3.5M H₂SO₄ electrolyte when compared to the pure γ -

Mo₂N [89]. Electrochemical properties of pure bimetallic compounds have, however, have not been studied.

In this chapter, bimetallic molybdenum tungsten oxynitride is synthesised by a solid state route, similar to the method reported by Yu and Oyama [88]. The synthesised material is characterised by a low temperature N₂ adsorption, XRD, SEM, TEM and EELS, and its electrochemical properties are tested in 1M H₂SO₄ electrolyte in the three-electrode, as well as the symmetric cell setup. The electrochemical performance of the bimetallic compound is evaluated by cyclic voltammetry, galvanostatic charge and discharge, as well as electrochemical impedance spectroscopy (EIS) measurements, and compared to the performance of the monometallic molybdenum and tungsten oxynitrides.

4.2 Experimental

Molybdenum tungsten oxynitride was synthesised by a temperature-programmed reduction of the bimetallic oxide precursor. 13.5 g of WO₃ (Sigma-Aldrich, 95410) and MoO₃ (Sigma-Aldrich, 267856), mixed in 1:1 ratio, were loaded inside a planetary mill (Fritsch Pulverisette 5) with steel balls (20 mm diameter, 1:20 powder to ball ratio) and milled for 50 hours with the rotor speed set to 150 rpm in order to achieve a highly homogenous mixture. The milled powder was subsequently pressed into pellets under the pressure load of 8 tonnes using a dye with a 13 mm diameter. Pellets were annealed at 785 °C during 6 hours in a horizontal tube furnace with open ends (Tetlow Kilns & Furnaces Pty Ltd, Australia) inside an alumina crucible. After cooling down to the room temperature naturally, pellets were crushed into powder with an agate mortar and placed in the same furnace under the ammonia flow. Temperature-programmed reduction of the mixed oxide precursor was performed by heating the furnace to ~ 700 °C with the heating rate of 5 °C min⁻¹, keeping that temperature for 3 hours and cooling down to the room temperature naturally, with the ammonia flow fixed to 0.4 l min⁻¹ throughout the procedure. Prior to exposure to the ambient air, samples were passivated with a flow of a special gas mixture (Ar + 0.1 vol.% O₂) during 1 hour at the flow rate of 0.5 l min⁻¹. Monometallic molybdenum and tungsten oxynitrides were synthesised by a temperature-programmed reduction from the

pure MoO₃ (Sigma-Aldrich, 267856) and WO₃ (Sigma-Aldrich, 95410) precursors, respectively, in the similar TPR conditions, with the maximum operating temperature of 700 °C. The detailed synthesis procedures for these compounds are described elsewhere [126, 127, 150]. For simplicity, the synthesised materials are denoted as MoW(N,O), Mo(N,O) and W(N,O).

The synthesised bimetallic oxynitride was extensively characterised by SEM, low temperature N₂ adsorption, XRD and TEM. In order to perform the electrochemical testing, electrodes were prepared by mixing active materials with carbon nanopowder and PVDF in a 90:5:5 weight ratio using NMP as a solvent. The slurry was subsequently coated onto Ti foils and dried overnight in a conventional oven at 90 °C in vacuum. For the three-electrode cell setup, Ag/AgCl reference electrodes, as well as a Pt wire as a counter-electrode were used. Symmetric cells, emulating the design of a real supercapacitor device, were assembled by separating two nearly identical electrodes by a microporous polyethylene film (MTI Corp., USA). All cells were filled with 1M H₂SO₄ electrolyte under vacuum. Electrochemical performance was evaluated with the cyclic voltammetry, galvanostatic charge and discharge, as well as electrochemical impedance spectroscopy measurements.

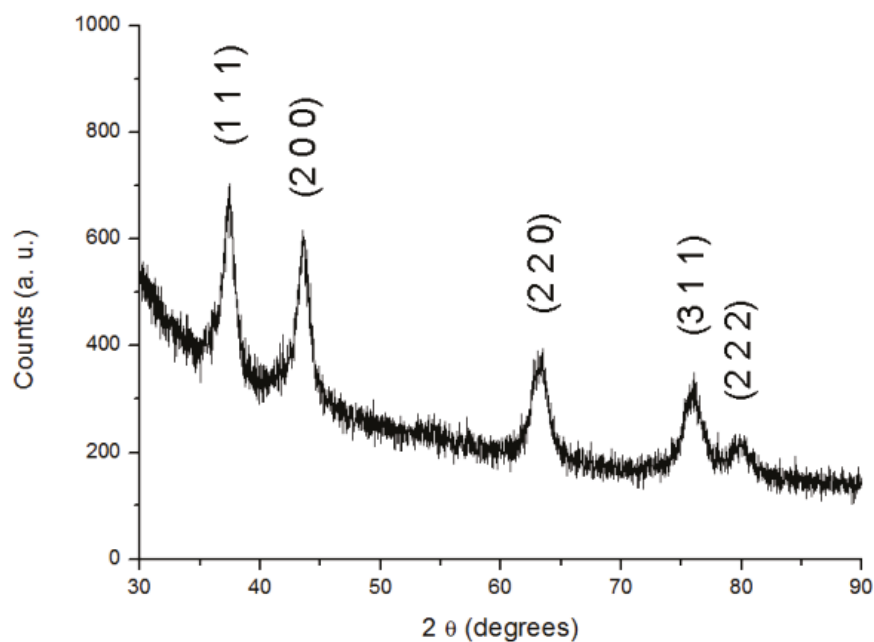


Figure 4.1. XRD pattern of the synthesised molybdenum tungsten oxynitride.

4.3 Structure and electrochemical properties of MoW(N,O)

The diffraction pattern of the bimetallic molybdenum tungsten oxynitride, revealed with the X-ray analysis (Figure 4.1), presents five peaks at $2\theta = 37.4^\circ$, 43.3° , 63.0° , 75.9° and 80.0° . The measured XRD pattern matches diffraction lines of $\text{MoWN}_{2.1}\text{O}_{2.4}$ (Powder Diffraction File #: 50-0134). The synthesised compound has a cubic structure and a small crystalline size, observed from the broadening of the diffraction peaks, in agreement with the previously reported data [87].

The surface area and pore size distribution of molybdenum tungsten oxynitride are measured with the low temperature N_2 adsorption (Figure 4.2). The isotherm corresponds to type IV and presents a hysteresis loop (Figure 4.2 a), indicating a porous nature of the solid. The surface area of $72.6 \text{ m}^2 \text{ g}^{-1}$ ($\pm 0.3347 \text{ m}^2 \text{ g}^{-1}$) is measured with BET method [137]. The pore size distribution, depicted on figure

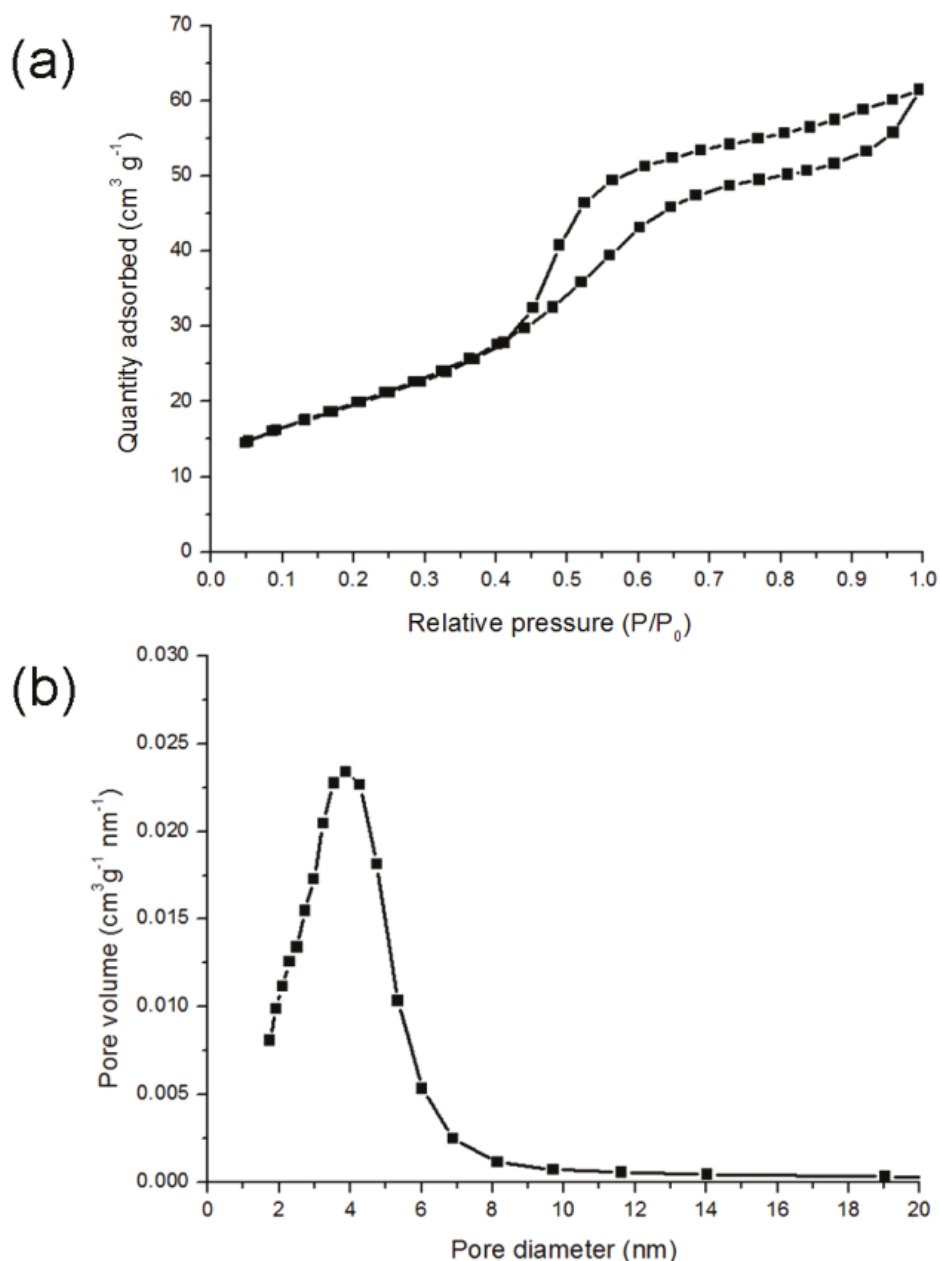


Figure 4.2. Low temperature N₂ adsorption-desorption isotherm (a) and pore size distribution (b) of MoW(N,O).

4.2 b, reveals that the material is mesoporous (pore diameters between 2 and 50 nm), with the maximum of the distribution centred around 4 nm. Further morphological characterisation of the synthesised material (Figure 4.3) confirms the porosity of the material, with surface pores of less than 10 nm diameter visible on the high resolution SEM image (Figure 4.3 b). Low resolution SEM image (Figure 4.3 a) shows that the synthesised dark grey powder consists of particles with sizes of approximately 1 μm .

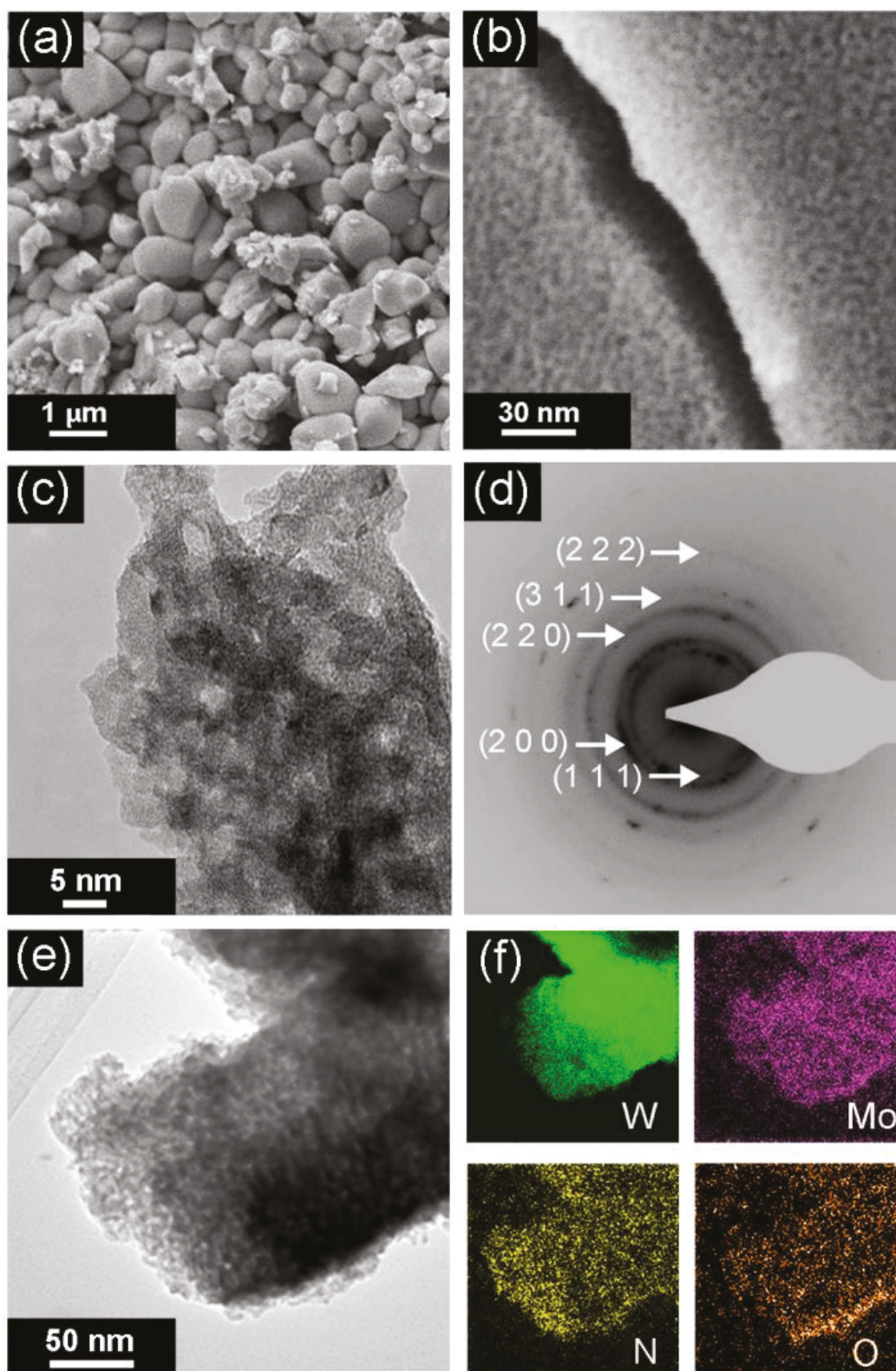


Figure 4.3. Low (a) and high (b) magnification SEM images; bright field TEM image (c) and electron diffraction pattern (d); EFTEM maps of Mo, W, N and O elements (f) and the corresponding TEM image (e).

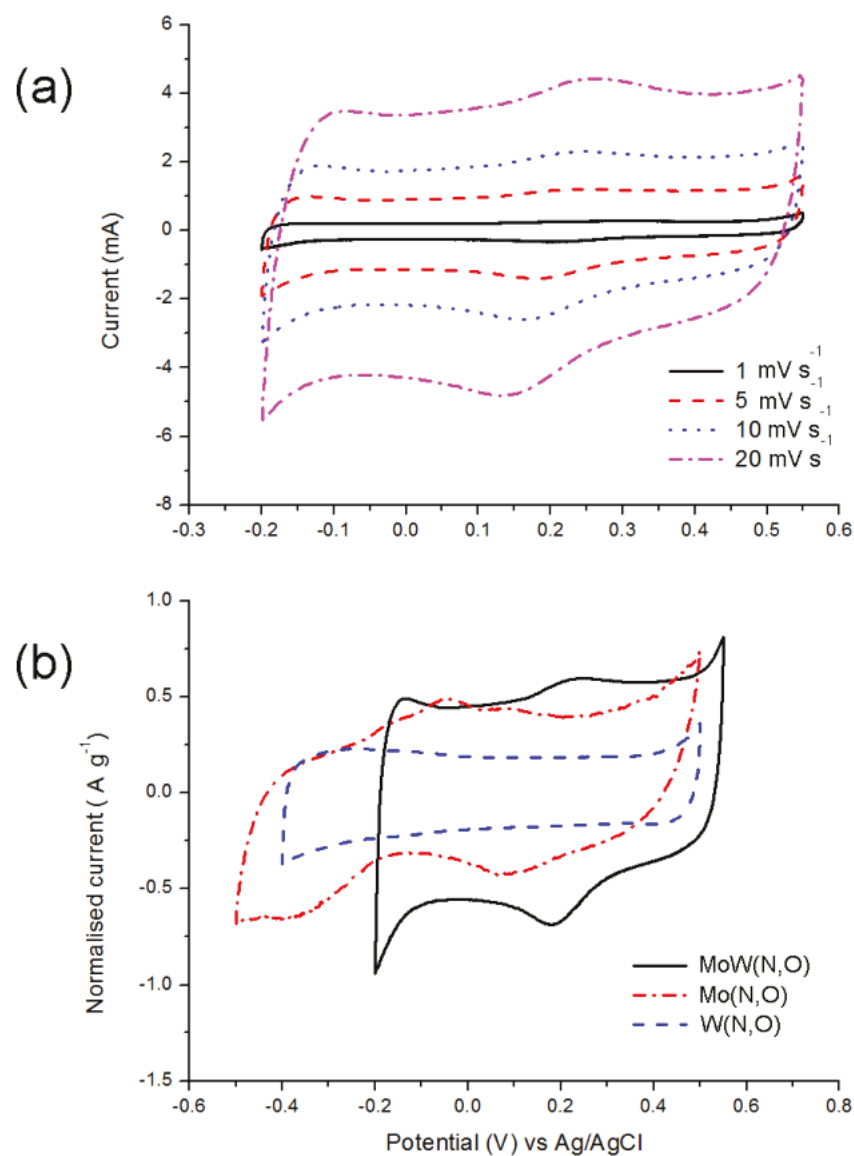


Figure 4.4. CV curves of MoW(N,O) in 1M H₂SO₄ electrolyte (a) and CV curve of MoW(N,O) compared to CV curves of Mo(N,O) and W(N,O), normalised to the weight, at the scan rate of 5 mV s⁻¹ (b).

TEM characterisation reveals the nanocrystalline nature of the synthesised material (Figure 4.3 c, e). The electron diffraction pattern, depicted on figure 4.3 d, presents five rings and is in agreement with the XRD data (Figure 4.1). EFTEM maps of Mo, W, N and O elements show that the elements are distributed throughout the sample (Figure 4.3 f).

Cyclic voltammetry curves of molybdenum tungsten oxynitride in 1M H₂SO₄ electrolyte possess nearly ideal, rectangular shapes, indicating good capacitive properties of the material (Figure 4.4 a). Two reversible redox peaks could be

observed on top of the CV curves, typical for the compounds possessing pseudocapacitive properties. The nearly rectangular shape of the CVs is preserved at the scan rates as high as 100 mV s^{-1} . The operating voltage window of MoW(N,O) is between -0.2 and $0.55 \text{ V vs. Ag/AgCl}$ in $1\text{M H}_2\text{SO}_4$ electrolyte. When comparing CV curves of MoW(N,O), Mo(N,O) and W(N,O), normalised to the weight of the active materials, at the scan rate of 5 mV s^{-1} (Figure 4.4 b), it can be observed that the shape of the cyclic voltammogram of MoW(N,O), as well as its operating voltage window, differ from both monometallic compounds. For instance, W(N,O) presents an ideal, rectangular shape of the CV curve and an operating voltage window between -0.4 and $0.5 \text{ V vs. Ag/AgCl}$, while Mo(N,O), operating between -0.5 and 0.5 V , shows a less rectangular curve with multiple redox peaks.

Galvanostatic charge and discharge curves of MoW(N,O) possess rectangular shapes, with small IR drops observed upon inverting the current at high scan rates (Figure 4.5 a). The maximum specific capacitance of 124 F g^{-1} ($172 \text{ }\mu\text{F cm}^{-2}$), measured at the current load of 0.05 A g^{-1} , indicates the presence of a pseudocapacitive charge storage mechanism in addition to the electric double layer. The bimetallic oxynitride demonstrates a very good rate capability, with 43% of the initial capacitance retention upon increasing the current load from 0.05 to 20 A g^{-1} (400-fold). Furthermore, at the same charge-discharge current densities, the bimetallic compound possesses higher specific capacitance values as well as a better rate capability when compared to both monometallic oxynitrides (Figure 4.5 b). In fact, when comparing specific capacitances at a high current load of 10 A g^{-1} , MoW(N,O), W(N,O) and Mo(N,O) show capacitance values of 67 F g^{-1} , 33 F g^{-1} and 2 F g^{-1} respectively, with the highest initial capacitance retention observed for MoW(N,O).

In order to investigate the difference in the electrochemical performance between MoW(N,O), Mo(N,O) and W(N,O) in more detail, electrochemical impedance spectroscopy measurements are performed for these compounds in the symmetric cell setup. Electrodes with nearly identical weights are selected for comparison. Nyquist plots of the impedance spectra measured for MoW(N,O), Mo(N,O) and W(N,O) (Figure 4.6) present depressed semi-circles at high frequencies,

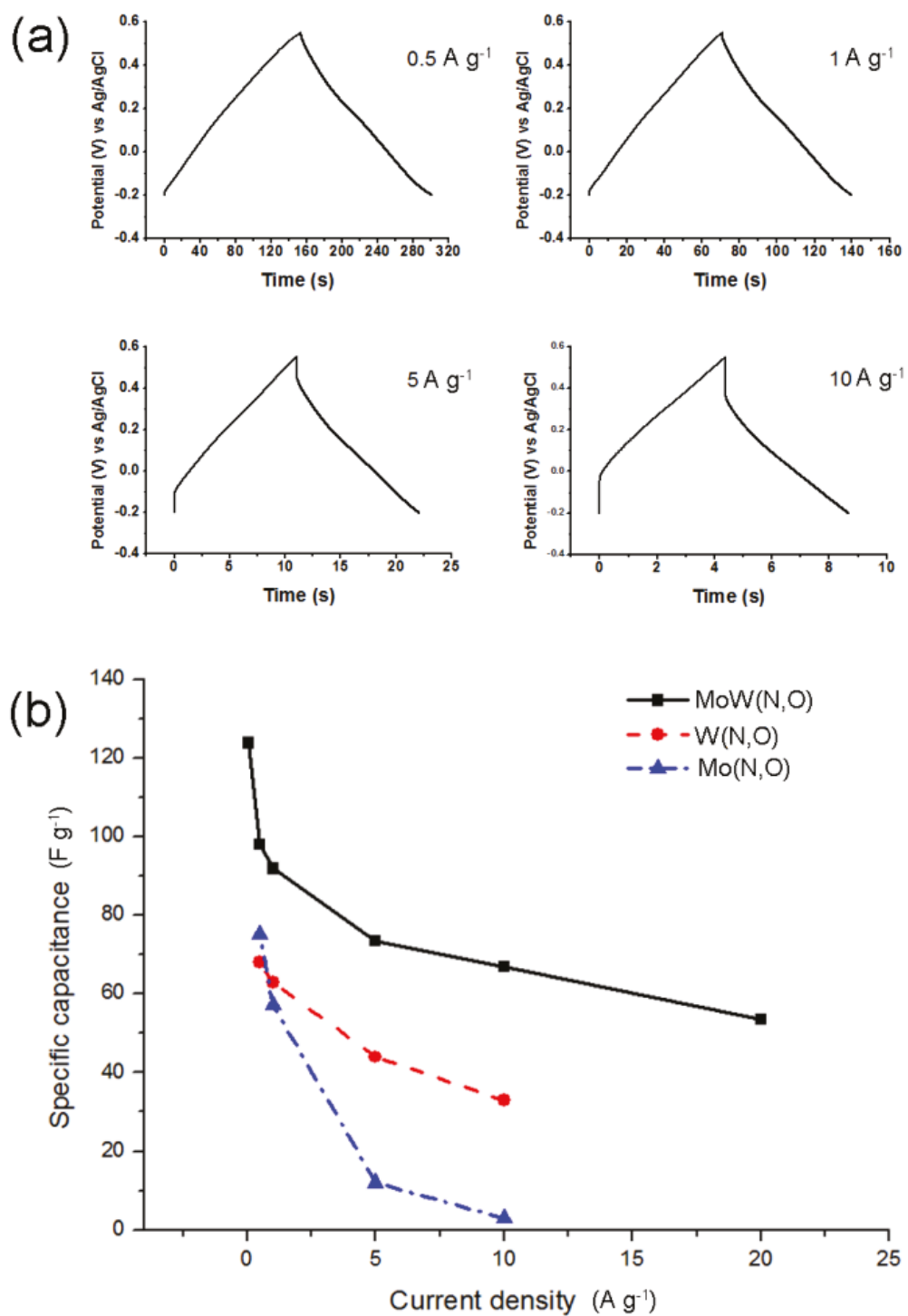


Figure 4.5. Galvanostatic charge and discharge curves of MoW(N,O) (a) and comparison of rate capabilities of MoW(N,O), Mo(N,O) and W(N,O) (b) in 1M H₂SO₄ electrolyte.

characteristic of charge transfer resistances and the double layer charging on the electrode surface, followed by inclined straight lines at lower frequencies, characteristic of the Warburg region [144, 151-153].

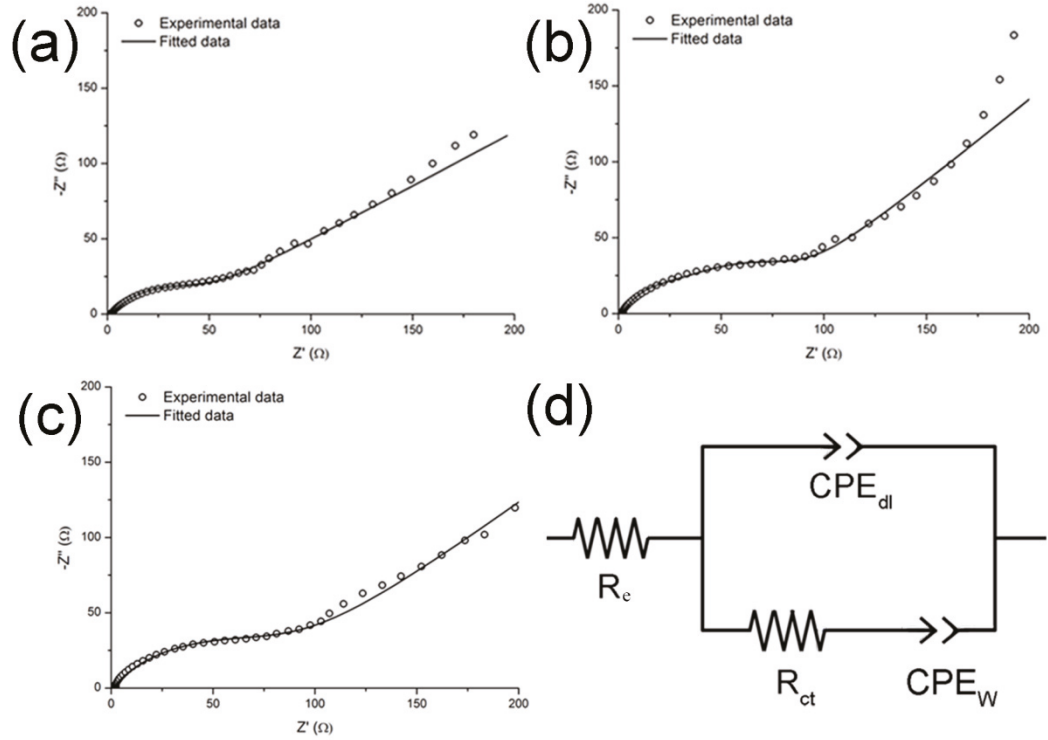


Figure 4.6. Electrochemical impedance spectroscopy measurements: Nyquist plots for MoW(N,O) (a), W(N,O) (b) and Mo(N,O) (c), as well as the equivalent circuit (d) used to fit the data.

In order to compare data in the medium-high frequency range, impedance spectra are modelled with Randles-type equivalent circuit (Figure 4.6 d), where R_e represents the resistance of the electrolyte, R_{ct} represents the charge transfer resistance and CPE_{dl} and CPE_W are constant phase elements used to model the double layer capacitance and diffusion impedance, respectively, in porous samples [144, 154, 155]. The equivalent circuit provides a good fit of the experimental data in the medium-high frequency range (Figures 4.6 a-c).

The impedance of the constant phase element is described with a formula [144, 151] :

$$Z_{CPE} = \frac{1}{Y_0(j\omega)^\alpha} \quad (4.1)$$

Y_0 is the admittance, j is the imaginary unit, ω is the modulation frequency and α is a dimensionless coefficient. When $\alpha=1$, Z_{CPE} represents an ideal capacitor, while at $\alpha=0.5$, a transmission line behaviour is observed, representing the mass

transport impedance in the pores [144, 151, 154, 155]. The impedance data for MoW(N,O), Mo(N,O) and W(N,O) are summarised in the Table 4.1.

Table 4.1 Fitted impedance data modelled with Randles-type equivalent circuit (Figure 4.6 d).

Sample	R_e (Ω)	R_{ct} (Ω)	R_w (Ω)/ α (-)	C_{dl} (F)/ α (-)
MoW(N,O)	1.6	60.5	111/ 0.46	0.00059/ 0.61
Mo(N,O)	1.0	90.8	141/ 0.50	0.00039/ 0.68
W(N,O)	1.2	101.3	118/ 0.58	0.00056/ 0.66

It can be observed from the modelled data (Table 4.1) that MoW(N,O) has a lowest R_{ct} value when compared to monometallic oxynitrides. R_{ct} is the charge transfer resistance, which is determined by the rate of electrons transfer towards the electrode/electrolyte interface, and represents intrinsic properties of the electrode such as, for example, its conductivity [144, 151-153]. The lowest R_{ct} value for MoW(N,O) could indicate its higher intrinsic conductivity when compared to the monometallic compounds and could explain the superior rate capability of the bimetallic compound (Figure 4.5 b).

Cyclic stability of molybdenum tungsten oxynitride is evaluated in 1M H_2SO_4 electrolyte during 5000 galvanostatic charge and discharge cycles at the current load of 5 A g^{-1} (Figure 4.7). The bimetallic compound demonstrates approximately 46 % of the starting capacitance retention after 5000 cycles. A larger IR drop observed in the galvanostatic charge and discharge curves after 5000 cycles (Figure 4.7, insert) could result from the progressive oxidation of the surface.

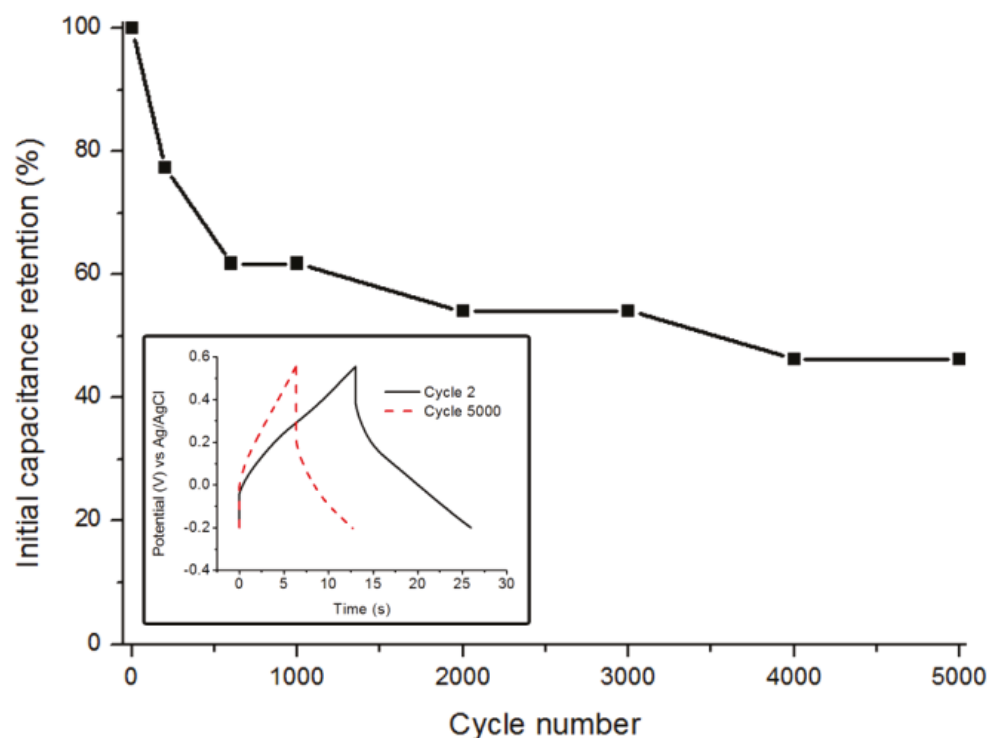


Figure 4.7. Cyclic stability of MoW(N,O) measured at the current load of 5 A g^{-1} . Galvanostatic charge and discharge curves in $1 \text{ M H}_2\text{SO}_4$ electrolyte (insert).

Finally, electrochemical properties of MoW(N,O) are investigated in a symmetric cell setup, emulating an accepted design of a real supercapacitor device (Figure 4.8) [11, 58, 68]. CV curves of the symmetric cell demonstrate ideal rectangular shapes with no redox peaks visible (Figure 4.8 a), in the operating potential range between 0 and 0.75 V in $1 \text{ M H}_2\text{SO}_4$ electrolyte. Galvanostatic charge and discharge curves have, similar to the three electrode setup, triangular shapes (Figure 4.8 b), with a small IR drop visible at the current load of 10 A g^{-1} . The maximum specific capacitance of 23 F g^{-1} is measured at 0.05 A g^{-1} . MoW(N,O) in a symmetric cell setup demonstrates a good rate capability, with approximately 50 % of the initial capacitance retention upon increasing the current load 400-fold from 0.05 to 20 A g^{-1} (Figure 4.8 c).

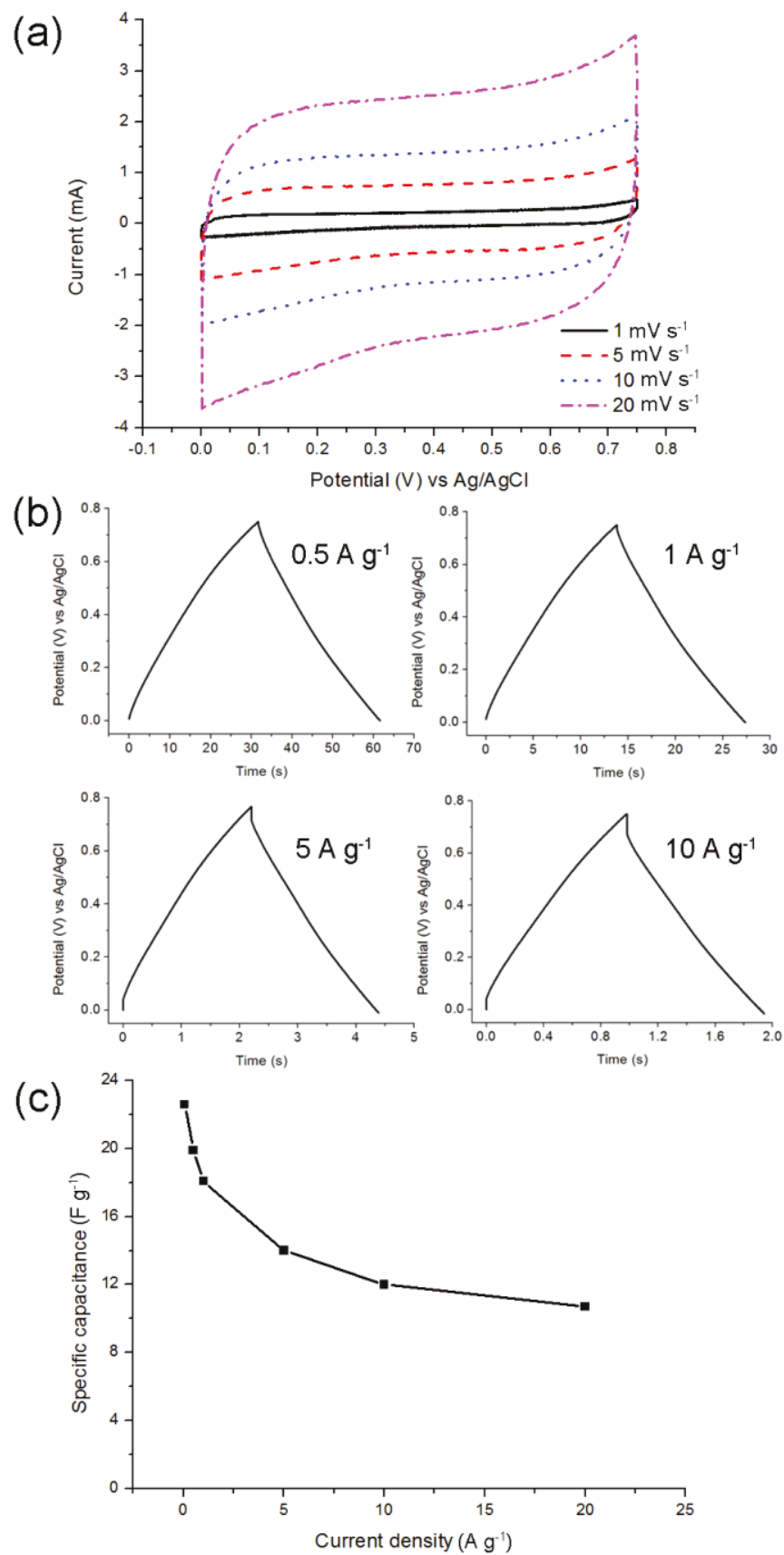


Figure 4.8. MoW(N₂O) in a symmetric cell: CV curves (a), galvanostatic charge/ discharge curves (b) and rate capability (c).

4.4 Conclusions

Molybdenum tungsten oxynitride is synthesised by a temperature-programmed reduction of a bimetallic precursor, prepared by ball milling and annealing the mixture of monometallic molybdenum and tungsten oxides. The product is extensively characterised by XRD, low temperature N₂ adsorption, SEM and TEM. The synthesised material is mesoporous and nanocrystalline, with the surface area of 72.6 m² g⁻¹. The XRD pattern of the compound matches the diffraction lines of MoWN_{2.1}O_{2.4} with cubic crystal structure, and EFTEM map show that W, Mo, N and O elements are distributed throughout the sample.

Electrochemical characterisation of bimetallic molybdenum tungsten oxynitride reveals nearly ideal, rectangular and triangular shapes of CVs and galvanostatic charge and discharge curves, respectively, indicating a good capacitive behaviour. The maximum specific capacitance, measured at 0.05 A g⁻¹ in 1M H₂SO₄ electrolyte, is 124 F g⁻¹, and 43 % of this value is maintained upon a 400-fold increase of the current load. MoW(N,O) demonstrates a superior rate capability when compared to monometallic Mo(N,O) and W(N,O) compounds, possibly due to the higher intrinsic electronic conductivity, as revealed by EIS measurements. Furthermore, its shape of the cyclic voltammogram, as well as the operating potential window in 1M H₂SO₄ electrolyte differs from the monometallic compounds. When assembled in a symmetric cell setup, molybdenum tungsten oxynitride electrodes show nearly ideal rectangular shapes of the CV and a high rate capability, with approximately 50 % of the initial capacitance retention upon increasing the current load from 0.05 to 20 A g⁻¹. Cyclic stability measurements indicate approximately 46 % of the capacitance retention after 5000 galvanostatic charge and discharge cycles, performed at the current load of 5 A g⁻¹ in 1M H₂SO₄ electrolyte.

Chapter 5. Ageing of molybdenum and tungsten oxynitrides and its influence on the electrochemical capacitance

5.1 Introduction

In supercapacitors, pseudocapacitive charge storage mechanisms often involve surface or sub-surface layers of the active materials. For instance, it has been proposed that the charge storage mechanism of nanocrystalline vanadium nitride is attributed to the presence of oxides on its surface, interacting with OH^- ions in alkaline electrolytes via the combination of the electrical double-layer and pseudocapacitive adsorption mechanisms [39]:



Here, $\text{VN}_x\text{O}_y \parallel \text{OH}^-$ represents the electrical double-layer adsorption of ions, while $\text{VN}_x\text{O}_y - \text{OH}$ represents a pseudocapacitive mechanism involving electrons transfer [39]. Properties and composition of the surface of transition metal nitrides and oxynitrides could therefore have a significant influence on the performance of these compounds as electrode materials and should therefore be carefully controlled.

It has previously been reported that transition metal nitrides and oxynitrides form an oxide layer on the surface at room temperature, and the composition of this layer is changing over time, the process also known as “ageing”. For instance, tungsten oxynitride stored in ambient air for 80 days has demonstrated an increase of the oxygen content on the surface, while no changes on the XRD patterns have been recorded [90]. Similar results have been reported for molybdenum

oxynitrides, where an increase of the oxygen content on the surface have been revealed by XPS or elemental analysis, while the XRD patterns have remained unchanged [91, 92]. This evolution of the surface composition of transition metal nitrides and oxynitrides in time and its influence on the capacitive properties of the materials remains almost unexplored. Since a number of these compounds are pyrophoric, they are usually passivated (i.e. exposed to a stream of a gas containing a small amount of oxygen) prior the exposure to air as a standard synthesis procedure, in order to form a protective oxide layer. The influence of the passivation on the ageing has not been explored as well. It is, in my view, important to investigate the influence of the synthesis and storage conditions of transition metal nitrides and oxynitrides on their surface properties, as these changes could have an influence on their electrochemical performance in supercapacitors.

In this work, ageing of molybdenum and tungsten oxynitrides is studied. More specifically, the materials, synthesised by the temperature-programmed reduction in ammonia, are exposed to ambient air for different periods and analysed by low temperature N₂ adsorption and XPS. Additionally, the influence of the passivation procedure, performed after the temperature-programmed reduction, is studied, in order to determine its effect on the ageing and the electrochemical properties of molybdenum and tungsten oxynitrides. Electrochemical properties of the samples are investigated with cyclic voltammetry and galvanostatic charge and discharge measurements. Recommendations are made regarding the synthesis procedure as well as the storage conditions for these compounds.

5.2 Experimental

Molybdenum and tungsten oxynitrides were synthesised by a temperature-programmed reduction of the commercially available MoO₃ (Sigma-Aldrich, 267856) and WO₃ (Sigma-Aldrich, 95410) precursors, respectively, in ammonia gas at 700° C. The detailed TPR procedure is described elsewhere [126, 127, 150]. Before bringing the synthesised materials in contact with air, the furnace was purged with the flow of the pure Ar (Coregas), with the flow rate of 0.5 l min⁻¹

Table 5.1 Description of the synthesised passivated and non-passivated samples exposed to ambient air for different periods.

Sample	Sample description	Storage period (days)	Weight of the active materials (mg) \pm 0.035 mg on the electrodes
A1	W(N,O)- non passivated	0 (fresh)	2.38
A2	W(N,O)- non passivated	5	2.31
A3	W(N,O)- non passivated	21	2.32
A4	W(N,O)- non passivated	48	2.4
B1	Mo(N,O)- non passivated	0 (fresh)	2.33
B2	Mo(N,O)- non passivated	21	2.35
B3	Mo(N,O)- non passivated	35	2.36
B4	Mo(N,O)- non passivated	48	2.48
AP1	W(N,O)- passivated	0 (fresh)	2.14
AP2	W(N,O)- passivated	5	2.02
AP3	W(N,O)- passivated	21	2.27
AP4	W(N,O)- passivated	48	2.02

during one hour. For simplicity, the synthesised materials are further denoted as non-passivated W(N,O) and Mo(N,O). In order to study the influence of the passivation on the ageing of oxynitrides and on the evolution of their electrochemical properties with time, passivated tungsten oxynitride samples were prepared by flowing a special passivating gas mixture (Ar + 0.1 vol.% O₂) over the synthesised material during one hour prior exposure to air. The flow rate of the gas mixture was fixed to 0.5 l min⁻¹.

Room temperature oxidation or ageing was performed by storing the synthesised samples in contact with ambient air (in open containers) for different time periods up to 48 days. The synthesised samples (Table 5.1) were characterised with low temperature N₂ adsorption, XPS and TEM measurements. Electrochemical testing was performed by cyclic voltammetry and galvanostatic charge and discharge measurements in 1M H₂SO₄ electrolyte. Electrode slurries were prepared by mixing the synthesised materials (A1-A4, B1-B4 and AP1-AP4) with carbon nanopowder and PVDF in 90:5:5 ratio. Slurries were coated onto Ti foils and dried at 90° C in vacuum overnight. Electrochemical measurements were performed in a three electrode cell setup with Ag/AgCl as a reference electrode and Pt wire as a counter-electrode. Electrodes with nearly identical weights were selected (Table 5.1).

5.3 Comparison of the structure and electrochemical performance of non-passivated samples exposed to ambient air for different periods.

5.3.1 Characterisation of tungsten oxynitride

Low temperature N₂ adsorption isotherms of non-passivated tungsten oxynitride samples exposed to ambient air for different periods (Figure 5.1 a) present a hysteresis between the adsorption and desorption branches, indicating that the materials are porous. Specific surface areas, measured with BET method, reveal surface areas of 54 (±0.2), 42 (±0.3), 44 (±0.2) and 48 (±0.3) m² g⁻¹ for samples

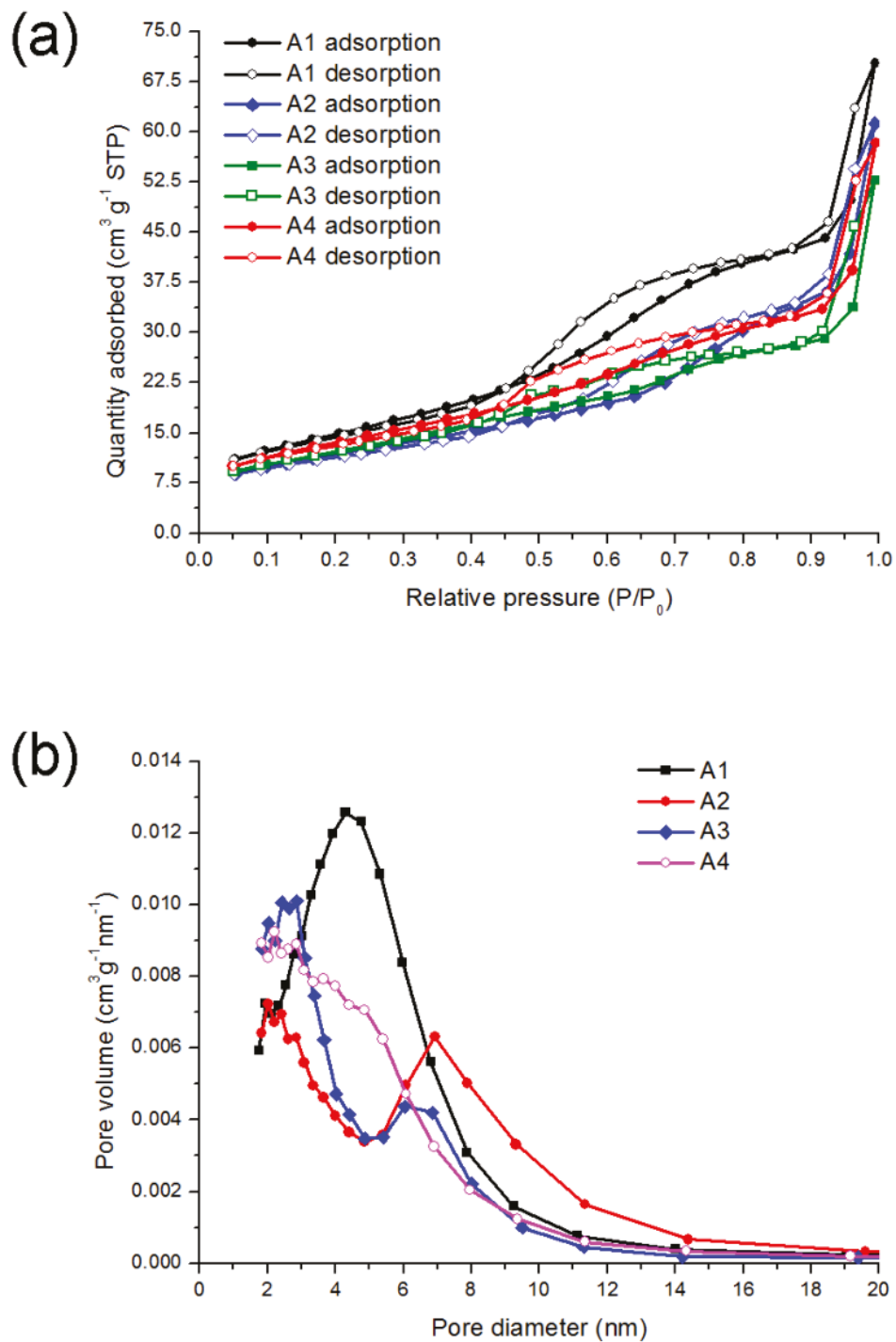


Figure 5.1. Low temperature N₂ adsorption characterisation of non-passivated tungsten oxynitride samples: isotherms (a) and pore size distributions (b).

A1, A2, A3 and A4, respectively. After an initial drop in the surface area from 54 to 42 m² g⁻¹ after exposure to ambient air for 5 days, no further decrease of the surface area could be detected. This observation differs from data reported by Cho *et al.* [90] for the passivated tungsten oxynitride, where a progressive decrease of

the surface area from 63.7 to 30 m² g⁻¹ is measured after the exposure of samples to air for 40 days.

The pore size distribution of the as-synthesised sample (Figure 5.1 b, sample A1) presents a maximum around 5 nm, with no pores larger than 20 nm visible. Upon exposure to ambient air for 5 days, this maximum disappears, giving rise to two different maxima, centred around 3 and 7 nm, respectively (Figure 5.1 b, sample A2). Further ageing leads to an increase in the proportion of mesopores with 3 nm diameters (Figure 5.1 b, sample A3). The evolution of the pore size distributions of the non-passivated tungsten oxynitrides is, as well, different from data measured for the passivated compounds. More specifically, Cho *et al.* reported that the pore size distribution of the as-synthesised compound presents three maxima, centred around 2.3, 3.5 and 4.2 nm. Upon ageing, the smaller pores disappear first, but larger mesopores (4.2 nm) remain intact, indicating that the oxide formation on the surface is blocking small pores [90]. For samples A1-A4, however, the oxide formation seems to progressively decrease the diameter of mesopores but not to block them (Figure 5.1 b). This difference could arise from the difference in the morphology of the pores, as the shape of the hysteresis loop for samples A1-A4 (Figure 5.1 a) is different from the shape previously reported for the passivated tungsten oxynitride samples [90].

In order to investigate the oxide species present on the surface of tungsten oxynitrides, the materials are characterised with XPS (Figure 5.2). XPS spectrum of the as-synthesised sample presents two core doublets (Figure 5.2 a, Table 5.2). The first doublet, characteristic of tungsten in WO₃ species and denoted as W⁶⁺, has binding energies of approximately 36.0 and 38.0 eV. The second doublet, with binding energies of approximately 32.7 and 34.8 eV, represents tungsten with lower oxidation states. Since the binding energies of this doublet are close to the values reported for the mixed W₂N + WN, as well as WO₂ + WO phases [90], it is difficult to assign the peaks to the exact species. They are therefore denoted as W^{δ+}, where δ < 6. XPS results indicate that the surface of the as-prepared

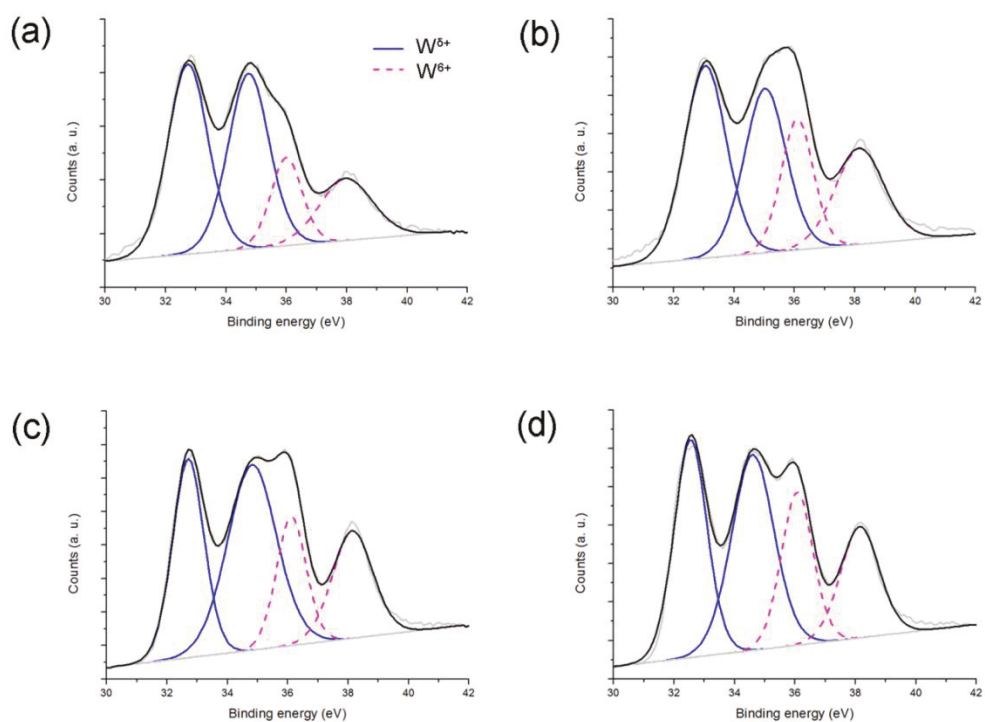


Figure 5.2. XPS spectra depicting W 4f deconvolution peaks for samples A1 (a), A2 (b), A3 (c) and A4 (d).

Table 5.2 Binding energies of W 4f deconvolution peaks for samples A1-A4.

Sample	W ⁶⁺		W ^{δ+}	
	W 4f _{5/2}	W 4f _{7/2}	W 4f _{5/2}	W 4f _{7/2}
A1	38.0	36.0	34.8	32.7
A2	38.2	36.1	35.0	33.0
A3	38.1	36.1	34.8	32.7
A4	38.1	36.1	34.6	32.5

Table 5.3 Ratio of W 4f_{7/2} peak areas for samples A1-A4.

Sample	W ⁶⁺ /W ^{δ+} ratio
A1	0.36
A2	0.61
A3	0.61
A4	0.68

tungsten oxynitride (Figure 5.2 a), as well as the samples exposed to air for different periods (Figure 5.2 b-d) contain WO₃. When comparing the change of the W⁶⁺/W^{δ+} ratio with time, calculated from the areas of W 4f_{7/2} peaks (Table 5.3), an increase of the proportion of WO₃ species could be observed on the surface. After an initial increase from 0.36 to 0.61, no further significant change in the W⁶⁺/W^{δ+} ratio is observed. This could indicate that upon exposure to air, the surface of tungsten oxynitride becomes progressively covered with a WO₃ layer, with a saturation observed shortly after the exposure.

5.3.2 Characterisation of molybdenum oxynitride

Low temperature N₂ adsorption isotherms of molybdenum oxynitride (Figure 5.3 a) correspond to type IV and demonstrate a hysteresis, indicating therefore the porosity of the synthesised dark grey powder. Surface areas of 123 (±2.6), 39 (±0.4), 60 (±0.5) and 67 (±0.6) m² g⁻¹ are measured for samples B1, B2, B3 and B4, respectively, with the BET method. After an initial drop of the surface area, an increase is observed. It is important to note that the samples are degassed at the same temperature prior the BET measurements, as degassing temperature could have an influence on the measured surface areas [91]. These results differ from the previously reported data, where a progressive decrease of the surface areas is

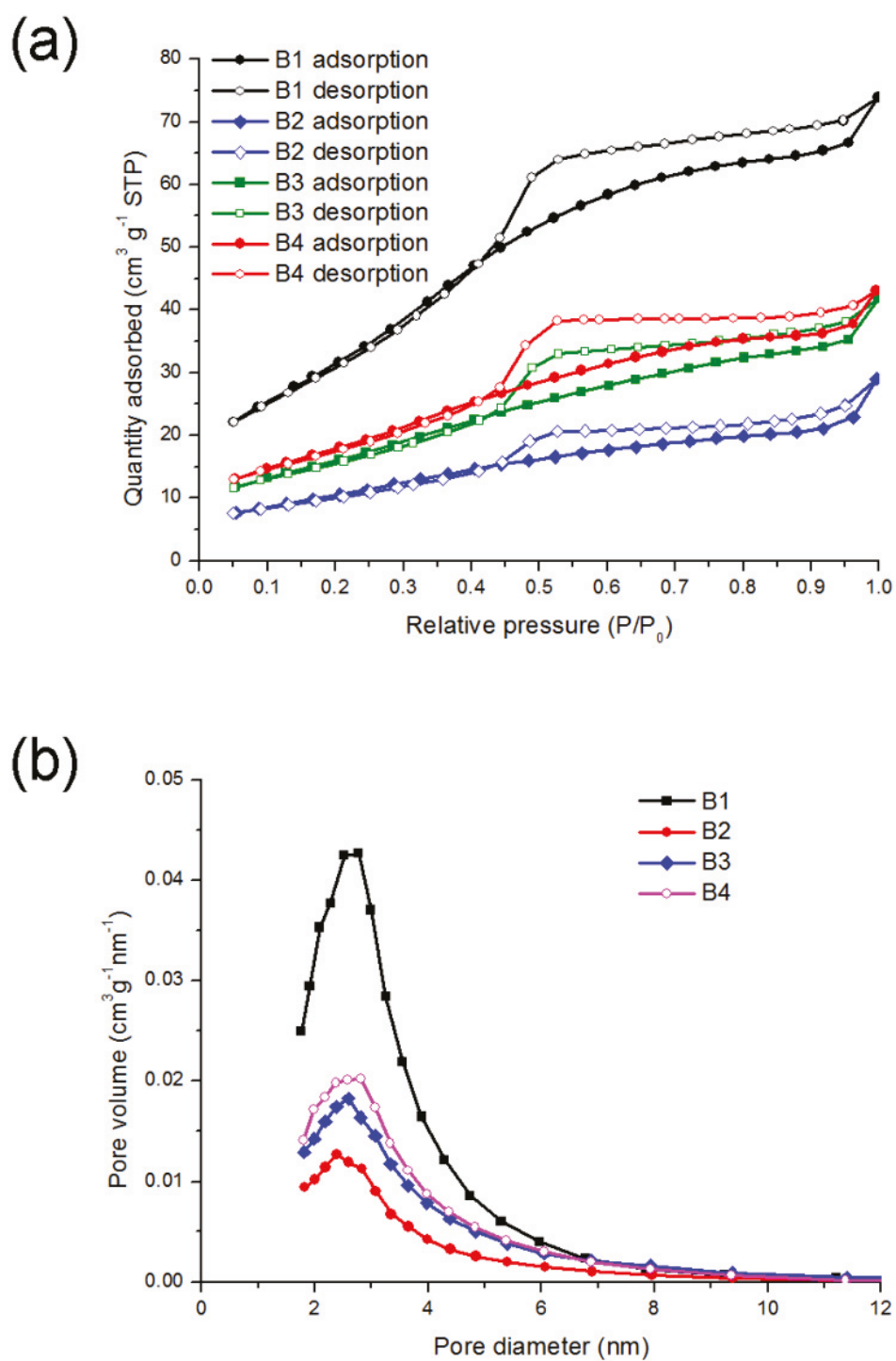


Figure 5.3. Low temperature N_2 adsorption characterisation of the non-passivated molybdenum oxynitride samples: isotherms (a) and pore size distributions (b).

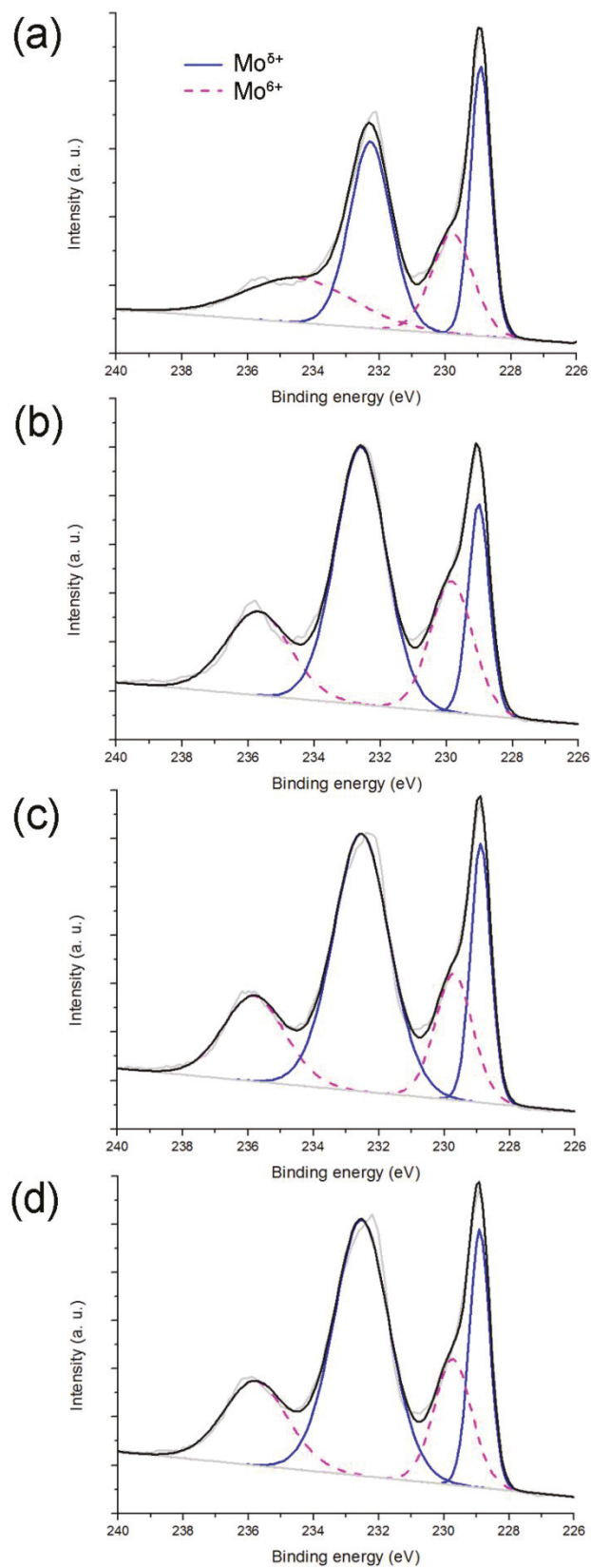


Figure 5.4. XPS spectra depicting Mo 3d deconvolution peaks for samples B1 (a), B2 (b), B3 (c) and B4 (d).

observed for the passivated molybdenum oxynitride samples stored in the ambient air for the period up to 7 weeks [91, 92]. The pore size distribution (Figure 5.3 b) presents a maximum at approximately 3nm, with no apparent shift in the maximum observed upon ageing.

XPS spectra of the as-synthesised molybdenum oxynitride (Figure 5.4 a) presents two doublets, the first centred around 232.2 and 235.9 eV and corresponding to Mo⁶⁺ in MoO₃, while the second is located at 229.1 and 232.3 eV and could be attributed to Mo^{δ+} species, with 0 < δ < 6 (Table 5.4) [156-158]. Similar to the XPS results measured for the non-passivated tungsten oxynitrides (Table 5.3), the Mo⁶⁺/Mo^{δ+} ratio increases upon ageing and reaches a saturation, indicating an increase of the proportion of MoO₃ species on the surface of the non-passivated molybdenum oxynitride upon exposure to ambient air (Table 5.5).

Table 5.4 Binding energies of Mo 3d deconvolution peaks for samples B1-B4.

Sample	Mo ⁶⁺		Mo ^{δ+}	
	Mo 3d _{3/2}	Mo 3d _{5/2}	Mo 3d _{3/2}	Mo 3d _{5/2}
B1	235.9	232.2	232.3	229.1
B2	236.0	232.4	232.6	229.2
B3	236.1	232.4	232.5	229.1
B4	236.1	232.5	232.5	229.1

Table 5.5 Ratio of Mo 3d_{5/2} peak areas for samples B1-B4.

Sample	Mo ⁶⁺ /Mo ^{δ+} ratio
B1	0.46
B2	0.71
B3	0.75
B4	0.72

5.3.3 Influence of ageing on the electrochemical properties of tungsten oxynitride

In order to evaluate the influence of ageing on the electrochemical properties of tungsten oxynitride, samples A1-A4, exposed to air for different periods, are characterised with cyclic voltammetry and galvanostatic charge and discharge measurements (Figures 5.5 and 5.6). The shape of the CV curve for the as-synthesised sample (A1) in 1M H₂SO₄ electrolyte is a nearly ideal rectangle (Figure 5.5 a). Upon ageing, however, small reversible redox peaks could be observed on the surface of the CV curves around -0.1 V. These peaks could be attributed to the electrochemical activity of additional WO₃ species present on the surface of the samples after exposure to air, revealed by XPS measurements (Figure 5.2). In fact, CV curves of mesoporous amorphous WO_{3-x} present redox peaks resembling those of the aged tungsten oxynitride samples [151]. The measurements of the maximum specific capacitance value, performed with the galvanostatic charge and discharge method, indicate its progressive increase upon ageing. In fact, the capacitance value, measured at 0.05 A g⁻¹, increases from 57 F g⁻¹ (106 μF cm⁻²) for the as-prepared sample (A1) to 75 F g⁻¹ (156 μF cm⁻²) for the sample exposed to the ambient air for 48 days (Figure 5.5 b).

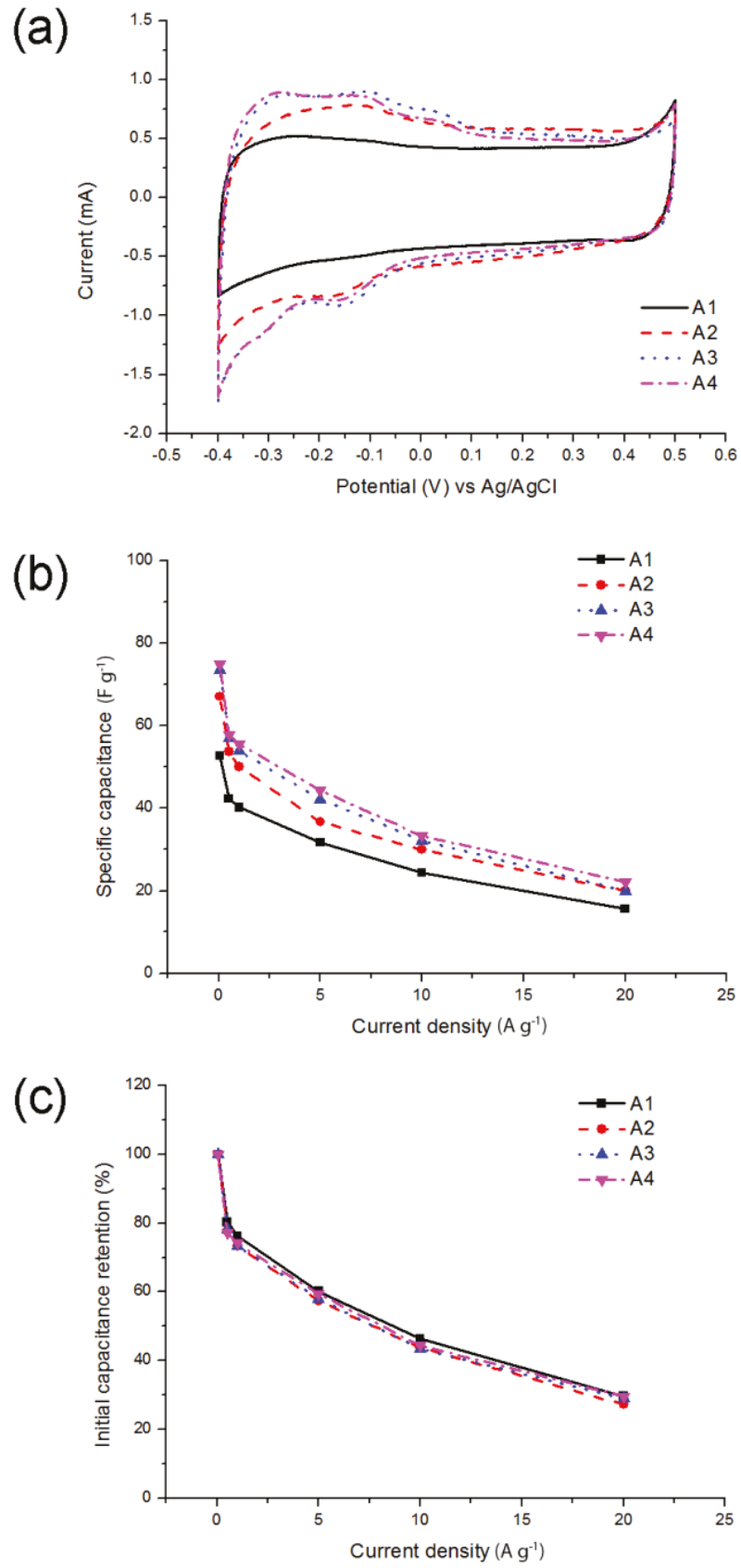


Figure 5.5. CV curves at the scan rate of 5 mV s⁻¹ (a) and rate capabilities (b, c) of tungsten oxynitride samples exposed to ambient air for different periods in 1M H₂SO₄ electrolyte.

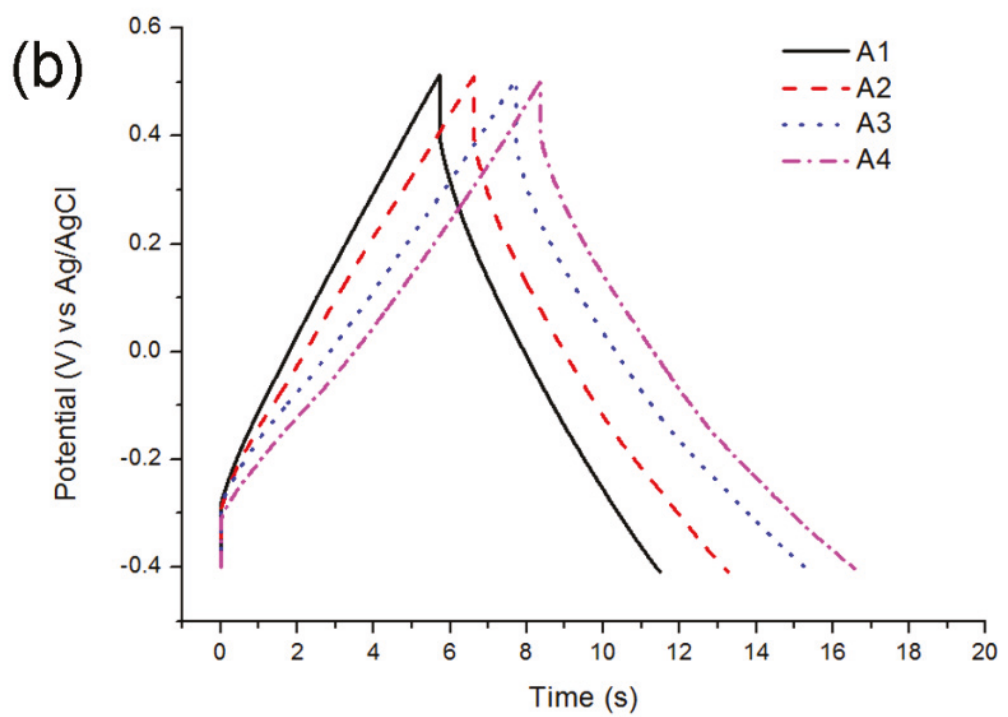
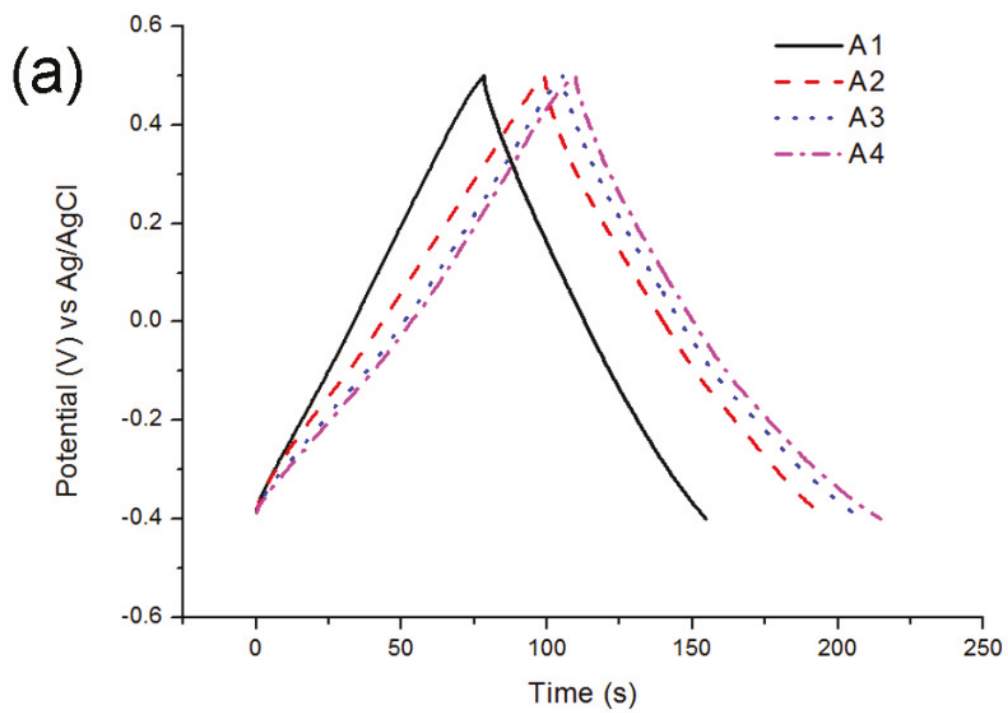


Figure 5.6. Galvanostatic charge and discharge curves measured for tungsten oxynitride samples at 0.5 (a) and 5 A g⁻¹ (b) in 1M H₂SO₄ electrolyte.

It is important to note that the weight of the active materials is carefully controlled and electrodes with nearly identical mass are selected for comparison (Table 5.1). When comparing the specific capacitance retention at high current loads for samples A1-A4 (Figure 5.5 b, c), it could be observed that the ageing does not have an influence on their rate capabilities. More specifically, for the as-prepared sample (A1), 29.6 % of the initial capacitance value is retained upon increasing the current load from 0.05 to 20 A g⁻¹. The same capacitance retention is reported for the sample exposed to air for 48 days (A4). These results are consistent with the assumption that the progressive oxidation of the surface of oxynitrides does not affect the bulk and therefore does not have an influence on the intrinsic conductivity of the active materials.

Galvanostatic charge and discharge curves (Figure 5.6), measured for samples A1-A4 at the current load of 0.5 A g⁻¹ (Figure 5.6 a) and 5 A g⁻¹ (Figure 5.6 b) have nearly ideal, triangular shapes, with small IR drops observed at the higher current (Figure 5.6 b). Ageing, however, has an influence on the Coulombic efficiencies of the samples, which could be observed from the distortion of the shapes of cyclic voltammograms (Figure 5.5 a). In fact, the Coulombic efficiency, measured from the galvanostatic charge and discharge curves at the current load of 0.05 A g⁻¹, drops from 94 % for the sample A1 to 77 % for the sample A4, indicating the presence of an irreversible process.

5.3.4 Influence of ageing on the electrochemical properties of molybdenum oxynitride

Similar to tungsten oxynitride, the influence of the ageing on the electrochemical properties of molybdenum oxynitride is evaluated by cyclic voltammetry and galvanostatic charge and discharge measurements (Figures 5.7 and 5.8). CV curves of samples B1-B4 are less rectangular (Figure 5.7 a), and ageing does not have an apparent influence on their shape. Rate capability measurements (Figure 5.7 b, c) indicate that the exposure to the ambient air has a significant influence on the capacitance retention at high current loads. In fact, the as-prepared sample (B1) retains only 2.7 % of its initial capacitance upon increasing the current from

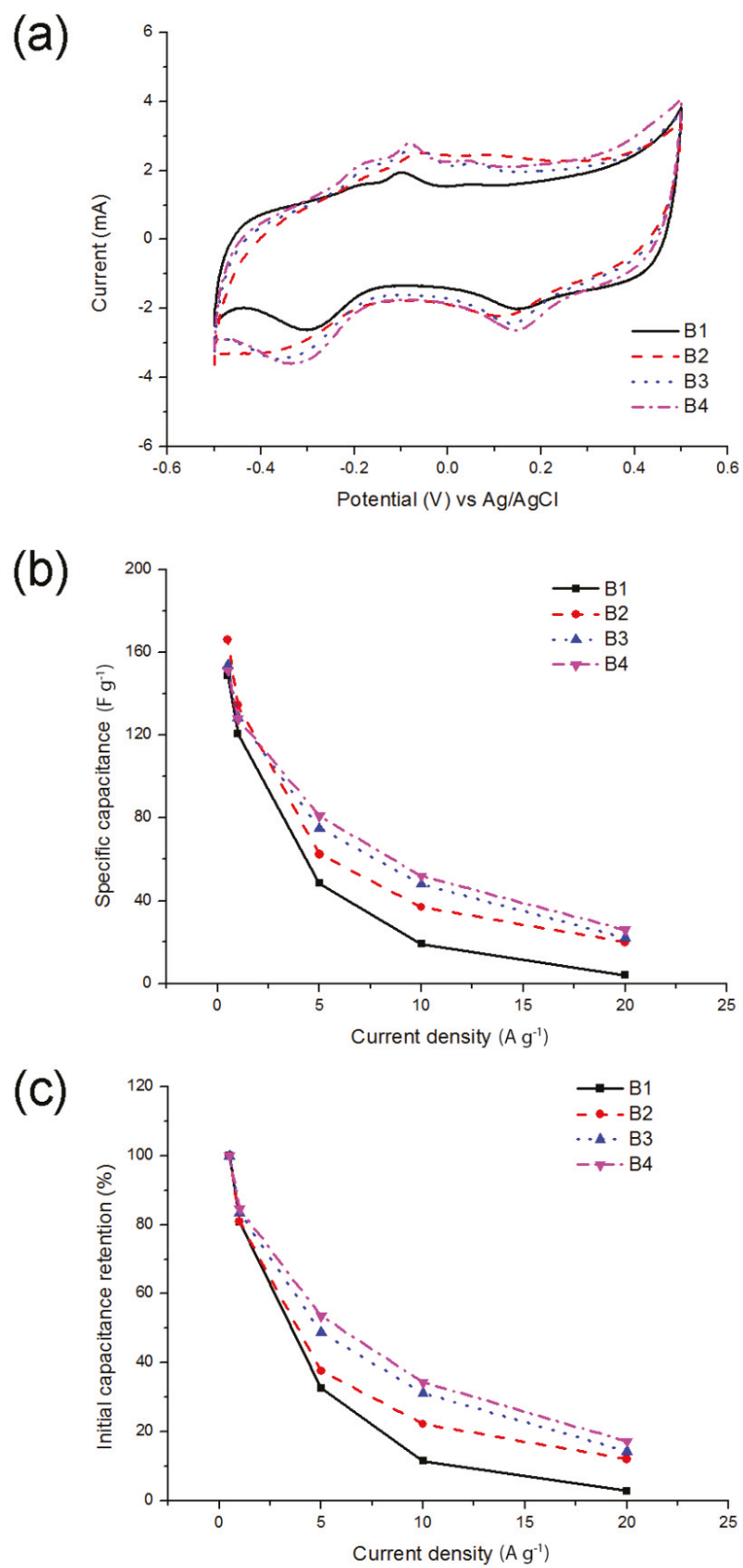


Figure 5.7. CV curves at the scan rate of 5 mV s⁻¹ (a) and rate capabilities (b, c) of molybdenum oxynitride samples exposed to ambient air for different periods in 1M H₂SO₄ electrolyte.

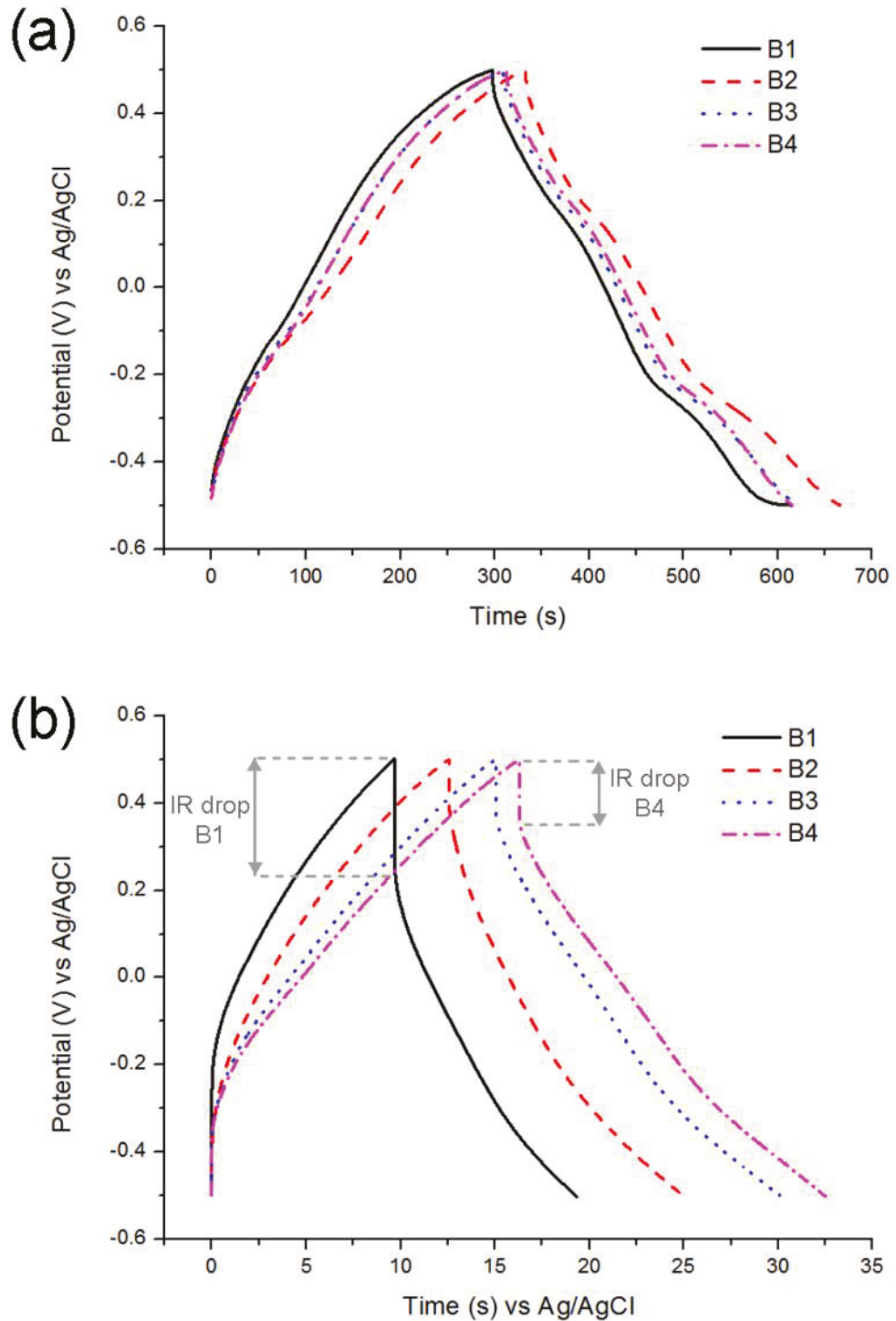


Figure 5.8. Galvanostatic charge and discharge curves measured for molybdenum oxynitride samples at 0.5 (a) and 5 A g⁻¹ (b) in 1M H₂SO₄ electrolyte.

0.5 to 20 A g⁻¹, while the sample exposed to air for 48 days (B4) retains 17.2 % of the initial value. Another change could be observed when comparing the galvanostatic charge and discharge curves of molybdenum oxynitride samples at the current load of 5 A g⁻¹ (Figure 5.8 b): for samples exposed to air, the IR drop

decreases. These results could indicate that oxidation at room temperature leads to an occurrence of faster electrochemical processes.

5.4 Influence of the passivation of tungsten oxynitride on the ageing process

As a standard synthesis procedure, transition metal nitrides and oxynitrides are usually passivated after the temperature-programmed reduction with a gas mixture containing a low percentage of oxygen in order to prevent the strong oxidation in the ambient air. In this work, the influence of the passivation on the ageing and on the electrochemical properties is studied. Low temperature nitrogen adsorption characterisation of the passivated samples AP1-AP4 is presented on figure 5.9. Similar to the non-passivated tungsten oxynitrides, the adsorption isotherms of the passivated compounds correspond to type IV (Figure 5.9 a), and specific surface areas, evaluated with the BET method, are 44.6, 40.1, 42.3 and 28.3 m² g⁻¹ for samples AP1, AP2, AP3 and AP4, respectively. The maximum of the pore size distribution of the as-synthesised sample AP1 (Figure 5.9 b) is centred at approximately 6 nm and upon ageing, this maximum shifts to larger pore sizes. These results, similar to the previously reported data, could indicate that the exposure to the ambient air leads to the blocking of the smaller pores [90].

XPS spectra of the passivated tungsten oxynitride samples (Figure 5.10) are similar to the spectra of the non-passivated compounds (Figure 5.2) and present two doublets corresponding to W³⁺ and W^{δ+} species (Table 5.6). The difference between the passivated and non-passivated samples could be observed when comparing the ratios of W⁶⁺/W^{δ+} species (Table 5.7). More specifically, for the as-synthesised sample, the ratio is 0.36 for the non-passivated and 0.16 for the passivated materials, respectively, indicating a stronger oxidation of A1-A4 compounds.

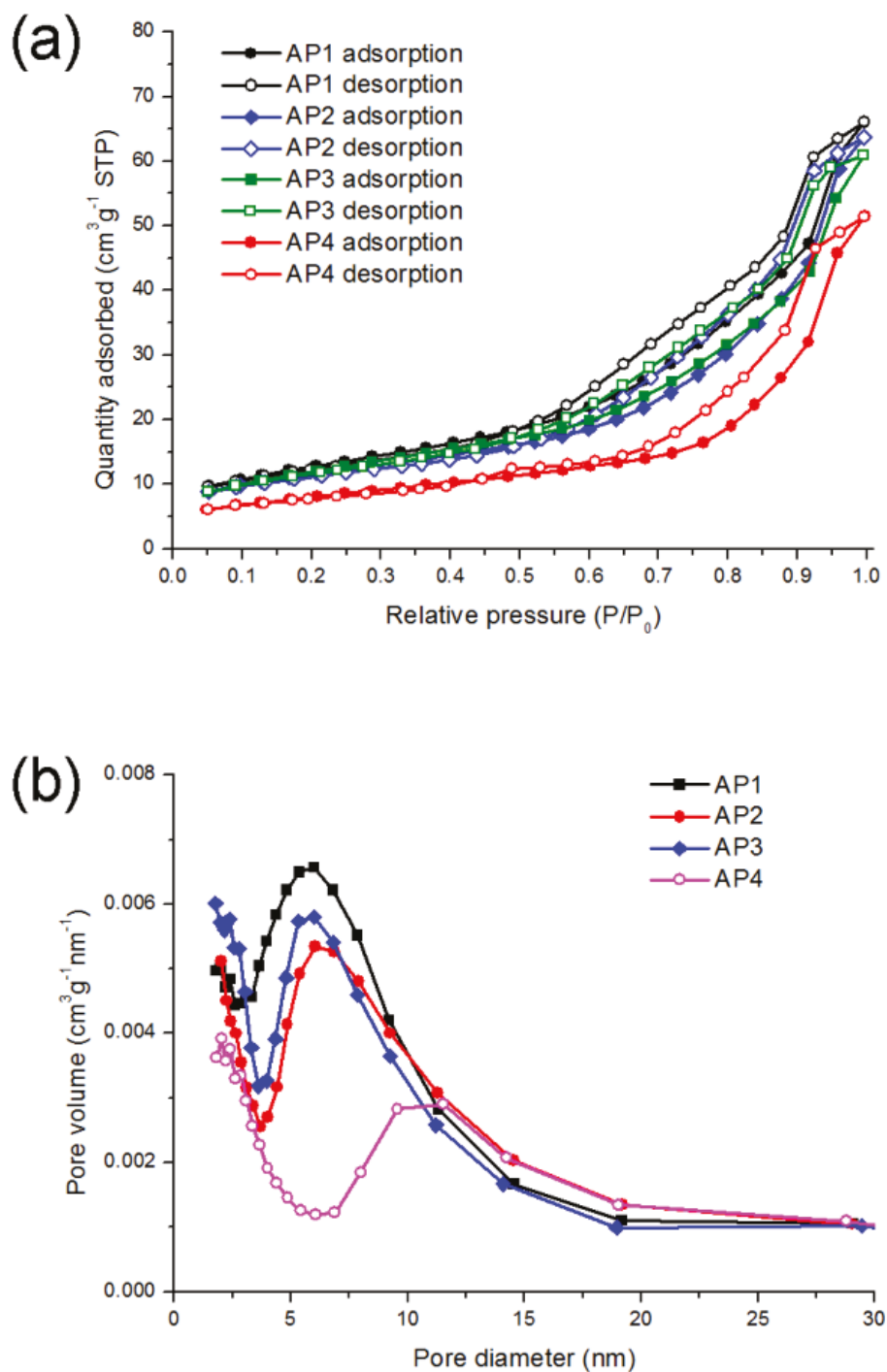


Figure 5.9. Low temperature N_2 adsorption characterisation of the passivated molybdenum oxynitride samples: isotherms (a) and pore size distributions (b).

Upon ageing, this ratio strongly increases for the non-passivated samples and reaches saturation already after 5 days of exposure to air, while for the passivated samples, the ratio increases progressively. These results indicate that the passivation slows down the room temperature oxidation but does not prevent it.

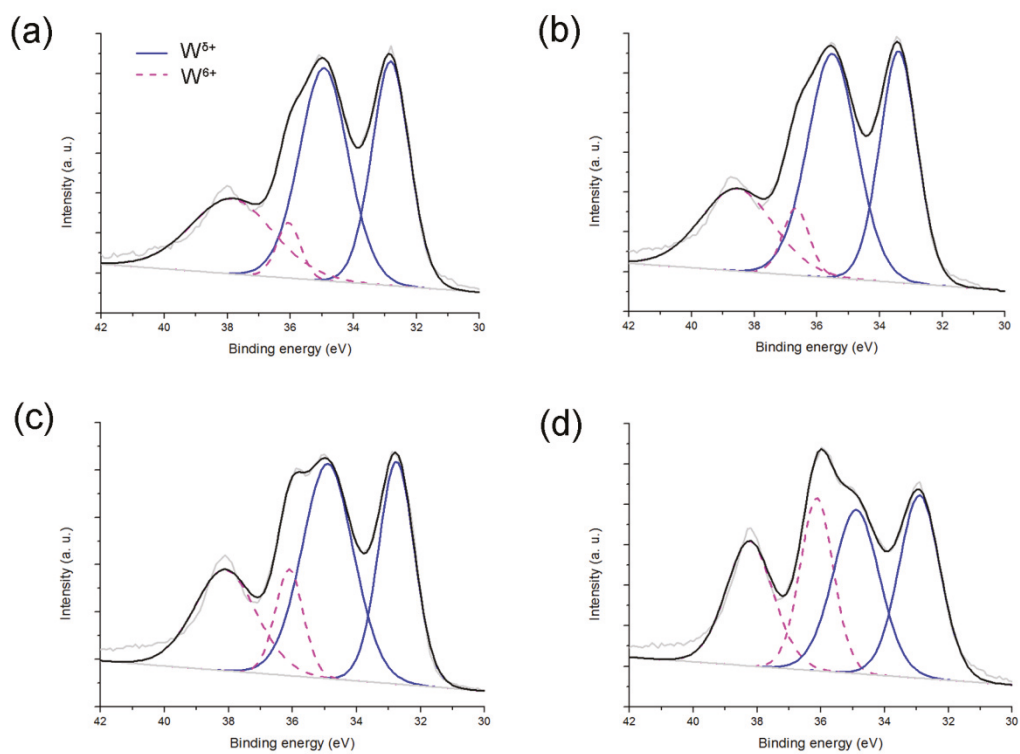


Figure 5.10. XPS spectra depicting W 4f deconvolution peaks for samples AP1 (a), AP2 (b), AP3 (c) and AP4 (d).

Table 5.6 Binding energies of W 4f deconvolution peaks for samples AP1-AP4.

Sample	W ⁶⁺		W ^{δ+}	
	W 4f _{5/2}	W 4f _{7/2}	W 4f _{5/2}	W 4f _{7/2}
AP1	37.6	36.0	34.9	32.8
AP2	38.6	36.7	35.5	33.4
AP3	38.1	36.1	34.9	32.8
AP4	38.2	36.1	34.9	32.9

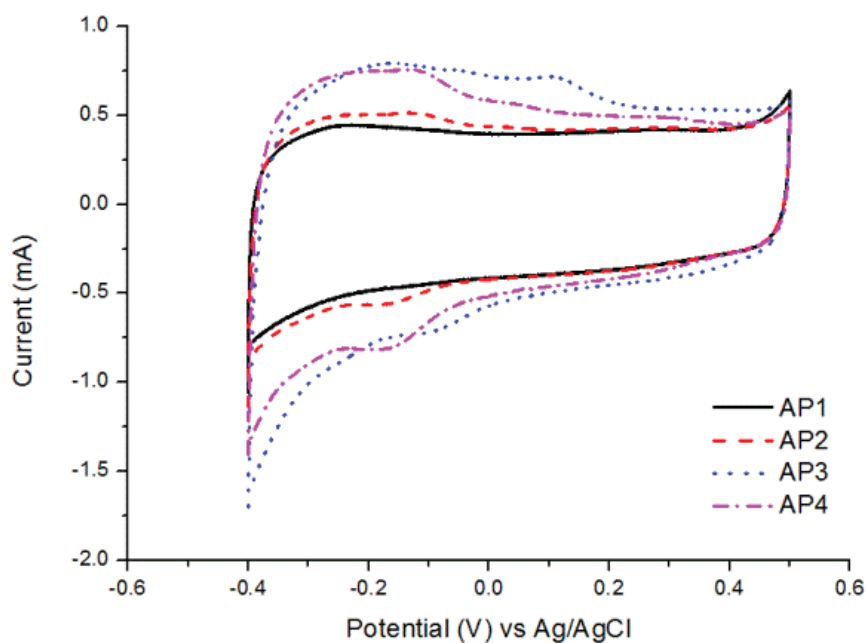


Figure 5.11. CV curves of the passivated tungsten oxynitride samples at the scan rate of 5 mV s^{-1} .

Table 5.7 Ratio of W $4f_{7/2}$ peak areas for samples AP1-AP4.

Sample	$\text{W}^{6+}/\text{W}^{\delta+}$ ratio
AP1	0.16
AP2	0.20
AP3	0.37
AP4	0.75

Cyclic voltammograms (Figure 5.11) of the passivated samples in 1M H_2SO_4 electrolyte shows that, similarly to the non-passivated samples, the shape of the cyclic voltammetry curves becomes distorted upon ageing, with redox peaks appearing on top of the CV around -0.1 V.

When comparing galvanostatic charge and discharge curves for the as-synthesised, passivated and non-passivated samples (A1 and AP1) as well as samples exposed to air for 48 days (A4 and AP4), it could be observed that at the charge and discharge curves for A1 and AP1, as well as for A4 and AP4 are nearly superimposed (Figure 5.12). At the current load of 0.5 A g^{-1} , the specific capacitance values, measured for the samples A1 and AP1, are 42.3 F g^{-1} and 43.6 F g^{-1} , respectively. Upon ageing, the specific capacitance values increase to 57.8 F g^{-1} and 58.3 F g^{-1} for samples A4 and AP4 (Figure 5.12 a). Upon the 10-fold increase of the current load (Figure 5.12 b), the specific capacitances measured are 31.7 , 35.6 , 44.4 and 46.7 F g^{-1} for samples A1, AP1, A4 and AP4, respectively, thus indicating that passivation does not have a significant influence on the rate capability of tungsten oxynitride.

The influence of the passivation could be, however, observed when comparing the increase of the specific capacitance values upon ageing (Figure 5.13). For samples A1-A4, a sharp increase of the specific capacitance, measured at the current load of 0.5 A g^{-1} , is observed already after five days of exposure to air, followed by a plateau, while for samples AP1-AP4, the specific capacitance values progressively increase with time. After 48 days of exposure, however, both non-passivated and passivated samples reach nearly identical specific capacitance values. Similar results are measured at a higher current load of 5 A g^{-1} . These results indicate that the change in the electrochemical properties of the non-passivated samples happens soon after exposure to air, followed by the saturation, while for the passivated samples, these changes occur progressively. The observed data correlate with the change of the $\text{W}^{6+}/\text{W}^{\delta+}$ species ratio measured with XPS for the passivated and non-passivated samples, respectively.

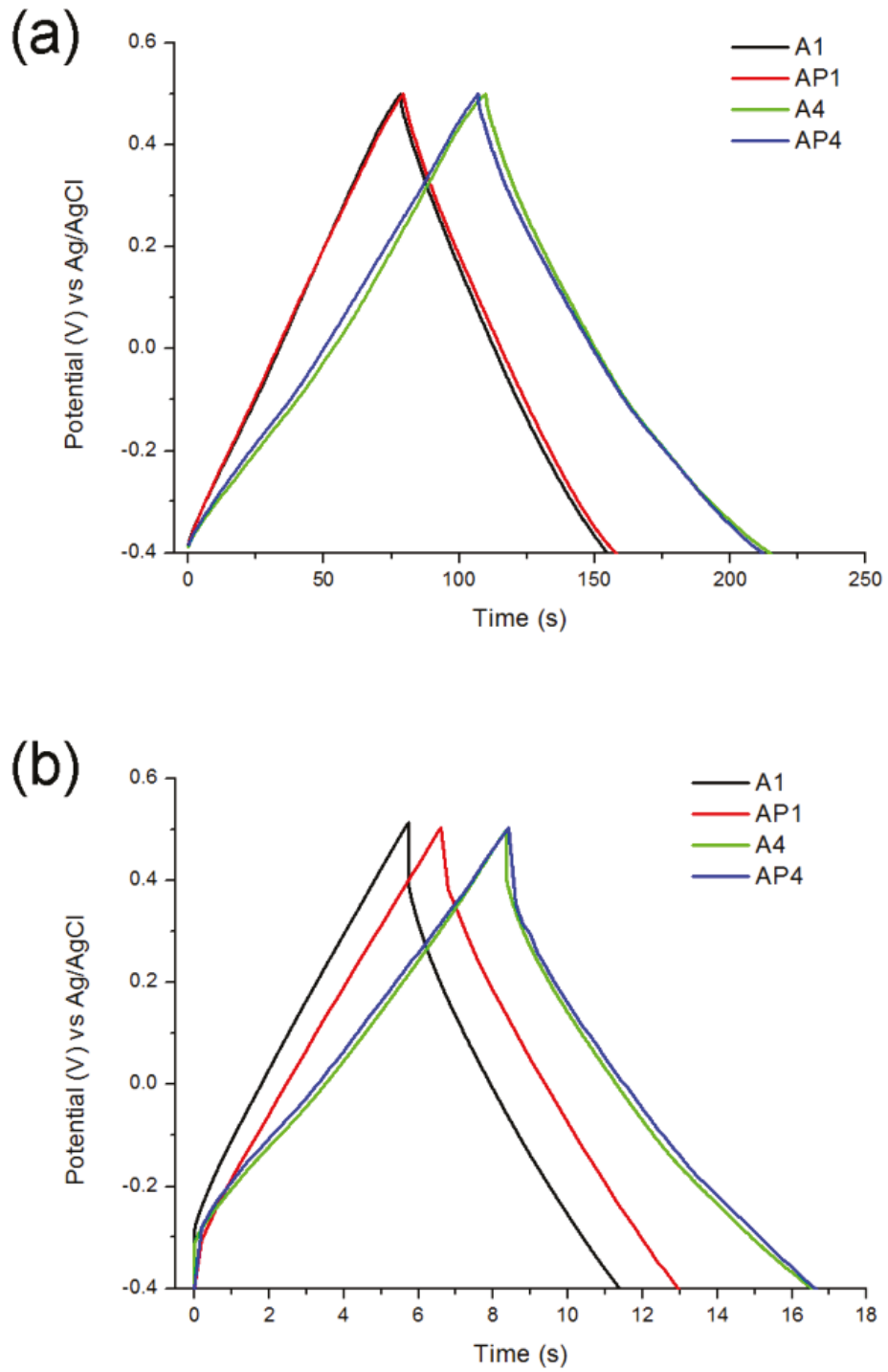


Figure 5.12. Galvanostatic charge and discharge curves of the passivated and non-passivated tungsten oxynitride samples at the current loads of 0.5 A g^{-1} (a) and 5 A g^{-1} (b).

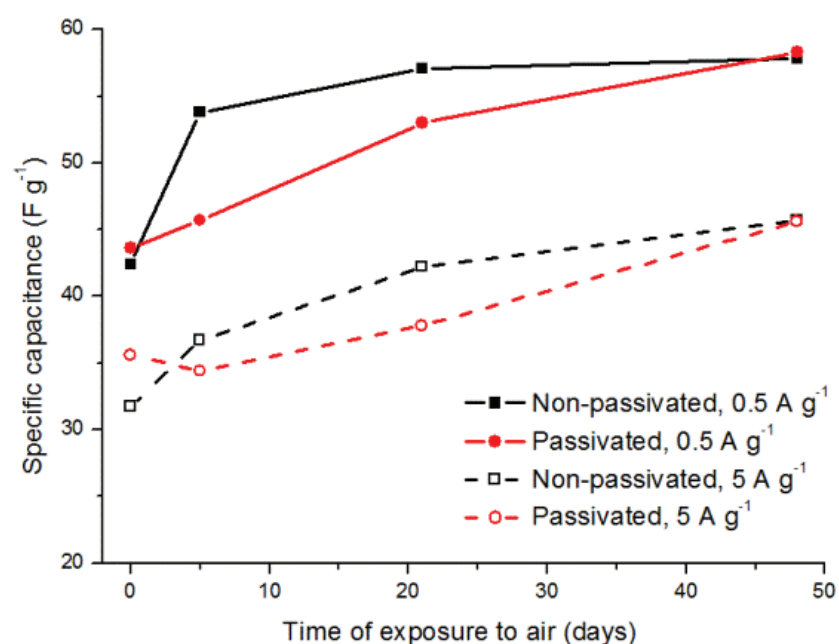


Figure 5.13. Evolution of the specific capacitance values of the passivated and non-passivated tungsten oxynitride samples upon exposure to air at different current loads.

5.5 Discussion: implications of the ageing on the preparation and storage of transition metal oxynitrides

The results presented in this work indicate that properties of molybdenum and tungsten oxynitrides are changing over time upon exposure to the ambient air at room temperature. XPS measurements indicate that the oxide composition on the surface of these compounds is evolving, and the compounds become progressively oxidised.

Ageing, in turn, has an influence on the electrochemical properties of transition metal oxynitrides in supercapacitors, and changes are material-specific. For instance, for tungsten oxynitrides, although an increase of the specific capacitance is observed upon exposure to air, ageing leads to the distortion of the cyclic voltammetry curves, and therefore decreases Coulombic efficiencies. For molybdenum oxynitrides, a completely different behaviour is observed, with an

increase of the rate capability upon ageing. These results indicate that the storage of these compounds in the ambient air could not only influence the electrochemical performance, but additionally affect the reproducibility of the measurements, or the comparison of the results to data reported in the literature. It could therefore be recommended to analyse the effect of the ageing on a particular nitride or oxynitride compound and select the appropriate storage conditions (controlled ageing in the ambient air or storage in an inert gas atmosphere).

Additionally, the effect of the passivation prior the exposure to air after the temperature-programmed reduction is studied in relation to the ageing. XPS results show that although the passivation slows down the oxidation of the surface of transition metal oxynitrides in the ambient air, it does not prevent it. Electrochemical measurements correlate with XPS results and demonstrate a progressive change in the specific capacitance values for the passivated samples, as opposed to the non-passivated samples, which show a strong change on the electrochemical performance soon after exposure to air and then reach saturation. Although after long storage periods both passivated and non-passivated tungsten oxynitride samples show similar changes in the electrochemical behaviour, this evolution of the performance is slower for the passivated samples. It could therefore be recommended to perform the passivation of the samples prior exposure to the ambient air. The passivation is typically performed by exposing the samples to the flow of an inert gas with a small amount of oxygen (0.1 vol. %) at the end of the temperature-programmed reduction.

5.6 Conclusions

In this work, the ageing of transition metal oxynitrides in the ambient air is studied. More specifically, molybdenum and tungsten oxynitrides are synthesised by the temperature-programmed reduction, exposed to the ambient air for different periods, and characterised by low temperature N₂ adsorption, X-ray photoelectron spectroscopy and electrochemical measurements. Additionally, the role of the passivation in the ageing of samples is investigated. Results indicate that upon exposure of the compounds to air for different periods, progressive oxidation of the surface occurs, which, in turn, leads to material-specific changes

in their electrochemical properties. For tungsten oxynitride, exposure to air induces an increase of the specific capacitance values but decreases Coulombic efficiencies, while for molybdenum oxynitride, an increase of the rate capability is observed. Finally, passivation of tungsten oxynitride samples prior exposure to air slows down the oxidation of the surface and therefore the evolution of the electrochemical properties. It is therefore recommended to analyse the effect of ageing on transition metal nitrides or oxynitrides and select the appropriate storage conditions.

Chapter 6. Transition metal oxynitrides: structure and electrocatalytic performance for the oxygen reduction reaction

6.1 Introduction

Due to their high intrinsic conductivity and good catalytic activity, transition metal nitrides and oxynitrides are promising candidates for applications as electrocatalysts for oxygen reduction reaction (ORR) [51-54, 93, 118-125, 159, 160]. In fact, compounds including TiN [52], MoN [53], Mo₂N [124], Mn₄N [121], CrN [121] and Co₃Mo₃N [122] have demonstrated good electrocatalytic performances with overall four-electron ORR pathways. Among these compounds, carbon-supported molybdenum nitrides MoN and Mo₂N have shown promising electrocatalytic activities, with $n = 3.8$ transferred electrons calculated for both materials in aqueous electrolytes [53, 124]. These compounds, however, have been prepared by the temperature-programmed reduction of the carbon-supported precursors, and Youn *et al.* [125] have demonstrated that nanocarbon supports could have a synergetic effect on the electrocatalytic activity on transition metal nitrides. More specifically, TiN on a hybrid carbon nanotube-graphene (CNT-GR) hybrid support has shown an enhanced performance when compared to the unsupported TiN [125]. This improvement of the electrocatalytic activity has been attributed to the formation of a 3D structure with a large surface area and mesopores, thus enabling the electrolyte to access the active sites of TiN, and the enhanced conductivity of the composite [125]. The electrocatalytic activity of the molybdenum nitride and oxynitride compounds without carbon supports should therefore be investigated in more detail.

In this chapter, oxynitrides of molybdenum, tungsten and vanadium are synthesised by the temperature-programmed reduction in NH_3 and characterised by XRD, SEM, low temperature N_2 adsorption and wavelength dispersive spectrometry in order to assign the correct phase to the synthesised compounds. Their electrocatalytic activity is compared by performing cyclic voltammetry with a rotating disk electrode in a neutral 0.1 M KCl aqueous solution, used as a chloride-containing model of hexyl(tetradecyl)phosphonium chloride ($\text{P}_{6,6,6,14}\text{Cl}$) ionic liquid electrolyte [161, 162]. The ORR mechanism of molybdenum oxynitride is investigated in detail by performing RDE and RRDE measurements, in order to determine the number of transferred electrons, as well as to calculate the percentage of the hydrogen peroxide formed.

6.2 Experimental

Molybdenum, tungsten and vanadium oxynitrides were synthesised by a temperature-programmed reduction in NH_3 . Molybdenum and tungsten oxynitrides were prepared by placing 0.5 g of the commercially available oxide precursors MoO_3 (Sigma-Aldrich, 267856) and WO_3 (Sigma-Aldrich, 95410), respectively, in a tube furnace (Tetlow Kilns & Furnaces PTY Ltd., Australia). The TPR was performed by bringing the furnace up to the final temperature of 700°C with a heating rate of 3°C min^{-1} , then maintaining the temperature for two hours before cooling down to the room temperature naturally. The flow of ammonia was fixed to 0.2 l min^{-1} throughout the experiment. The synthesised materials were passivated with a special gas mixture ($\text{Ar} + 0.1\text{ vol.}\% \text{O}_2$, 0.5 l min^{-1}) during one hour prior the exposure to air. Vanadium oxynitride was synthesised from 20 g of V_2O_5 precursor (Sigma-Aldrich, 221899) using an in-house built fluid bed reactor. The temperature of the reactor was first gradually brought to 500°C with the flow rate of NH_3 fixed to 4 l min^{-1} . The flow was decreased to 1.5 l min^{-1} when the temperature of the reactor reached 500°C . Finally, when the final TPR temperature of 700°C was attained, the flow rate of ammonia was set to 1 l min^{-1} and the reactor was kept at this temperature for two hours. During the cooling down procedure, the NH_3 was replaced with N_2 when the temperature dropped down to 400°C . Similar to molybdenum and tungsten

oxynitrides, the synthesised vanadium oxynitride was passivated with Ar + 0.1 vol.% O₂ during two hours.

The synthesised materials were extensively characterised by XRD, SEM, low temperature N₂ adsorption and WDS. Electrodes for RDE and RRDE measurements were prepared by mixing the active materials with Super PTM Li carbon black (TIMCAL) and PVDF (Solvay) in a 69.86:22.95:7.19 weight ratio. NMP (Scharlau) was added to mixtures and slurries are mixed by sonication during 1 hour. The as-prepared slurries were deposited onto the glassy carbon disk electrode (4 mm diameter, 0.1256 cm², ALS Co. Ltd., Japan) and dried for one hour in a conventional oven at 50° C in vacuum. Electrocatalytic performance of the synthesised materials was compared by performing cyclic voltammetry measurements in the potential range between 0.2 and -0.7 V vs. Ag/AgCl reference electrode at the scan rate of 20 mV s⁻¹, with a Pt wire used as a counter electrode in 0.1 M KCl electrolyte. In order to determine the percentage of hydrogen peroxide formed during the ORR, rotating ring-disk electrode measurements were made with a Pt ring-modified electrode (0.188 cm², ALS Co. Ltd., Japan) in a four-electrode cell setup. The potential of the disk electrode was scanned at the scan rate of 20 mV s⁻¹ between 0.2 and -1 V vs. Ag/AgCl reference electrode, with a Pt wire as a counter electrode. Meanwhile, the potential of the ring electrode was fixed to 0.2 V vs. Ag/AgCl. The collection efficiency was calculated by performing RRDE measurements in 5 mM K₃[Fe(CN)₆] in 0.1 M KCl solution, deaerated with a flow of nitrogen for 30 minutes. The potential of the disk, rotating at 700-2300 rpm, was scanned from 0.45 to 0V at 20 mV s⁻¹, while the potential of the ring electrode was kept at 0.45 V.

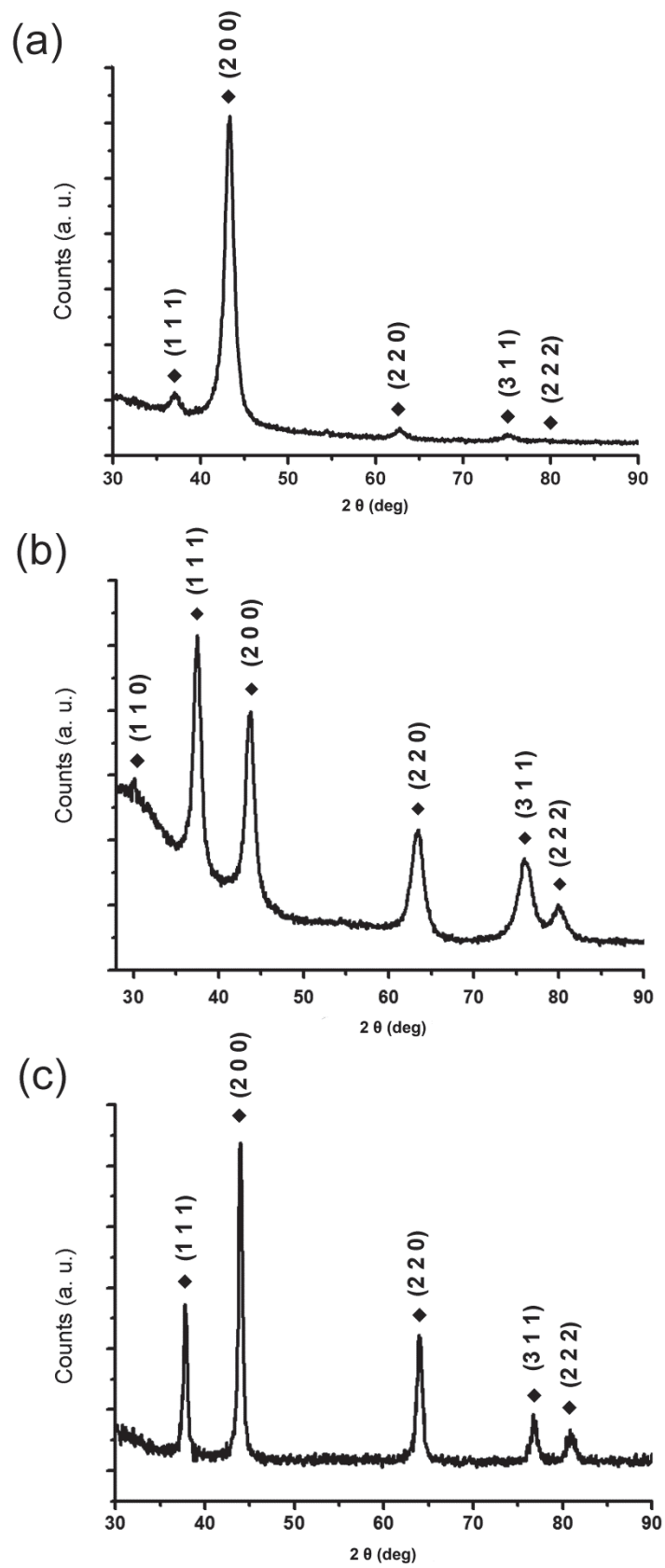


Figure 6.1. XRD patterns of molybdenum (a), tungsten (b) and vanadium (c) oxynitrides.

6.3 Characterisation of molybdenum, tungsten and vanadium oxynitrides

XRD patterns of the synthesised dark grey powders are presented on Figure 6.1. The diffractions peaks of molybdenum oxynitride (Figure 6.1 a) are located at 36.8°, 43.3°, 62.7°, 75.1° and 79.2° and match diffraction lines of γ -Mo₂N (Powder Diffraction File #: 25-1366) and Mo₃N₂ (PDF #: 89-3712). The XRD pattern of tungsten oxynitride (Figure 6.1 b), presenting diffraction peaks located at 30.1°, 37.5°, 43.7°, 63.4°, 76.1° and 80.1°, fits diffractions lines of W_{0.75}(N,O) (PDF#: 25-1255) and W₃N₄ (PDF#: 75-1002). Finally, peaks of vanadium oxynitride (Figure 6.1 c) match diffraction lines of VN (PDF#: 73-2038) and VO (PDF#: 75-0048), which both have cubic crystalline structures. It is known that this class of materials can exist in a broad range of compositions containing atoms of a transition metal, nitrogen and oxygen [17]. It is therefore difficult to determine the phase of these transition metal compounds based on XRD patterns alone.

Table 6.1 Average atomic percentages of elements in molybdenum, tungsten and vanadium oxynitrides.

	Metal (at. %)	Nitrogen (at. %)	Oxygen (at. %)	M/(N,O) ratio	O/N ratio
Mo(N,O)	38	45	16	0.6	0.4
W(N,O)	36	40	24	0.6	0.6
V(N,O)	42	44	15	0.7	0.3

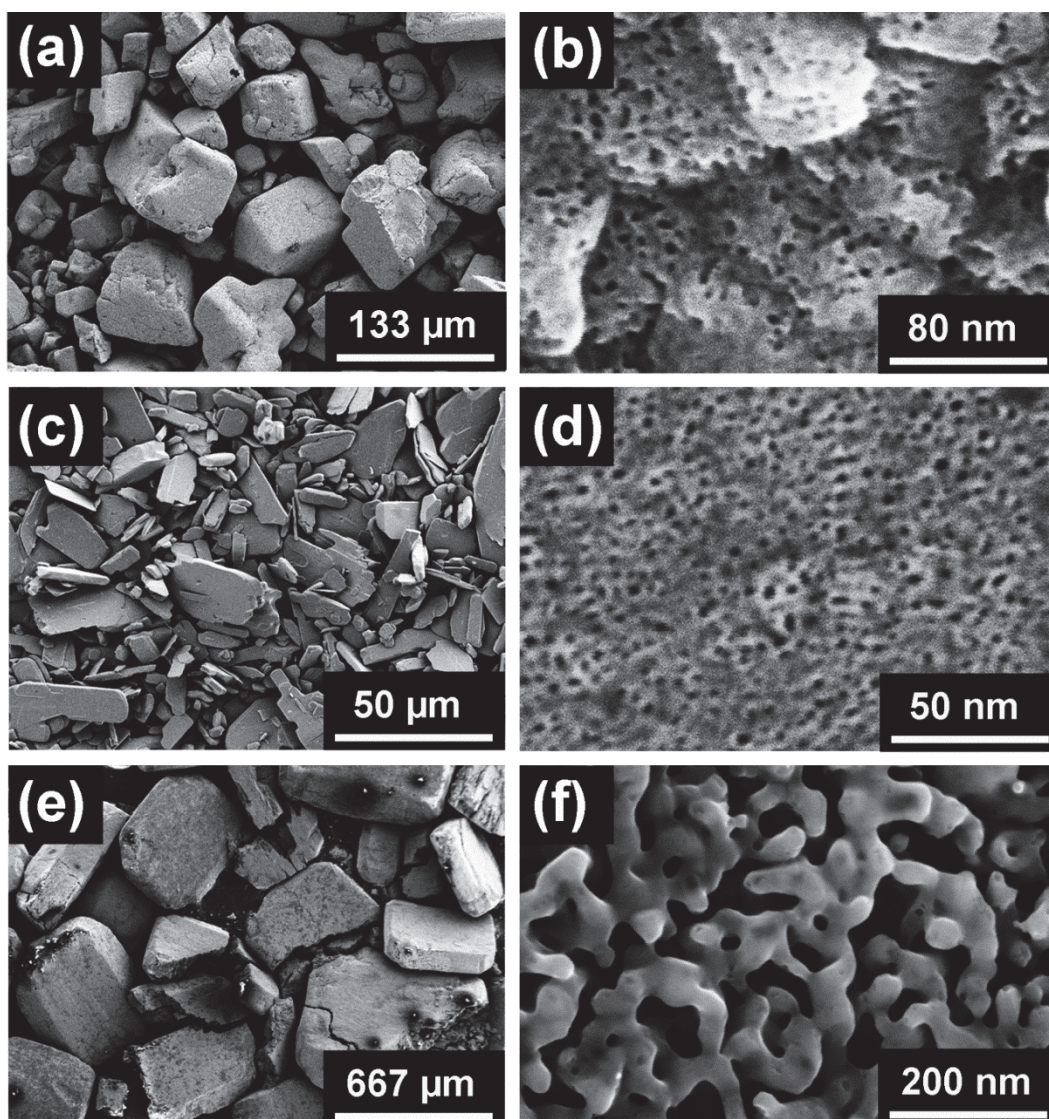


Figure 6.2. Low and high-magnification SEM images of tungsten (a, b), molybdenum (c, d) and vanadium (e, f) oxynitrides.

In order to investigate the composition of the synthesised materials in more detail, the elemental composition of each compound is analysed with WDS, using an electron microprobe. The results of WDS analysis are summarised in Table 6.1. It is important to note that this analysis is approximate due to the fact that samples are porous and contain light elements (WDS is more adapted for heavier elements). Furthermore, for V(N,O), the peaks of V and O overlap in WDS. The approximate elemental composition of molybdenum, tungsten and vanadium oxynitrides reveals the presence of non-negligible amount of oxygen (between 14.8 and 24.2 at. %) in all samples, thus confirming that the synthesised compounds are oxynitrides. In fact, the oxygen/ nitrogen ratios are 0.3 for

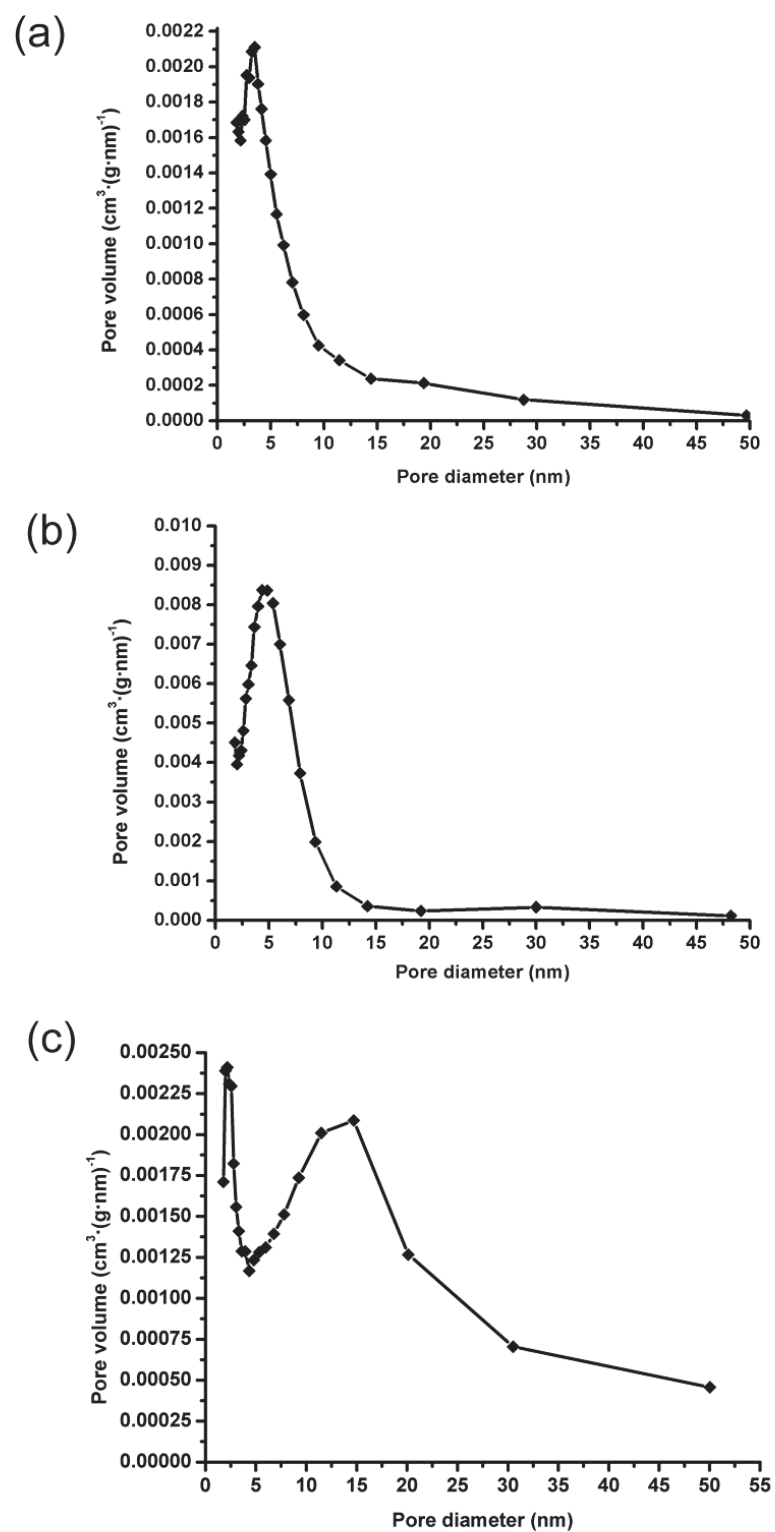


Figure 6.3. Pore size distribution for molybdenum (a), tungsten (b) and vanadium (c) oxynitrides.

V(N,O), 0.4 for Mo(N,O) and 0.6 for W(N,O) (Table 6.1). The metal to non-metal ratios indicate that the approximate stoichiometric compositions of the oxynitrides are $\text{Mo}_{0.6}(\text{N},\text{O})$, $\text{W}_{0.6}(\text{N},\text{O})$ and $\text{V}_{0.7}(\text{N},\text{O})$. Interestingly, $\text{Mo}_{0.6}(\text{N},\text{O})$ seems to deviate from the $\text{Mo}_2(\text{N},\text{O})$ and $\text{Mo}_3(\text{N},\text{O})_2$ phases expected from the XRD pattern (Figure 6.1 a). It has, however, been previously reported that a cubic $\text{Mo}_2\text{N}_{3-x}\text{O}_x$ is present near the surface in molybdenum nitrides [163], which correlates with our characterisation data. For simplicity, the oxynitrides are further denoted as Mo(N,O), W(N,O) and V(N,O).

Morphological characterisation of the synthesised materials (Figure 6.2) by SEM reveals porous structures at a high magnification (Figures 6.2 b, d, f). Low temperature N_2 adsorption measurements (Figure 6.3) confirm that the synthesised materials are mesoporous, with the maximum of the pore size distributions centred around 4 nm and 5 nm for molybdenum (Figure 6.3 a) and tungsten (Figure 6.3 b) oxynitrides, respectively. Vanadium oxynitride (Figure 6.3 c) possesses a bimodal pore size distribution and has, in addition to small pores centred around 3 nm, larger pores with diameters centred around 15 nm. These measurements are in agreement with the high-magnification SEM images (Figure 6.2 b, d, f). Surface areas of 42, 12 and 19 $\text{m}^2 \text{g}^{-1}$ are calculated with the BET method for tungsten, molybdenum and vanadium oxynitrides, respectively.

6.4 Electrocatalytic performance of molybdenum, tungsten and vanadium oxynitrides and oxygen reduction mechanism of molybdenum oxynitride

6.4.1 Comparison of the electrocatalytic performance of Mo(N,O), W(N,O) and V(N,O)

In order to compare the electrocatalytic performance of molybdenum, tungsten and vanadium oxynitrides, cyclic voltammograms are measured using a rotating disk electrode (RDE) technique (Figure 6.4) at the scan rate of 20 mV s^{-1} in the potential range between -0.7 and 0.2 V vs. Ag/AgCl reference electrode. When

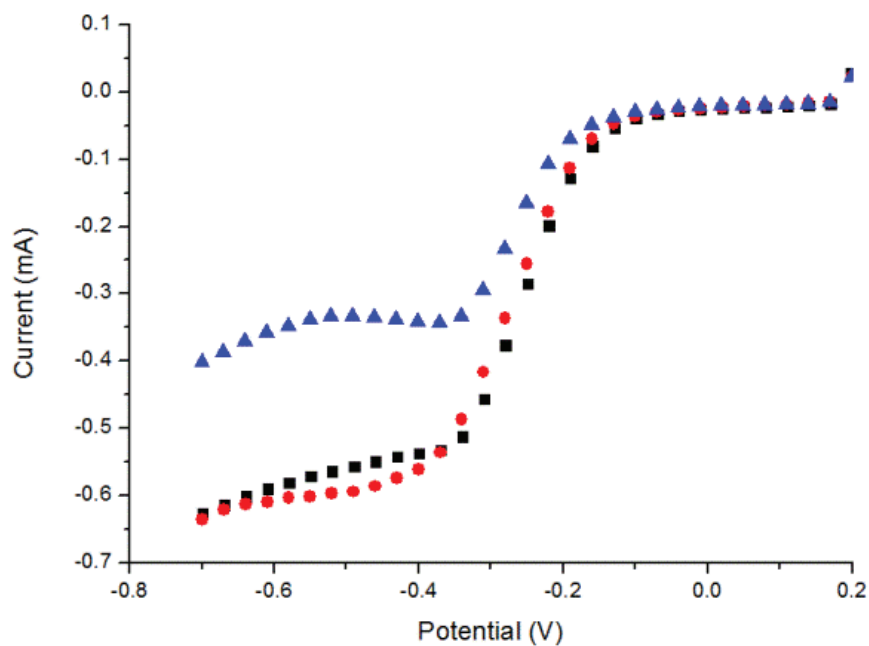


Figure 6.4. Voltammograms of tungsten (▲), molybdenum (■) and vanadium (●) oxynitrides performed with RDE at the rotation rate of 1000 rpm in 0.1 M KCl electrolyte.

comparing the cyclic voltammograms representing the ORR, it could be noted that molybdenum and vanadium oxynitrides demonstrate a similar electrocatalytic activity, with an onset potential of -0.156 V. Tungsten oxynitride, however, shows a more negative onset potential of -0.196 V, indicating that this compound is less active towards oxygen reduction reaction when compared to molybdenum and vanadium oxynitrides. Since tungsten oxynitride has the highest surface area among the three compounds, this behaviour could be explained by the presence of different active sites for ORR on the surface, as well as by the varying bulk properties of the materials. Since tungsten oxynitride possesses the highest amount of oxygen (Table 6.1), which is nearly the double of the amount present in vanadium and molybdenum oxynitrides, it could be speculated that oxygen content in oxynitrides could have an influence on the electrocatalytic performance.

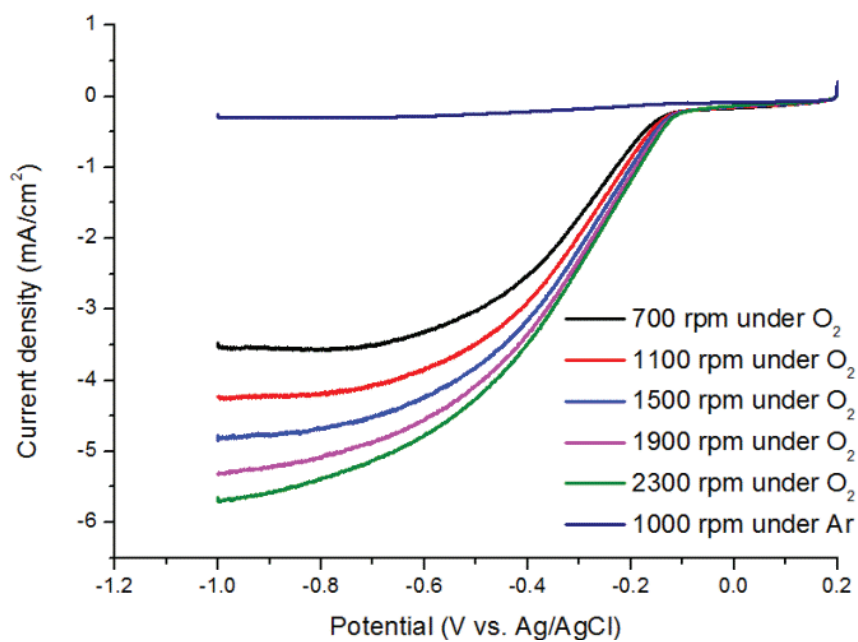


Figure 6.5. Voltammogram of molybdenum oxynitride at different rotation rates in 0.1 M KCl electrolyte.

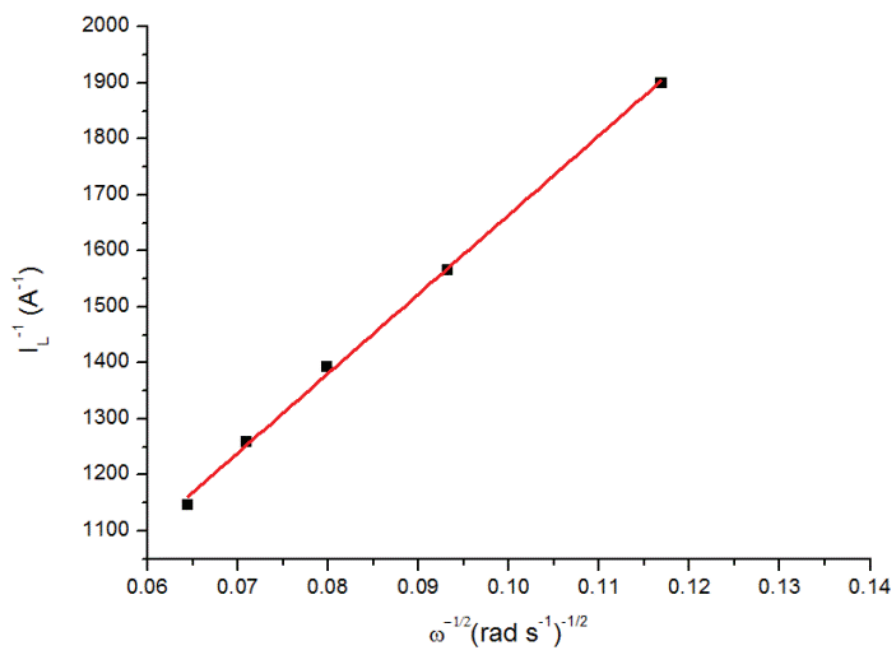


Figure 6.6. Koutecky-Levich plot for molybdenum oxynitride at the potential of -0.8 V vs. Ag/AgCl.

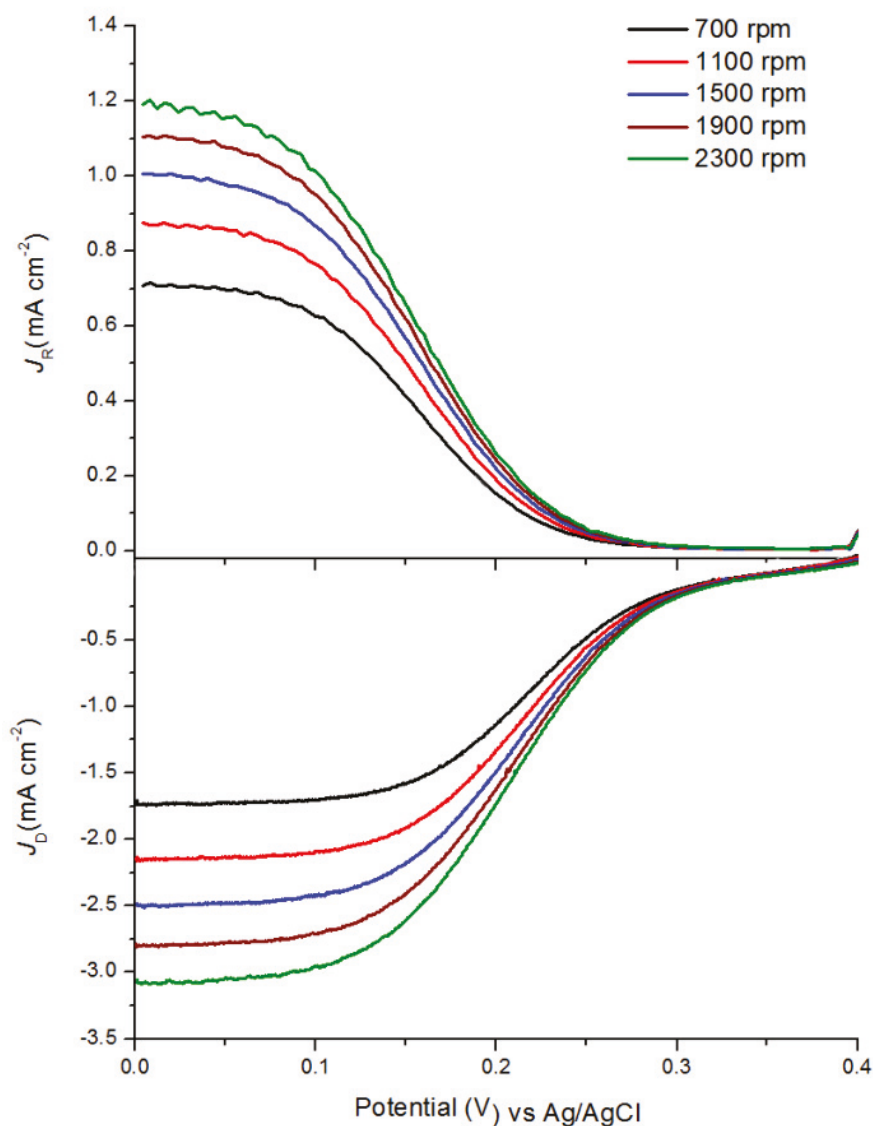


Figure 6.7. Ring (top) and disk (bottom) current densities for RRDE measurements performed in 5 mM $K_3[Fe(CN)_6]$ in 0.1 M KCl solution at different rotation rates.

6.4.2 Investigation of the oxygen reduction mechanism for molybdenum oxynitride

In order to determine the total number of transferred electrons, RDE measurements (Figure 6.5) in the potential range between 0.2 and -1 V vs. Ag/AgCl are performed, with the rotation rates varying from 700 to 2300 rpm under the flow of O_2 . Blank RDE measurement is performed under the flow of

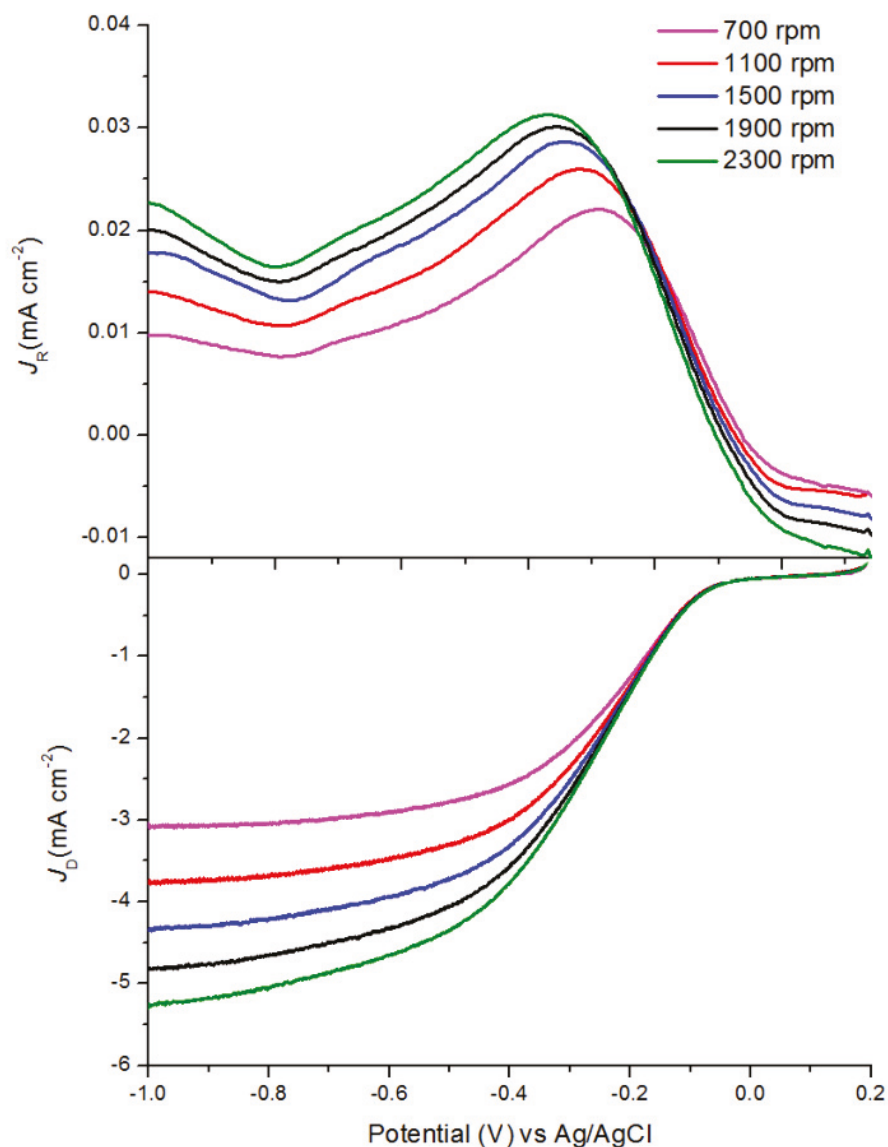


Figure 6.8. Ring (top) and disk (bottom) current densities for RRDE measurements performed in 0.1 M KCl solution at different rotation rates.

argon. To calculate the number of electrons, current in the diffusion-controlled potential range (-0.8 V vs. Ag/AgCl) is plotted as a function of the rotation rate (Koutecky-Levich plot, Figure 6.6). The number of electrons (n) is given by the equation 2.11 (Chapter 2). Here, n is equal to 4, indicating a four-electron ORR pathway.

In order to confirm the overall four-electron pathway and obtain more quantitative information on the ORR mechanism, the percentage of H₂O₂ generated is measured with rotating ring-disk electrode. In case of four-electron ORR mechanism, the amount hydrogen peroxide should be close to 0 %. First, the collection efficiency (N) is determined by performing RRDE studies using 5 mM K₃[Fe(CN)₆] in 0.1 M KCl solution (Figure 6.7). Afterwards, RRDE measurements are made in 0.1 M KCl electrolyte (Figure 6.8), and the percentage of hydrogen peroxide is determined by the procedure described in the experimental part (Chapter 2, section 2.3.5). For molybdenum oxynitride electrocatalyst, the calculated amount of hydrogen peroxide is 2.35 ± 0.18 %, which confirms the four-electron ORR pathway.

6.5 Conclusions

In this chapter, molybdenum, tungsten and vanadium oxynitrides are synthesised by the temperature-programmed reduction of the corresponding oxide precursors and extensively characterised by XRD, WDS, SEM and low temperature N₂ adsorption. The analysis reveals that although the XRD patterns of the synthesised materials match diffraction lines of nitrides, the compounds contain significant amounts of oxygen (between 15 at.% and 24 at.%), and therefore should be described as oxynitrides. The approximate stoichiometric compositions of molybdenum, tungsten and vanadium oxynitrides, estimated from the WDS analysis, are Mo_{0.6}(N,O), W_{0.6}(N,O) and V_{0.7}(N,O), respectively. Morphological characterisation by SEM shows the presence of pores, and the low temperature N₂ adsorption measurements confirm that the synthesised materials are, in fact, mesoporous.

Electrocatalytic performances of molybdenum, tungsten and vanadium oxynitrides for oxygen reduction reaction are compared using a cyclic voltammetry analysis with a rotating disk electrode in 0.1 M KCl electrolyte. These measurements reveal that molybdenum and vanadium oxynitrides have a similar electrocatalytic activity for ORR, with an onset potential at -0.156 V vs. Ag/AgCl, while tungsten oxynitride has a lower performance, with a more

negative onset potential of -0.196 V vs. Ag/AgCl. A more detailed analysis of the ORR mechanism is performed for molybdenum oxynitride. RDE and RRDE measurements reveal that oxygen is reduced via the four-electron pathway, as the number of transferred electrons, calculated from the Koutecky-Levich plot, is equal to four, and the amount of the generated peroxide, measured with RRDE, is only 2.35 ± 0.18 %.

Chapter 7. Summary and recommendations

In this thesis, transition metal oxynitrides have been investigated as candidates for applications in supercapacitors and as electrocatalysts for oxygen reduction reaction, and a number of gaps in the knowledge have been addressed. The materials investigated in this work are tungsten, molybdenum and vanadium oxynitrides. Furthermore, a bimetallic molybdenum tungsten oxynitride compound has been explored in supercapacitors for the first time.

In supercapacitors, many transition metal oxynitrides show a nearly ideal capacitive behaviour. For instance, tungsten oxynitride and molybdenum tungsten oxynitride demonstrate rectangular cyclic voltammograms and triangular galvanostatic charge and discharge curves, as well as a high reversibility of the charge storage mechanism. In this thesis, it is shown that this nearly ideal capacitive behaviour is very sensitive to the electrolyte, as well as the preparation and storage conditions of the compounds. More specifically, in case of tungsten oxynitride, upon electrochemical testing in a range of aqueous solutions containing alkaline and alkaline-earth metal cations (KCl, NaCl, LiCl and CaCl₂), the shape of the cyclic voltammogram shows changes depending on the presence of particular cations in the electrolyte. Additionally, it is reported for the first time that capacitive properties of transition metal oxynitrides evolve upon storage in the ambient air and these changes are material-specific. Tungsten oxynitride, for instance, demonstrates distortions of the shapes of cyclic voltammograms and a loss of reversibility upon ageing due to the oxidation of the surface, while molybdenum oxynitride shows an increase of the rate capability. Furthermore, it is demonstrated that although the passivation of the samples prior exposure to air slows down the oxidation, it does not prevent it. It is therefore recommended to carefully control the storage conditions of the oxynitrides.

In addition to nearly ideal shapes of cyclic voltammograms, transition metal oxynitrides predominantly show good rate capabilities due to their high intrinsic conductivities, as opposed to their corresponding oxides. For example, tungsten oxynitride demonstrates approximately 40 % of the initial capacitance retention upon a 200-fold increase of the current load, while molybdenum tungsten oxynitride retains up to 50 % of the initial capacitance upon a 400-fold increase of the current density in a symmetric cell setup. This property is particularly important for high-power applications of supercapacitors for instance, in the automotive sector.

Additionally, good cyclic stabilities are observed for tungsten and molybdenum tungsten oxynitrides. These stabilities, however, show variations depending on the electrolyte. Tungsten oxynitride, for instance, is tested for up to 1000 galvanostatic charge and discharge cycles in 1M KOH solution, while only 300 and 400 cycles are performed in 1M H₂SO₄ and 3 M NaCl electrolytes, respectively, before a significant loss of the reversibility is observed. It is suggested that the difference in the stability between the acidic and alkaline solutions could be explained by the oxidation of tungsten oxynitride in 1M H₂SO₄ electrolyte. Furthermore, it is proposed in this thesis to use galvanostatic charging and discharging, in addition to cyclic voltammetry, as a standard procedure to measure the long-term cyclic stability, as a different cyclic behaviour is observed when comparing data measured with cyclic voltammetry and galvanostatic charge/discharge experiments. More specifically, a faster loss of reversibility is observed upon galvanostatic cycling. The galvanostatic charging and discharging technique could also be coupled with floating potential tests.

The observed specific capacitance values per unit of electrode area indicate a presence of pseudocapacitive processes in addition to the electrical double-layer formation for the compounds presented in this thesis, as the measured values largely exceed the 20-50 $\mu\text{F cm}^{-2}$ typical for the EDLC. Based on the comparison of the charged and discharged tungsten oxynitride electrodes by the X-ray diffraction, it is proposed that for this particular compound, the pseudocapacitive ion/proton intercalation does not take place, while ion/proton adsorption is a possible charge storage mechanism.

Although the larger portion of the thesis is dedicated to the electrochemical properties of transition metal oxynitrides in supercapacitors, electrocatalytic properties of these compounds are investigated as well. More specifically, electrocatalytic activities of molybdenum, tungsten and vanadium oxynitrides towards oxygen reduction reaction are compared. In addition, the ORR mechanism is explored for a pure, unsupported molybdenum oxynitride, and an overall four-electron oxygen reduction pathway is measured, demonstrating a good electrocatalytic performance.

Results presented in this thesis confirm that a number of transition metal oxynitrides are promising candidates for applications in the new energy storage devices such as supercapacitors and metal-air batteries. Particularly, in supercapacitors, active electrode materials should possess high specific capacitance values, good rate capabilities as well as high cyclic stabilities. Transition metal oxynitrides presented in this work show a nearly ideal capacitive behaviour with a pseudocapacitive charge storage mechanism, high rate capabilities as well as good cyclic stabilities. Although the maximum specific capacitance values for oxynitrides presented in this thesis are modest, in a range between 85 and 124 F g⁻¹, it would be interesting, in my view, to compare the volumetric rather than gravimetric capacitance values. The volumetric capacitance for this type of pseudocapacitive materials exceed the corresponding values for the carbon-based compounds, as pointed out by Y. Gogotsi *et al.* [164], which is an advantage for a range of specific, space-limited applications. Additionally, it is suggested in this thesis that particular attention should be paid to the fact that electrochemical properties of these compounds are very sensitive to the preparation and storage conditions, as well as to the electrolyte used. Furthermore, it is observed that transition metal oxynitrides are subjected to self-discharge, *i.e.* the decline of the voltage after charging [58]. It would be, in my view, important to explore this phenomenon. In summary, although transition metal oxynitrides demonstrate an attractive electrochemical performance, further work addressing the self-discharge is required in order to evaluate advantages and limitation of this type of compounds in view of the application in the real devices.

References

- [1] R. A. Huggins, *Energy storage*, Springer, New York; London, 2010.
- [2] M. Beaudin, H. Zareipour, A. Schellenberglabe, W. Rosehart, *Energy storage for mitigating the variability of renewable electricity sources: an updated review*, *Energy Sustain. Dev.*, 14 (2010) 302-314.
- [3] R.-S. Liu, L. Zhang, X. Sun, H. Lui, JiuJun Zhang, *Electrochemical technologies for energy storage and conversion*, Wiley-VCH, Weinheim, 2012.
- [4] B. Dunn, H. Kamath, J. M. Tarascon, *Electrical energy storage for the grid: a battery of choices*, *Science*, 334 (2011) 928-935.
- [5] E. Karden, S. Ploumen, B. Fricke, T. Miller, K. Snyder, *Energy storage devices for future hybrid electric vehicles*, *J. Power Sources*, 168 (2007) 2-11.
- [6] H. Ibrahim, A. Ilinca, J. Perron, *Energy storage systems - characteristics and comparisons*, *Renew. Sust. Energ. Rev.*, 12 (2008) 1221-1250.
- [7] C. Lefrou, P. Fabry, J.-C. Poignet, *Electrochemistry: the basics, with examples*, Springer, Heidelberg; New York; Dordrecht; London, 2012.
- [8] B. L. Ellis, L. F. Nazar, *Sodium and sodium-ion energy storage batteries*, *Curr. Opin. Solid St. M.*, 16 (2012) 168-177.
- [9] N. S. Choi, Z. H. Chen, S. A. Freunberger, X. L. Ji, Y. K. Sun, K. Amine, G. Yushin, L. F. Nazar, J. Cho, P. G. Bruce, *Challenges facing lithium batteries and electrical double-layer capacitors*, *Angew. Chem. Int. Edit.*, 51 (2012) 9994-10024.
- [10] J. Christensen, P. Albertus, R. S. Sanchez-Carrera, T. Lohmann, B. Kozinsky, R. Liedtke, J. Ahmed, A. Kojic, *A critical review of Li/Air batteries*, *J. Electrochem. Soc.*, 159 (2012) R1-R30.
- [11] M. Conte, *Supercapacitors Technical Requirements for New Applications*, *Fuel Cells*, 10 (2010) 806-818.
- [12] G. Girishkumar, B. McCloskey, A. C. Luntz, S. Swanson, W. Wilcke, *Lithium - air battery: promise and challenges*, *J. Phys. Chem. Lett.*, 1 (2010) 2193-2203.

- [13] A. Yu, V. Chabot, J. Zhang, Electrochemical supercapacitors for energy storage and delivery: fundamental applications, CRC Press: Taylor and Francis group, Boca Raton (FL), 2013 .
- [14] R. Cao, J. S. Lee, M. L. Liu, J. Cho, Recent progress in non-precious catalysts for metal-air batteries, *Adv. Energy Mater.*, 2 (2012) 816-829.
- [15] F. Y. Cheng, J. Chen, Metal-air batteries: from oxygen reduction electrochemistry to cathode catalysts, *Chem. Soc. Rev.*, 41 (2012) 2172-2192.
- [16] B. W. Downing, Metal-air technology, in: R.-S. Liu, L. Zhang, X. Sun, H. Lui, J. Zhang, *Electrochemical technologies for energy storage and conversion*, Wiley-VCH, Weinheim, 2012.
- [17] L. E. Toth, *Transition metal carbides and nitrides*, Academic Press, New York; London, 1971.
- [18] S. T. Oyama, *The chemistry of transition metal carbides and nitrides*, Blackie Academic & Professional, an imprint of Chapman & Hall, Glasgow, 1996.
- [19] S. T. Oyama, J. C. Schlatter, J. E. Metcalfe, J. M. Lambert, Preparation and characterization of early transition-metal carbides and nitrides, *Ind. Eng. Chem. Res.*, 27 (1988) 1639-1648.
- [20] S. T. Oyama, Crystal-structure and chemical-reactivity of transition-metal carbides and nitrides, *J. Solid State Chem.*, 96 (1992) 442-445.
- [21] S. M. Dong, X. Chen, X. Y. Zhang, G. L. Cui, Nanostructured transition metal nitrides for energy storage and fuel cells, *Coordin. Chem. Rev.*, 257 (2013) 1946-1956.
- [22] A. M. Glushenkov, D. Hulicova-Jurcakova, D. Llewellyn, G. Q. Lu, Y. Chen, Structure and capacitive properties of porous nanocrystalline VN prepared by temperature-programmed ammonia reduction of V₂O₅, *Chem. Mater.*, 22 (2010) 914-921.
- [23] X. H. Zhou, C. Q. Shang, L. Gu, S. M. Dong, X. Chen, P. X. Han, L. F. Li, J. H. Yao, Z. H. Liu, H. X. Xu, Y. W. Zhu, G. L. Cui, Mesoporous coaxial titanium nitride-vanadium nitride fibers of core-shell structures for high-performance supercapacitors, *ACS Appl. Mater. Inter.*, 3 (2011) 3058-3063.
- [24] H. O. Pierson, *Handbook of refractory carbides and nitrides : properties, characteristics, processing, and applications*, Noyes Publications, Park Ridge (NJ), 1996.

- [25] S. T. Oyama, Preparation and catalytic properties of transition-metal carbides and nitrides, *Catal. Today*, 15 (1992) 179-200.
- [26] Q. Sun, Z. W. Fu, Vanadium nitride as a novel thin film anode material for rechargeable lithium batteries, *Electrochim. Acta*, 54 (2008) 403-409.
- [27] Q. Sun, Z. W. Fu, An anode material of CrN for lithium-ion batteries, *Electrochem. Solid State Lett.*, 10 (2007) A189-A193.
- [28] Z. W. Fu, Y. Wang, X. L. Yue, S. L. Zhao, Q. Z. Qin, Electrochemical reactions of lithium with transition metal nitride electrodes, *J. Phys. Chem. B*, 108 (2004) 2236-2244.
- [29] Q. Sun, Z. W. Fu, Mn_3N_2 as a novel negative electrode material for rechargeable lithium batteries, *Appl. Surf. Sci.*, 258 (2012) 3197-3201.
- [30] S. Bouhtiyya, R. L. Porto, B. Laik, P. Boulet, F. Capon, J. P. Pereira-Ramos, T. Brousse, J. F. Pierson, Application of sputtered ruthenium nitride thin films as electrode material for energy-storage devices, *Scripta Mater.*, 68 (2013) 659-662.
- [31] Y. N. Zhou, C. Liu, H. J. Chen, L. Zhang, W. J. Li, Z. W. Fu, Electrochemistry of V_2ON with lithium, *Electrochim. Acta*, 56 (2011) 5532-5537.
- [32] B. Das, M. V. Reddy, G. V. S. Rao, B. V. R. Chowdari, Synthesis and Li-storage behavior of CrN nanoparticles, *RSC Adv.*, 2 (2012) 9022-9028.
- [33] B. Das, M. V. Reddy, G. V. S. Rao, B. V. R. Chowdari, Synthesis of porous-CoN nanoparticles and their application as a high capacity anode for lithium-ion batteries, *J. Mater. Chem.*, 22 (2012) 17505-17510.
- [34] B. Das, M. V. Reddy, B. V. R. Chowdari, X-ray absorption spectroscopy and energy storage of Ni-doped cobalt nitride, $(Ni_{0.33}Co_{0.67})N$, prepared by a simple synthesis route, *Nanoscale*, 5 (2013) 1961-1966.
- [35] B. Das, M. V. Reddy, P. Malar, T. Osipowicz, G. V. S. Rao, B. V. R. Chowdari, Nanoflake CoN as a high capacity anode for Li-ion batteries, *Solid State Ionics*, 180 (2009) 1061-1068.
- [36] P. Pande, P. G. Rasmussen, L. T. Thompson, Charge storage on nanostructured early transition metal nitrides and carbides, *J. Power Sources*, 207 (2012) 212-215.
- [37] X. P. Zhou, H. Y. Chen, D. Shu, C. He, J. M. Nan, Study on the electrochemical behavior of vanadium nitride as a promising supercapacitor material, *J. Phys. Chem. Solids*, 70 (2009) 495-500.

- [38] F. K. Cheng, C. He, D. Shu, H. Y. Chen, J. Zhang, S. Q. Tang, D. E. Finlow, Preparation of nanocrystalline VN by the melamine reduction of V_2O_5 xerogel and its supercapacitive behavior, *Mater. Chem. Phys.*, 131 (2011) 268-273.
- [39] D. Choi, G. E. Blomgren, P. N. Kumta, Fast and reversible surface redox reaction in nanocrystalline vanadium nitride supercapacitors, *Adv. Mater.*, 18 (2006) 1178-1182.
- [40] A. R. Ko, S. B. Han, Y. W. Lee, K. W. Park, Template-free synthesis and characterization of mesoporous tungsten nitride nanoplates, *Phys. Chem. Chem. Phys.*, 13 (2011) 12705-12707.
- [41] D. Choi, P. N. Kumta, Synthesis, structure, and electrochemical characterization of nanocrystalline tantalum and tungsten nitrides, *J. Am. Ceram. Soc.*, 90 (2007) 3113-3120.
- [42] M. Wixom, L. Owens, J. Parker, J. Lee, I. Song, L. T. Thompson, High surface area metal nitride and carbide electrode materials, *Proceedings of the symposium on electrochemical capacitors II*, 96 (1997) 63-74.
- [43] C. Z. Deng, K. C. Tsai, Characterization of molybdenum nitride as an ultracapacitor material, *Proceedings of the symposium on electrochemical capacitors II*, 96 (1997) 75-84.
- [44] X. L. Li, Y. Xing, H. Wang, H. L. Wang, W. D. Wang, X. Y. Chen, Synthesis and characterization of uniform nanoparticles of γ - Mo_2N for supercapacitors, *Trans. Nonferrous Met. Soc. China*, 19 (2009) 620-625.
- [45] G. L. Cui, S. M. Dong, X. A. Chen, L. Gu, X. H. Zhou, H. X. Xu, H. B. Wang, Z. H. Liu, P. X. Han, J. H. Yao, L. Wang, L. Q. Chen, Facile preparation of mesoporous titanium nitride microspheres for electrochemical energy storage, *ACS Appl. Mater. Inter.*, 3 (2011) 93-98.
- [46] D. Choi, P. N. Kumta, Nanocrystalline TiN derived by a two-step halide approach for electrochemical capacitors, *J. Electrochem. Soc.*, 153 (2006) A2298-A2303.
- [47] R. L. Porto, R. Frappier, J. B. Ducros, C. Aucher, H. Mosqueda, S. Chenu, B. Chavillon, F. Tessier, F. Chevire, T. Brousse, Titanium and vanadium oxynitride powders as pseudo-capacitive materials for electrochemical capacitors, *Electrochim. Acta*, 82 (2012) 257-262.

- [48] G. R. Li, J. Song, G. L. Pan, X. P. Gao, Highly Pt-like electrocatalytic activity of transition metal nitrides for dye-sensitized solar cells, *Energy Environ. Sci.*, 4 (2011) 1680-1683.
- [49] Y. D. Wang, M. X. Wu, X. Lin, Z. C. Shi, A. Hagfeldt, T. L. Ma, Several highly efficient catalysts for Pt-free and FTO-free counter electrodes of dye-sensitized solar cells, *J. Mater. Chem.*, 22 (2012) 4009-4014.
- [50] T. L. Ma, M. X. Wu, Q. Y. Zhang, J. Q. Xiao, C. Y. Ma, X. Lin, C. Y. Miao, Y. J. He, Y. R. Gao, A. Hagfeldt, Two flexible counter electrodes based on molybdenum and tungsten nitrides for dye-sensitized solar cells, *J. Mater. Chem.*, 21 (2011) 10761-10766.
- [51] J. Giner, L. Swette, Oxygen reduction on titanium nitride in alkaline electrolyte, *Nature*, 211 (1966) 1291-1292.
- [52] Y. R. Wang, R. H. Ohnishi, E. Yoo, P. He, J. Kubota, K. Domen, H. S. Zhou, Nano- and micro-sized TiN as the electrocatalysts for ORR in Li-air fuel cell with alkaline aqueous electrolyte, *J. Mater. Chem.*, 22 (2012) 15549-15555.
- [53] D. G. Xia, S. Z. Liu, Z. Y. Wang, G. Chen, L. J. Zhang, L. Zhang, S. Q. Hui, J. J. Zhang, Methanol-tolerant MoN electrocatalyst synthesized through heat treatment of molybdenum tetraphenylporphyrin for four-electron oxygen reduction reaction, *J. Power Sources*, 177 (2008) 296-302.
- [54] J. Qi, L. H. Jiang, Q. A. Jiang, S. L. Wang, G. Q. Sun, Theoretical and experimental studies on the relationship between the structures of molybdenum nitrides and their catalytic activities toward the oxygen reduction reaction, *J. Phys. Chem. C*, 114 (2010) 18159-18166.
- [55] H. M. Zhang, H. X. Zhong, G. Liu, Y. M. Liang, J. W. Hu, B. L. Yi, A novel non-noble electrocatalyst for PEM fuel cell based on molybdenum nitride, *Electrochem. Commun.*, 8 (2006) 707-712.
- [56] S. Doi, A. Ishihara, S. Mitsushima, N. Kamiya, K. I. Ota, Zirconium-based compounds for cathode of polymer electrolyte fuel cell, *J. Electrochem. Soc.*, 154 (2007) B362-B369.
- [57] A. Ishihara, S. Doi, S. Mitsushima, K. Ota, Tantalum (oxy)nitrides prepared using reactive sputtering for new nonplatinum cathodes of polymer electrolyte fuel cell, *Electrochim. Acta*, 53 (2008) 5442-5450.
- [58] B. E. Conway, *Electrochemical Supercapacitors: Scientific Fundamentals and Technological Applications*, Kluwer Academic, New York, 1999.

- [59] R. Kotz, M. Carlen, Principles and applications of electrochemical capacitors, *Electrochim. Acta*, 45 (2000) 2483-2498.
- [60] A. Burke, Ultracapacitors: why, how, and where is the technology, *J. Power Sources*, 91 (2000) 37-50.
- [61] B. E. Conway, V. Birss, J. Wojtowicz, The role and utilization of pseudocapacitance for energy storage by supercapacitors, *J. Power Sources*, 66 (1997) 1-14.
- [62] A. G. Pandolfo, A. F. Hollenkamp, Carbon properties and their role in supercapacitors, *J. Power Sources*, 157 (2006) 11-27.
- [63] X. Zhao, B. M. Sanchez, P. J. Dobson, P. S. Grant, The role of nanomaterials in redox-based supercapacitors for next generation energy storage devices, *Nanoscale*, 3 (2011) 839-855.
- [64] G. P. Wang, L. Zhang, J. J. Zhang, A review of electrode materials for electrochemical supercapacitors, *Chem. Soc. Rev.*, 41 (2012) 797-828.
- [65] W. T. Deng, X. B. Ji, Q. Y. Chen, C. E. Banks, Electrochemical capacitors utilising transition metal oxides: an update of recent developments, *RSC Adv.*, 1 (2011) 1171-1178.
- [66] B. E. Conway, Transition from supercapacitor to battery behavior in electrochemical energy-storage, *J. Electrochem. Soc.*, 138 (1991) 1539-1548.
- [67] J. P. Zheng, T. R. Jow, A new charge storage mechanism for electrochemical capacitors, *J. Electrochem. Soc.*, 142 (1995) L6-L8.
- [68] P. Simon, Y. Gogotsi, Materials for electrochemical capacitors, *Nat. Mater.*, 7 (2008) 845-854.
- [69] J. P. Zheng, P. J. Cygan, T. R. Jow, Hydrrous ruthenium oxide as an electrode material for electrochemical capacitors, *J. Electrochem. Soc.*, 142 (1995) 2699-2703.
- [70] C. J. Xu, F. Y. Kang, B. H. Li, H. D. Du, Recent progress on manganese dioxide based supercapacitors, *J. Mater. Res.*, 25 (2010) 1421-1432.
- [71] H. Y. Lee, V. Manivannan, J. B. Goodenough, Electrochemical capacitors with KCl electrolyte, *C. R. Acad. Sci. II C*, 2 (1999) 565-577.
- [72] R. G. Reddy, R. N. Reddy, Sol-gel MnO₂ as an electrode material for electrochemical capacitors, *J. Power Sources*, 124 (2003) 330-337.

- [73] Y. U. Jeong, A. Manthiram, Nanocrystalline manganese oxides for electrochemical capacitors with neutral electrolytes, *J. Electrochem. Soc.*, 149 (2002) A1419-A1422.
- [74] S. L. Kuo, N. L. Wu, Investigation of pseudocapacitive charge-storage reaction of $\text{MnO}_2 \cdot n\text{H}_2\text{O}$ supercapacitors in aqueous electrolytes, *J. Electrochem. Soc.*, 153 (2006) A1317-A1324.
- [75] L. Athouel, F. Moser, R. Dugas, O. Crosnier, D. Belanger, T. Brousse, Variation of the MnO_2 birnessite structure upon charge/discharge in an electrochemical supercapacitor electrode in aqueous Na_2SO_4 electrolyte, *J. Phys. Chem. C*, 112 (2008) 7270-7277.
- [76] H. Kanoh, W. P. Tang, Y. Makita, K. Ooi, Electrochemical intercalation of alkali-metal ions into birnessite-type manganese oxide in aqueous solution, *Langmuir*, 13 (1997) 6845-6849.
- [77] O. Ghodbane, J. L. Pascal, F. Favier, Microstructural effects on charge-storage properties in MnO_2 -based electrochemical supercapacitors, *ACS Appl. Mater. Inter.*, 1 (2009) 1130-1139.
- [78] C. J. Xu, C. G. Wei, B. H. Li, F. Y. Kang, Z. C. Guan, Charge storage mechanism of manganese dioxide for capacitor application: Effect of the mild electrolytes containing alkaline and alkaline-earth metal cations, *J. Power Sources*, 196 (2011) 7854-7859.
- [79] D. Belanger, M. Toupin, T. Brousse, Influence of microstructure on the charge storage properties of chemically synthesized manganese dioxide, *Chem. Mater.*, 14 (2002) 3946-3952.
- [80] P. Ragupathy, H. N. Vasan, N. Munichandraiah, Synthesis and characterization of nano- MnO_2 for electrochemical supercapacitor studies, *J. Electrochem. Soc.*, 155 (2008) A34-A40.
- [81] S. Devaraj, N. Munichandraiah, Effect of crystallographic structure of MnO_2 on its electrochemical capacitance properties, *J. Phys. Chem. C*, 112 (2008) 4406-4417.
- [82] T. Brousse, M. Toupin, R. Dugas, L. Athouel, O. Crosnier, D. Belanger, Crystalline MnO_2 as possible alternatives to amorphous compounds in electrochemical supercapacitors, *J. Electrochem. Soc.*, 153 (2006) A2171-A2180.

- [83] O. Ghodbane, J. L. Pascal, F. Favier, Microstructural effects on charge-storage properties in MnO₂-based electrochemical supercapacitors, *ACS Appl. Mater. Inter.*, 1 (2009) 1130-1139.
- [84] M. J. Zhi, C. C. Xiang, J. T. Li, M. Li, N. Q. Wu, Nanostructured carbon-metal oxide composite electrodes for supercapacitors: a review, *Nanoscale*, 5 (2013) 72-88.
- [85] C. D. Lokhande, D. P. Dubal, O. S. Joo, Metal oxide thin film based supercapacitors, *Curr. Appl. Phys.*, 11 (2011) 255-270.
- [86] Y. Li, Y. Zhang, R. Raval, C. Li, R. Zhai, Q. Xin, The modification of molybdenum nitrides: the effect of the second metal component, *Catal. Lett.*, 48 (1997) 239-245.
- [87] C. C. Yu, S. T. Oyama, Synthesis and characterization of new bimetallic transition-metal oxynitrides - M(I)-M(II)-O-N (M(I), M(II)=V, Mo, W and Nb), *J. Mater. Sci.*, 30 (1995) 4037-4042.
- [88] C. C. Yu, S. Ramanathan, F. Sherif, S. T. Oyama, Structural, surface, and catalytic properties of a new bimetallic V-Mo oxynitride catalyst for hydrodenitrogenation, *J. Phys. Chem.*, 98 (1994) 13038-13041.
- [89] C. L. Chen, D. L. Zhao, D. Xu, X. K. Wang, Gamma-Mo₂N/Co₃Mo₃N composite material for electrochemical supercapacitor electrode, *Mater. Chem. Phys.*, 95 (2006) 84-88.
- [90] D. H. Cho, T. S. Chang, C. H. Shin, Variations in the surface structure and composition of tungsten oxynitride catalyst caused by exposure to air, *Catal. Lett.*, 67 (2000) 163-169.
- [91] X. Gouin, R. Marchand, P. Lharidon, Y. Laurent, Reaction of ammonia with molybdenum oxide - physicochemical characterization of an Mo₂N-gamma type oxynitride phase, *J. Solid State Chem.*, 109 (1994) 175-180.
- [92] C. Sayag, G. Bugli, P. Havi, G. Djega-Mariadassou, Surface studies of passivated molybdenum oxynitride, *J. Catal.*, 167 (1997) 372-378.
- [93] J. Zhang, PEM fuel cell electrocatalysts and catalyst layers: fundamentals and applications, Springer, London, 2008.
- [94] Z. W. Chen, D. Higgins, A. P. Yu, L. Zhang, J. J. Zhang, A review on non-precious metal electrocatalysts for PEM fuel cells, *Energy Environ. Sci.*, 4 (2011) 3167-3192.

- [95] V. Neburchilov, H. J. Wang, J. J. Martin, W. Qu, A review on air cathodes for zinc-air fuel cells, *J. Power Sources*, 195 (2010) 1271-1291.
- [96] N. M. Markovic, T. J. Schmidt, V. Stamenkovic, P. N. Ross, Oxygen reduction reaction on Pt and Pt bimetallic surfaces: a selective review, *Fuel Cells*, 1 (2001) 105-116.
- [97] Y. H. Bing, H. S. Liu, L. Zhang, D. Ghosh, J. J. Zhang, Nanostructured Pt-alloy electrocatalysts for PEM fuel cell oxygen reduction reaction, *Chem. Soc. Rev.*, 39 (2010) 2184-2202.
- [98] D. Y. Qu, Investigation of oxygen reduction on activated carbon electrodes in alkaline solution, *Carbon*, 45 (2007) 1296-1301.
- [99] Y. G. Li, W. Zhou, H. L. Wang, L. M. Xie, Y. Y. Liang, F. Wei, J. C. Idrobo, S. J. Pennycook, H. J. Dai, An oxygen reduction electrocatalyst based on carbon nanotube-graphene complexes, *Nat. Nanotechnol.*, 7 (2012) 394-400.
- [100] M. N. Zhang, Y. M. Yan, K. P. Gong, L. Q. Mao, Z. X. Guo, Y. Chen, Electrostatic layer-by-layer assembled carbon nanotube multilayer film and its electrocatalytic activity for O₂ reduction, *Langmuir*, 20 (2004) 8781-8785.
- [101] G. Liu, X. G. Li, J. W. Lee, B. N. Popov, A review of the development of nitrogen-modified carbon-based catalysts for oxygen reduction at USC, *Catal. Sci. Technol.*, 1 (2011) 207-217.
- [102] S. R. Stoyanov, A. V. Titov, P. Kral, Transition metal and nitrogen doped carbon nanostructures, *Coordin. Chem. Rev.*, 253 (2009) 2852-2871.
- [103] K. P. Gong, F. Du, Z. H. Xia, M. Durstock, L. M. Dai, Nitrogen-doped carbon nanotube arrays with high electrocatalytic activity for oxygen reduction, *Science*, 323 (2009) 760-764.
- [104] Y. L. Li, J. J. Wang, X. F. Li, D. S. Geng, R. Y. Li, X. L. Sun, Superior energy capacity of graphene nanosheets for a nonaqueous lithium-oxygen battery, *Chem. Commun.*, 47 (2011) 9438-9440.
- [105] C. Z. Zhu, S. J. Dong, Recent progress in graphene-based nanomaterials as advanced electrocatalysts towards oxygen reduction reaction, *Nanoscale*, 5 (2013) 1753-1767.
- [106] F. H. B. Lima, M. L. Calegari, E. A. Ticianelli, Electrocatalytic activity of manganese oxides prepared by thermal decomposition for oxygen reduction, *Electrochim. Acta*, 52 (2007) 3732-3738.

- [107] L. Q. Mao, T. Sotomura, K. Nakatsu, N. Koshiba, D. Zhang, T. Ohsaka, Electrochemical characterization of catalytic activities of manganese oxides to oxygen reduction in alkaline aqueous solution, *J. Electrochem. Soc.*, 149 (2002) A504-A507.
- [108] K. M. Parida, S. B. Kanungo, B. R. Sant, Studies on MnO₂. 1. Chemical-composition, microstructure and other characteristics of some synthetic MnO₂ of various crystalline modifications, *Electrochim. Acta*, 26 (1981) 435-443.
- [109] F. Y. Cheng, J. Shen, W. Q. Ji, Z. L. Tao, J. Chen, Selective synthesis of manganese oxide nanostructures for electrocatalytic oxygen reduction, *ACS Appl. Mater. Inter.*, 1 (2009) 460-466.
- [110] F. Y. Cheng, Y. Su, J. Liang, Z. L. Tao, J. Chen, MnO₂-based nanostructures as catalysts for electrochemical oxygen reduction in alkaline media, *Chem. Mater.*, 22 (2010) 898-905.
- [111] F. H. B. Lima, M. L. Calegari, E. A. Ticianelli, Investigations of the catalytic properties of manganese oxides for the oxygen reduction reaction in alkaline media, *J. Electroanal. Chem.*, 590 (2006) 152-160.
- [112] J. B. Xu, P. Gao, T. S. Zhao, Non-precious Co₃O₄ nano-rod electrocatalyst for oxygen reduction reaction in anion-exchange membrane fuel cells, *Energy Environ. Sci.*, 5 (2012) 5333-5339.
- [113] J. W. Xiao, Q. Kuang, S. H. Yang, F. Xiao, S. Wang, L. Guo, Surface structure dependent electrocatalytic activity of Co₃O₄ anchored on graphene sheets toward oxygen reduction reaction, *Sci. Rep.*, 3 (2013) 1-8.
- [114] M. Y. Wang, J. R. Huang, M. Wang, D. G. Zhang, W. M. Zhang, W. H. Li, J. Chen, Co₃O₄ nanorods decorated reduced graphene oxide composite for oxygen reduction reaction in alkaline electrolyte, *Electrochem. Commun.*, 34 (2013) 299-303.
- [115] J. H. Kim, A. Ishihara, S. Mitsushima, N. Kamiya, K. I. Ota, Catalytic activity of titanium oxide for oxygen reduction reaction as a non-platinum catalyst for PEFC, *Electrochim. Acta*, 52 (2007) 2492-2497.
- [116] S. V. Mentus, Oxygen reduction on anodically formed titanium dioxide, *Electrochim. Acta*, 50 (2004) 27-32.
- [117] J. Sunarso, A. A. J. Torriero, W. Zhou, P. C. Howlett, M. Forsyth, Oxygen reduction reaction activity of La-based perovskite oxides in alkaline medium: a

thin-film rotating ring-disk electrode study, *J. Phys. Chem. C*, 116 (2012) 5827-5834.

[118] J. Chen, K. Takanabe, R. Ohnishi, D. L. Lu, S. Okada, H. Hatasawa, H. Morioka, M. Antonietti, J. Kubota, K. Domen, Nano-sized TiN on carbon black as an efficient electrocatalyst for the oxygen reduction reaction prepared using an mpg-C₃N₄ template, *Chem. Commun.*, 46 (2010) 7492-7494.

[119] P. He, Y.G. Wang, H. S. Zhou, Titanium nitride catalyst cathode in a Li-air fuel cell with an acidic aqueous solution, *Chem. Commun.*, 47 (2011) 10701-10703.

[120] R. Ohnishi, K. Takanabe, M. Katayama, J. Kubota, K. Domen, Nano-nitride cathode catalysts of Ti, Ta, and Nb for polymer electrolyte fuel cells: temperature-programmed desorption investigation of molecularly adsorbed oxygen at low temperature, *J. Phys. Chem. C*, 117 (2013) 496-502.

[121] N. Miura, H. Horiuchi, Y. Shimizu, N. Yamazoe, Gas-diffusion electrodes for oxygen reduction loaded with transition-metal nitrides, *Nippon Kagaku Kaishi*, (1987) 617-622.

[122] K. J. Zhang, L. X. Zhang, X. Chen, X. He, X. G. Wang, S. M. Dong, P. X. Han, C. J. Zhang, S. Wang, L. Gu, G. L. Cui, Mesoporous cobalt molybdenum nitride: a highly active bifunctional electrocatalyst and its application in lithium-O₂ Batteries, *J. Phys. Chem. C*, 117 (2013) 858-865.

[123] H. Tominaga, M. Nagai, Cathode catalysts for fuel cell development: a theoretical study based on band structure calculations for tungsten nitride and cobalt tungsten nitrides, *Electrochim. Acta*, 54 (2009) 6732-6739.

[124] H. X. Zhong, H. M. Zhang, G. Liu, Y. M. Liang, J. W. Hu, B. L. Yi, A novel non-noble electrocatalyst for PEM fuel cell based on molybdenum nitride, *Electrochem. Commun.*, 8 (2006) 707-712.

[125] D. H. Youn, G. Bae, S. Han, J. Y. Kim, J. W. Jang, H. Park, S. H. Choi, J. S. Lee, A highly efficient transition metal nitride-based electrocatalyst for oxygen reduction reaction: TiN on a CNT-graphene hybrid support, *J. Mater. Chem. A*, 1 (2013) 8007-8015.

[126] L. Volpe, M. Boudart, Compounds of molybdenum and tungsten with high specific surface-area. 1. Nitrides, *J. Solid State Chem.*, 59 (1985) 332-347.

- [127] S. Z. Li, W. B. Kim, J. S. Lee, Effect of the reactive gas on the solid-state transformation of molybdenum trioxide to carbides and nitrides, *Chem. Mater.*, 10 (1998) 1853-1862.
- [128] R. Kapoor, S. T. Oyama, Synthesis of high surface-area vanadium nitride, *J. Solid State Chem.*, 99 (1992) 303-312.
- [129] Y. Waseda, E. Matsubara, K. Shinoda, X-Ray diffraction crystallography: introduction, examples and solved problems, Springer, Berlin; London, 2011.
- [130] L.V. Azaroff, R. Kaplow, N. Kato, R. J. Weiss, A. J. C. Wilson, R. A. Young, X-ray diffraction, McGraw-Hill, New York, 1974.
- [131] O. C. Wells, with portions contributed by A. Boyde, E. Lifshin and A. Rezanowich, Scanning electron microscopy, McGraw-Hill, New York, 1974.
- [132] R. Jenkins, X-ray fluorescence spectrometry, 2nd edition, Wiley, New York, 1999.
- [133] L. Reimer, H. Kohl, Transmission electron microscopy: physics of image formation, 5th edition, Springer, New York, 2008.
- [134] S. L. Flegler, J. W. Heckman, Jr., K. L. Klomparens, Scanning and transmission electron microscopy : an introduction, W.H. Freeman, New York, 1993.
- [135] D. B. Williams, C. B. carter, Transmission electron microscopy: a textbook for materials science, 2nd edition, Springer, New York; London, 2009.
- [136] B. Fultz, J. M. Howe, Transmission electron microscopy and diffractometry of materials, 3rd edition, Springer-Verlag, Berlin, 2008.
- [137] S. J. Gregg, K. S. W.Sing, Adsorption, surface area and porosity, Academic Press, London;New York, 1967.
- [138] J. B. Condon, Surface area and porosity determinations by physisorption: measurements and theory, Elsevier, Amsterdam, 2006.
- [139] E.P. Barrett, L.G. Joyner, P.P. Halenda, The Determination of Pore Volume and Area Distributions in Porous Substances .1. Computations from Nitrogen Isotherms, *J Am Chem Soc*, 73 (1951) 373-380.
- [140] P. van der Heide, X-Ray Photoelectron Spectroscopy : An introduction to principles and practices, Wiley, Hoboken (NJ), 2011.
- [141] S. Hofmann, Auger- and X-ray photoelectron spectroscopy in materials science : a user-oriented guide, Springer, Heidelberg; London, 2013.

- [142] F. Béguin, E. Frackowiak, Supercapacitors: materials, systems, and applications, Wiley-VCH, Weinheim, 2013.
- [143] E. Barsoukov, J. R. Macdonald, Impedance spectroscopy: theory, experiment, and applications, 2nd edition, Wiley-Interscience, Hoboken (NJ), 2005.
- [144] V.F. Lvovich, Impedance spectroscopy: Applications to electrochemical and dielectric phenomena, Wiley, Hoboken (NJ), 2012.
- [145] H. Liu, J. Zhang, Electrocatalysis of direct methanol fuel cells: from fundamentals to applications, Wiley-VCH, Weinheim; Chichester, 2009.
- [146] S. L. Kuo, N. L. Wu, Investigation of pseudocapacitive charge-storage reaction of $\text{MnO}_2 \cdot n\text{H}_2\text{O}$ supercapacitors in aqueous electrolytes, *J. Electrochem. Soc.*, 153 (2006) A1317-A1324.
- [147] Y. M. Zhao, W. B. Hu, Y. D. Xia, E. F. Smith, Y. Q. Zhu, C. W. Dunnill, D. H. Gregory, Preparation and characterization of tungsten oxynitride nanowires, *J. Mater. Chem.*, 17 (2007) 4436-4440.
- [148] T. Nakajima, K. Watanabe, N. Watanabe, Preparation of tungsten nitride film by CVD method using WF_6 , *J. Electrochem. Soc.*, 134 (1987) 3175-3178.
- [149] A. M. Glushenkov, D. Hulicova-Jurcakova, D. Llewellyn, G. Q. Lu, Y. Chen, Structure and capacitive properties of porous nanocrystalline VN prepared by temperature-programmed ammonia reduction of V_2O_5 , *Chem. Mater.*, 22 (2010) 914-921.
- [150] J. B. Claridge, A. P. E. York, A. J. Brungs, M. L. H. Green, Study of the temperature-programmed reaction synthesis of early transition metal carbide and nitride catalyst materials from oxide precursors, *Chem. Mater.*, 12 (2000) 132-142.
- [151] C. Jo, I. Hwang, J. Lee, C. W. Lee, S. Yoon, Investigation of Pseudocapacitive charge-storage behavior in highly conductive ordered mesoporous tungsten oxide electrodes, *J. Phys. Chem. C*, 115 (2011) 11880-11886.
- [152] W. Sugimoto, H. Iwata, K. Yokoshima, Y. Murakami, Y. Takasu, Proton and electron conductivity in hydrous ruthenium oxides evaluated by electrochemical impedance spectroscopy: the origin of large capacitance, *J. Phys. Chem. B*, 109 (2005) 7330-7338.

- [153] S. E. Chun, S. I. Pyun, G. J. Lee, A study on mechanism of charging/discharging at amorphous manganese oxide electrode in 0.1 M Na₂SO₄ solution, *Electrochim. Acta*, 51 (2006) 6479-6486.
- [154] R. de Levie, On porous electrodes in electrolyte solutions, *Electrochim. Acta*, 8 (1963) 751-780.
- [155] G. J. Brug, A. L. G. Vandeneeden, M. Sluytersrehabach, J. H. Sluyters, The analysis of electrode impedances complicated by the presence of a constant phase element, *J. Electroanal. Chem.*, 176 (1984) 275-295.
- [156] Z. B. Z. Wei, P. Grange, B. Delmon, XPS and XRD studies of fresh and sulfided Mo₂N, *Appl. Surf. Sci.*, 135 (1998) 107-114.
- [157] Y. J. Zhang, Q. Xin, I. Rodriguez-Ramos, A. Guerrero-Ruiz, Temperature dependence of the pseudomorphic transformation of MoO₃ to gamma-Mo₂N, *Mater. Res. Bull.*, 34 (1999) 145-156.
- [158] J. G. Choi, J. R. Brenner, C. W. Colling, B. G. Demczyk, J. L. Dunning, L. T. Thompson, Synthesis and characterization of molybdenum nitride hydrodenitrogenation catalysts, *Catal. Today*, 15 (1992) 201-222.
- [159] R. Ohnishi, M. Katayama, D. K. Cha, K. Takanabe, J. Kubota, K. Domen, Titanium nitride nanoparticle electrocatalysts for oxygen reduction reaction in alkaline solution, *J. Electrochem. Soc.*, 160 (2013) F501-F506.
- [160] H. X. Zhong, H. M. Zhang, Y. M. Liang, J. L. Zhang, M. R. Wang, X. L. Wang, A novel non-noble electrocatalyst for oxygen reduction in proton exchange membrane fuel cells, *J. Power Sources*, 164 (2007) 572-577.
- [161] T. Khoo, P. C. Howlett, M. Tsagouria, D. R. MacFarlane, M. Forsyth, The potential for ionic liquid electrolytes to stabilise the magnesium interface for magnesium/air batteries, *Electrochim. Acta*, 58 (2011) 583-588.
- [162] P. C. Howlett, T. Khoo, G. Mooketsi, J. Efthimiadis, D. R. MacFarlane, M. Forsyth, The effect of potential bias on the formation of ionic liquid generated surface films on Mg alloys, *Electrochim. Acta*, 55 (2010) 2377-2383.
- [163] B. G. Demczyk, J. G. Choi, L.T. Thompson, Surface-structure and composition of high-surface-area molybdenum nitrides, *Appl. Surf. Sci.*, 78 (1994) 63-69.
- [164] M. R. Lukatskaya, O. Mashtalir, C. E. Ren, Y. Dall'Agnese, P. Rozier, P. L. Taberna, M. Naguib, P. Simon, M. W. Barsoum, Y. Gogotsi, Cation intercalation

and high volumetric capacitance of two-dimensional titanium carbide, *Science*, 341 (2013) 1502-1505.